In the Name of God

Journal of
Information Systems & Telecommunication
Vol. 5, No. 2, April-June 2017, Serial Number 18

Research Institute for Information and Communication Technology
Iranian Association of Information and Communication Technology
Affiliated to: Academic Center for Education, Culture and Research (ACECR)

Print ISSN: 2322-1437
Online ISSN: 2345-2773
Publication License: 91/13216

Editorial Office Address: No.5, Saeedi Alley, Kalej Intersection., Enghelab Ave., Tehran, Iran,
P.O.Box: 13145-799 Tel: (+9821) 88930150 Fax: (+9821) 88930157
E-mail: info@jist.ir
URL: www.jist.ir

Indexed by:
- Index Copernicus International www.indexcopernicus.com
- Islamic World Science Citation Center (ISC) www.isc.gov.ir
- Directory of open Access Journals www.Doaj.org
- Scientific Information Database (SID) www.sid.ir
- Regional Information Center for Science and Technology (RICeST) www.ricest.ac.ir
- Iranian Magazines Databases www.magiran.com

Publisher:
Regional Information Center for Science and Technology **(RICeST)**
Islamic World Science Citation Center **(ISC)**

This Journal is published under scientific support of
Advanced Information Systems (AIS) Research Group and
Digital & Signal Processing Research Group, ICTRC

Acknowledgement

JIST Editorial-Board would like to gratefully appreciate the following distinguished referees for spending their valuable time and expertise in reviewing the manuscripts and their constructive suggestions, which had a great impact on the enhancement of this issue of the JIST Journal.

(A-Z)

- Ahmadi, Ali, khaje Nasir-edin Toosi University, Tehran, Iran
- Alizadeh, Somayeh, khaje Nasir-edin Toosi University, Tehran, Iran
- Ashrafi Payaman, Nosratali, Kharazmi University, Tehran, Iran
- Aghaeizadeh Zoroofi, Reza, Tehran University, Tehran, Iran
- Charmi, Mostafa, University of Zanjan, Zanjan, Iran
- Fazli, Saeed, Azad University, Kermanshah Branch, Kermanshah, Iran
- Hamidi, Hojjatollah, khaje Nasir-edin Toosi University, Tehran, Iran
- Kabudian, Seyed Jahanshah, Razi University, Kermanshah, Iran
- Montazemi, Alireza, McMaster University, Hamilton, Ontario, Canada
- Mosallanejad, Ali, Iran University of Science and Technology, Tehran, Iran
- Nilforoushan, Zahra, Kharazmi University, Tehran, Iran
- Ramezannia, Seyed Bagher, khaje Nasir-edin Toosi University, Tehran, Iran
- Rouhani, Saeed, Tehran, University, Tehran, Iran
- Sadatrasoul, Seyed Mahdi, Kharazmi University, Tehran, Iran
- Saeidi, Rahim, Aalto University, Helsinki, Finland
- Soleimanian Gharechopogh, Farhad, Hacettepe University, Ankara, TURKEY

Table of Contents

A Hybrid Cuckoo Search for Direct Blockmodeling

Saeed NasehiMoghaddam*
Faculty of Engineering,University of Zanjan, Zanjan, Iran
nasehi@znu.ac.ir
Mehdi Ghazanfari
Faculty of Industrial Engineering, Iran University of Science and Technology, Tehran, Iran
mehdi@iust.ac.ir
Babak Teimourpour
Faculty of Systems and Industrial Engineering, Tarbiat Modares University, Tehran, Iran
b.teimourpour@modares.ac.ir

Received: 18/Oct/2016 Revised: 20/May/2017 Accepted: 27/May/2017

Abstract

Block modeling as a social structure discovery process needs to find and adopt a partitioning of actors to equivalent classes or positions. The best partitioning, naturally, must provide the closest estimation of network ties and show the most agreement with original network data. This interpretation of the best, leads to the structure with the most fitness to original network data. Finding this best partition vector can be formulated as an optimization problem and can be solved by Meta heuristic algorithms. In this paper, we use cuckoo search and genetic algorithm as a basis for comparison with cuckoo search. In addition to simple cuckoo search, we apply a hybrid cuckoo search algorithm to find the solution. The results of experiments through multiple samples reveals that while genetic algorithm shows the better performance in terms of convergence time and small iteration, the hybrid cuckoo search finds the better solutions than genetic algorithm in large iteration in terms of quality of solutions measured by fitness function. Furthermore, the hybrid cuckoo search shows no significant superiority over the simple cuckoo search, unless the large iteration numbered is used. In addition to block model problem, the proposed hybrid cuckoo search shows clear superiority over the greedy discrete PSO for community detection problem .

Keywords: Social Network Analysis (SNA): blockmodeling: Genetic Algorithm: Cuckoo Search: likelihood ratio statistics G^2.

1. Introduction

The social structure of a given network is discovered during blockmodeling process in the framework of positional analysis. During this process using a partitioning vector of actors to equivalent classes, called positions, network relational data is summarized to reduced network of structural positions which is assumed as the structure of a given network. This structure can be shown by density/image matrices or reduced graphs and reflects the whole original network of actors in the simplified small network of structural positions. Thus structure discovery process, similar to community detection process, depends on the partition vector of actors to positions, but a community is not assumed as a structural position. As mentioned by[1], the term "community" was used by "physicists" instead of term "cohesive group" which "is foundational in sociology". It is clear that grouping actors based on cohesion, does not necessarily means that members of a cohesive subgroup have similar ties to/ from the other actors. However if the structure of a given network discovered during blockmodeling is "cohesive subgroup" then the structural positions of that network will correspond to communities of the network. The partitioning of actors to structural positions is done so that all actors of a position are equivalent and similar in terms of their relational pattern. In conventional blockmodeling, several definitions of equivalency were used to find this partition vector. Pioneer of them is structural equivalence (SE), introduced by [2], which implies that two actors belong to the same structural equivalent class iff they have identical ties to / from all other actors. In addition to SE, automorphic, isomorphic and regular equivalence were proposed by researchers, and for each definition, an algorithm for partitioning actors to positions was proposed by researchers. Since for social structure discovery of a given network, the original network data is summarized by actor partitioning, and the inconsistent partition vectors produced by these equivalence definitions, leads to several structures for the same network and the question is that which of these structures is the best representative of the network?, and which equivalence definition is suitable for finding the structure of a network?, and a fundamental question is that is it necessary to use an equivalence definition for structure discovery purpose?, if not is it possible to adopt a computational approach in the form of an optimization problem to find the best social structure of a given network?, if so how to solve this optimization problem?

In this paper, we consider the social structure discovery as an optimization problem and intend to find the best social structure of a network. The best structure, naturally, provides the best estimation of network relational data. Since the social structure of a given network, depends on a partition vector of actors to

* Corresponding Author

positions, a partition vector, producing the closest estimation of network relational data, prepares the best social structure of a given network. This interpretation of the best, which is mentioned in none of the previous contributions of optimized block model problem, is the basis of our definition of block model problem. In order to solve our definition of block model problem, we employ two of Meta heuristics: cuckoo search and genetic algorithm as a basis for comparison with cuckoo search. In addition to simple cuckoo search, we apply a hybrid cuckoo search algorithm to find the solution. Now in the next section we briefly review the previous contributions pertinent to the optimal block model problem and then in section 3, we propose our definition for the block model problem along with algorithms used to optimize this problem and in section 4 the results of experiments for investigating the performance of the proposed algorithm are presented and finally the results summarized at section 5.

2. Related Works

In this section we review contributions relevant to applying optimization approach in block modeling and then a brief introductory subsection for meta heuristic algorithms generally and for cuckoo search algorithm specifically is provided.

2.1 Optimization Approaches In Block Modeling

While conventional block modeling allocates actors to positions by clustering, based on distances of actors from each other according to several equivalence definitions, such as structural and regular equivalence, generalized blockmodeling procedure of [3], using a local optimization procedure, searches the best partition vector conforming with a predetermined social structure. In fact, in generalized blockmodeling, actor partitioning is done without need to any equivalence definition, and the social structure of network is assumed known; therefore the structure of network is not sought. The independency from equivalence definitions provides direct approach for generalized blockmodeling. This generalization of blockmodeling could be adopted for two-mode network by [4], signed network by [5], sparse network by [6], multilevel network by [7], and valued networks by [8] , which were implemented in Pajek software and blockmodeling R package. However if the predefined social structure is unknown, the applicability and feasibility of generalized blockmodeling will be limited.

Besides generalized blockmodeling, the other direct approaches to structure discovery in the framework of an optimization problem have recently been proposed by authors. James, et al. [9] suggested a novel genetic algorithm with some ad hoc operators, for blockmodeling and showed its applicability in large network. But the usage of Herfindahl-Hirschman Index ([10]; [11]), HHI, which is just the sum of squared position sizes over all positions, as fitness function is not suitable in all cases such as valued relations; because maximized (HHI) prepares solution with high dense diagonal blocks for single binary network, (a network with one relation whose socio matrix includes zero- one entries), which makes this algorithm be classified for community detection algorithm rather than block model problem. The other contribution based on structural equivalence, as an application of tab u-search algorithm, was presented by [12] for block modeling of a two-mode network, (a network with two sets of: actors and events whose data is recorded in the incidence matrix so that if an actor participate in an event, the corresponding element set as 1, otherwise set as 0), and followed with an adaptation of variable neighborhood search by [13] for finding ideal zero and one blocks, which is only applicable for binary network data. The greedy discrete PSO algorithm of [14] is the one of the latest contribution in partitioning networks which made PSO applicable, effective, and competitive in community detection problem for finding cohesive subgroups. Although PSO algorithm, originally was not designed for discrete valued problem, the greedy discrete PSO of [14] works well and produces high quality solutions for community detection problems in terms of modularity index of Girvan and Newman [15]. However this algorithm, as mentioned by authors, is not fit and parsimonious for large networks, because of high time consuming for its convergence. In addition, it is designed for community problem and is not suitable for block model problem.

2.2 Cuckoo Search Algorithm (CS)

Metaheuristic methods usually are nature inspired algorithm and originally coordinate the interaction between local improvement procedures and procedures for avoiding local optimum and have capabilities to accomplish a robust search in a solution space. In fact, these methods employ strategies for conquering the trap of local optimality in complex solution spaces. Essentially, metaheuristics are approximate optimization methods which provide acceptable solutions in a reasonable time for solving hard and complex problems in science and engineering. There are two natural phenomena which is inspired by researchers during the development of metaheuristic algorithms as mentioned by [16]: the Darwinian evolution, and the social behavior of living animals and insects (e.g., birds, bees, ant colonies, fireflies). While evolutionary algorithms (EAs), as a species of these methods, refers to a family of algorithms which have been induced from the Darwinian nature evolution, swarm intelligence (SI) based algorithms are influenced from the social behavior of animals. Among evolutionary algorithms, the Genetic Algorithm (GA), as the most applicable and famous algorithm, is a probabilistic search algorithm that iteratively transforms a set (population) of objects (usually a fixed-length binary string), each with an associated fitness value, into a new population of offspring objects using the Darwinian

principle of natural selection and operations that mimic naturally occurring genetic operations such as mating recombination (crossover) and mutation.

In the family of the swarm intelligence algorithms, the Cuckoo Search algorithm (CS) as the one of the latest nature inspired metaheuristics, was developed by Yang and Deb [17], and is inspired by the brood parasitism of some cuckoo species laying their eggs in the nests of other bird species. According to Yang and Deb [17] cuckoo have the aggressive reproduction strategy. The term "brood parasitism" means that some species of cuckoo lays their eggs in the nests of other host birds (often other species) and includes three types: intraspecific brood parasitism, cooperative breeding, and nest takeover. There is a possibility that a conflict between some host birds and the intruding cuckoos is occurred. That is if a host bird discovers the extrinsic eggs, the discard of these foreign eggs or leave the nest and builds a new nest elsewhere will be chosen by the host birds. To adopt this behavior of cuckoo reproduction in forming an algorithm, Yang and Deb [17] constructed three rules:

1. Each cuckoo lays one egg at a time, and dumps it in a randomly chosen nest.
2. The best nests with high quality eggs will be carried over to the next generations.
3. The number of available host nests is fixed and any egg laid by a cuckoo may be discovered by the host bird with a probability $p_a \in (0, 1)$. In this case, the host bird can either get rid of the egg, or simply abandon the nest and build a completely new one.

Yang and Deb [17] using these rules, constructed cuckoo search algorithm as follows

CUCKOO SEARCH: **According to Yang and Deb [17]**

Data: α,λ,*maxGenerations*
Result: The best solution

Objective function $f(x)$, $x = (x_1, x_2, \ldots x_d)^T$
Generate initial population, of n host nests x_i $(i = 1, 2, \ldots, n)$
while *(t ≤ maxGenerations) or(stop criterion)* **do**
  $C_i \leftarrow$ *Get a cuckoo randomely by levy flight and evaluate its quality* $\rightarrow F_i$
  $C_j \leftarrow$ *Choose a nest randomely among n nests*
  if C_i *is better than* C_j **then** $C_j \leftarrow C_i$
  A fraction p_a *of worse nests are abondened and new ones are built*
  Keep the best solutions
  best $\leftarrow$ *Rank the solutions and find the current best*
return(best)

Figure 1. Cuckoo Search Algorithm of Yang and Deb

Yang and Deb [17] demonstrated he superiority of cuckoo search over genetic algorithm and PSO through several standard tests. In all experiments, the solution space is continuous and results corroborate that cuckoo search clearly outperforms GA and PSO. The results reported by Yang and Deb [17], motivated us to employ cuckoo search to find the optimal blockmodel. Because PSO algorithm was dominated by GA in blockmodel problem, we adopt GA as a basis for comparison with cuckoo search.

3. Proposed Method

In this section, required definitions of our research is presented. The definition of the blockmodel problem is prepared at the first subsection. In addition, the specification of genetic algorithm and cuckoo search algorithm is prepared

3.1 Blockmodel Problem

As mentioned in the previous section, we search for the best structure agree with the original network data. This means that our goal is to find the structure which estimates relatively close to original network ties. The closeness to original network data can be measured by either statistically goodness of fit indices or deviance indices. This measurement, simply is done by comparison of original network data with estimated network data by a given blockmodel. Thus it is necessary to define the estimation of network ties under a given blockmodel. This estimation is defined in general form to be applied in wide range of network data and then it is revised to be applicable for calculation of the log likelihood ratio statistics, in the special case of discrete ordinal network data.

Suppose $\mathcal{N} = \{1,2, \ldots, n\}$ is a set of actors in network $\mathcal{S}$ and $\mathcal{R} = \{1,2, \ldots, R\}$ is a set of R valued relations measured on $\mathcal{N}$, and $\mathcal{X}_r$ is the sociomatrix of rth relation where $\mathcal{X}_{rij}$ is the strength of the tie from actor i to actor j on the rth relation. In addition, let $\mathcal{P} = \{\mathcal{P}_1, \mathcal{P}_2, \ldots, \mathcal{P}_p\}$ be a set of positions and Φ be a mapping function, which assigns actors to positions; that is:

$$\phi: \mathcal{N} \longrightarrow \mathcal{P}$$
$$\forall\, i \in \mathcal{N}\ \exists!\ j \in \mathcal{P} \ni \phi(i) = j \qquad (1)$$

The relation between and within positions can be represented by density matrices. Suppose $\Delta = [\delta_{ruv}]_{r\times p\times p}$ is an array of density matrices among these p positions such that if n_k , n_l are respectively the number of members in positions k and l, we have:

$$\Delta_{rkl} = \begin{cases} \sum_{i\in\mathcal{P}_k}\sum_{j\in\mathcal{P}_l} x_{rij}/n_k n_l\,, & if\ k \neq l \\ \sum_{i\in\mathcal{P}_k}\sum_{i\in\mathcal{P}_k} x_{rij}/n_k(n_k-1)\,, & if\ k = l \end{cases} \qquad (2)$$

Now, the blockmodel $\mathcal{B}$ can be defined as: $\mathcal{B} = \langle \phi, \Delta \rangle$. The hypothetical nature of a blockmodel makes it capable to estimate the strength of each tie, and once a partition is established, either posteriori or a priori, the model can estimate relational ties. In the other words, we have:

$$E\left(x_{rij} \middle| \mathcal{B} = \langle \phi, \Delta \rangle\right) = \hat{x}^{\mathcal{B}}_{rij} = \Delta_{r\phi(i)\phi(j)} \qquad (3)$$

In fact, $\hat{\boldsymbol{x}}^{\boldsymbol{\mathcal{B}}}_{\boldsymbol{rij}}$ is the expected strength of tie, from actor i to actor j in the rth relation under hypothesis $\mathcal{B}$.

In order to calculate goodness of fit of a given blockmodel, in terms of G^2, we need to assume strengths of ties is categorical. Suppose $\mathcal{R} = \{1,2, \ldots, R\}$ is a set of R ordinal valued relations measured on $\mathcal{N}$, and $\mathcal{X}_r$ is the sociomatrix of rth relation where $\mathcal{X}_{rij}$ is the strength of

the tie from actor i to actor j, on the rth relation. In addition, assume that these strengths of ties come from a bounded ordinary set $\mathcal{V}_r$ which has C_r categories on the rth relation. Let ψ be a mapping function from $\mathcal{V}_r$ to $\{1,2,3,\dots,C_r\}$ ordinary set such that:

$$\forall\, v \in \mathcal{V}_r\ \exists!\ c \in \{1,2,\dots,C_r\} \ni \psi(v) = c \quad (4)$$

Now, we define a four dimensional $(n \times n \times C_r \times C_r)$ cross-classified array $\boldsymbol{Y} = \{Y_{rijkl}\}$ as:

$$Y_{rijkl} = \begin{cases} 1 & if\ \left(\psi(\mathcal{X}_{rij}), \psi(\mathcal{X}_{rji})\right) = (k,l)\ , where\ k,l \in \{1,2,\dots,C_r\} \\ 0 & otherwise \end{cases} \quad (5)$$

As noted by [18], the (i,j) th cell of Y is a $C_r \times C_r$ submatrix which has a single 1 in the (k, l) th cell and the remaining $C_r^2 - 1$ elements will be 0. Thus, these submatrices can be simply viewed as indicator matrices, giving the "state" of each $(\boldsymbol{\mathcal{X}_{rij}}, \boldsymbol{\mathcal{X}_{rji}})$ dyad. Now the estimation under blockmodel B for the state of $(\boldsymbol{\mathcal{X}_{rij}}, \boldsymbol{\mathcal{X}_{rji}})$ dyad is:

$$\hat{y}^{\mathcal{B}}_{rijkl} = Pr\left(y_{rijkl} = 1\right) = \begin{cases} \sum_{i\in\mathcal{P}_u}\sum_{j\in\mathcal{P}_v} Y_{rijkl}/(n_u n_v)\ , & u \neq v \\ \sum_{i\in\mathcal{P}_u}\sum_{j\in\mathcal{P}_u} Y_{rijkl}/n_u(n_u-1)\ , & u = v \end{cases} \quad (6)$$

Where counts n_u and n_v are the number of actors in positions $\mathcal{P}_u$ and, $\mathcal{P}_v$, respectively. Now, estimation of relational ties can be written as:

$$\hat{x}^{\mathcal{B}}_{rij} = \sum_{v\in\mathcal{V}_r} v\hat{y}^{\mathcal{B}}_{rijk+} = \sum_{v\in\mathcal{V}_r} v \sum_{l=1}^{C_r} \hat{y}^{\mathcal{B}}_{rijkl} \quad (7)$$
$$where\ i \neq j, \quad \psi(v) = k, and\ \ l = 1,2,\dots,C_r$$

In order to assess how close a given blockmodel estimation is to original relational data, deviance indices such as sum of absolute error, sum of squared error (SSE), inconsistency index[5] and goodness of fit indices such as matrix correlation, ρ, and the log ratio statistics, G^2, can be used.

$$SAE = \delta_{x1} = \sum_{r,i,j} \left|x_{rij} - \hat{x}^{\mathcal{B}}_{rij}\right| \quad (8)$$

$$SSE = \sum_{r,i,j} \left(x_{rij} - \hat{x}^{\mathcal{B}}_{rij}\right)^2 \quad (9)$$

$$\rho = \left(\sum \left(x_{rij} - \bar{x}_r\right)\left(\hat{x}^{\mathcal{B}}_{rij} - \bar{x}_r\right)\right) \Big/ \left(\sqrt{\sum \left(x_{rij} - \bar{x}_r\right)^2}\sqrt{\sum \left(\hat{x}^{\mathcal{B}}_{rij} - \bar{x}_r\right)^2}\right) \quad (10)$$

$$Inconsistency = \sum_{\phi(i),\phi(j)} \alpha \left\| x^{+}_{rij} \middle| \Delta_{r\phi(i)\phi(j)} < 0 \right\| + (1-\alpha) \left\| x^{-}_{rij} \middle| \Delta_{r\phi(i)\phi(j)} > 0 \right\| \quad (11)$$

$$G^2_{\mathcal{B}} = 2\sum_r \sum_{i<j} \sum_{k,l} y_{rijkl} log\left(y_{rijkl}/\hat{y}^{\mathcal{B}}_{rijkl}\right) \quad (12)$$

Inconsistency index was defined by [5] as an average count of positive ties in negative blocks and negative ties in positive blocks and if there are no specific preferences between inconsistency in positive blocks and inconsistency in negative blocks then $\alpha = 0.5$. Except for G^2, the other measures are not used for statistical goodness of fit test statistics, so we called them as descriptive indices. While SAE and SSE are measures of dissimilarity, ρ is a measure of similarity between the two matrices, and so $(1-\rho)$ can measure dissimilarity. That is, SAE, SSE and $(1-\rho)$ can be viewed as indices of lack of fitness of a given blockmodel. These indices have the advantage of applicability in any one mode relational data such as dichotomous, signed, ordered valued and valued relation, while G^2/ inconsistency index is suitable for ordinal / signed relations. Now, blockmodeling problem can be formulated as:

$$\begin{gathered} Minimize\ Lack\ of\ Fit \\ subject\ to: \\ \forall\, u \in \mathcal{P}: n_u \geq 1 \\ Where\ Lack\ of\ Fit \in \{SAE, SSE, (1-\rho), G^2, Inconsistency\} \end{gathered} \quad (13)$$

3.2 Genetic Algorithm for Blockmodel Problem (BMGA)

In all application of GA, at first, the chromosome structure must be defined. In blockmodeling problem, chromosome structure corresponds to partition vector; that is a chromosome string is a vector of length n such that the value of each element is the position (class) number of each actor. In fact, a partition vector corresponds to a chromosome (string), and each solution decodes as partition vector.

1	2	3		n-2	n-1	n
2	4	1	....	3	8	7

Figure 2. Partition vector as Chromosome

In the second step is recombination process of algorithm must be clarified. In GA recombination process consist of two major operators: crossover and mutation. Crossover operates on couple chromosomes; that is the mating process can be done between two chromosomes through crossover operators. Although there are several types of crossover: single point, multiple point, and uniform, we adopt uniform crossover in each run of algorithm in all experiments.

Another operator is mutation. Mutation operator increases the possibility of escape from local optimum and attempts to change the value of one or more genes of a given chromosome to a new randomly-generated value. Several types of mutation operators are proposed in the literature such as single point, double point, multiple point, swap, etc. Among various types of mutation, single point mutation is more common, which operates on a single chromosome, but the multiple point mutation is also used in our experiments

A selection method for choosing parent chromosomes to reproduce new child chromosomes is needed. Among various selection methods such as roulette wheel, tournament and rank, we used tournament methods with tour size equals to 2.

In order to make algorithm be converged we unify successive generations as new generation. Thus we have an elitist genetic algorithm which is shown in figure 3

ELITIST GENETIC ALGORITHM FOR DIRECT BLOCKMODELING: BMGA

Data: *network*,*popSize*,*pCount*,*function*,*selection*,*mutation*,*crossover*,$\mathcal{P}_m$,*maxGen*
Result: The best solution

1 $\langle population, fitness\rangle \leftarrow random\ Initialize(popSize, pCount)$
2 $\langle best, bestFitness\rangle \leftarrow bestFinding(population, fitness)$
3 **for** $i \in (1 : maxGen)$ **do**
4 **while** $\|offsprings\| \leq popSize$ **do**
5 $\langle P_1, P_2\rangle \leftarrow select\ (population, tournamentSelection\ (tourSize = 2\ ))$
6 $\langle C_1, C_2\rangle \leftarrow recombine\ (P_1, P_2, uniformCrossover)$
7 $\langle C_1, C_2\rangle \leftarrow mutate\ (C_1, C_2, \mathcal{P}_m, mutation \in \{SinglePoint, MultiplePoint\})$
8 $\langle F_1, F_2\rangle \leftarrow evaluate\ (C_1, C_2, function \in \{SAE, SSE, Inconsistency, \rho, G^2\})$
9 $\langle offspring, newFitness\rangle \leftarrow Add(\langle C_1, C_2\rangle, \langle F_1, F_2\rangle)$
10 $\langle population, fitness\rangle \leftarrow \langle (population \cup offspring), (fitness \cup newFitness)\rangle$
11 $\langle best, bestFitness\rangle \leftarrow bestFinding(population, fitness)$
12 $return(best, bestFitness)$

Figure 3.Elitist Genetic Algorithm for blockmodeling

3.3 Cuckoo Search for Blockmodel Problem (BMCS)

According to figure 1, a new cuckoo from existing cuckoo is recreated by levy flight random walk; that is for cuckoo i, new cuckoo is obtained by levy flight as:

$$x_i^{(t+1)} = x_i^{(t)} + \alpha \oplus Levy(\lambda) \quad (14)$$

Where α > 0 is the step size which is related to the scales of the given problem. As noted by Yang and Deb [17], in most cases, α = 1 is suitable step size. The equation (9) is essentially the stochastic equation for random walk which is in turn a Markov chain whose next status only depends on the current state (the first term in the above equation) and the transition probability (the second term). The operator ⊕ indicates entry-wise multiplications. Yang and Deb notes: "This entry-wise product is similar to those used in PSO, but the random walk via Levy flight is more efficient in exploring the search space as its step length is much longer in the long run". The Levy flight essentially provides a random walk while the random step length is drawn from a Levy distribution with infinitive mean and variance:

$$Levy \sim u = t^{-\lambda}, \qquad where\ 1 < \lambda \leq 3 \quad (15)$$

In order to draw a sample from Levy distribution, Yang [19] used Mantegna's algorithm which calculates a Levy distribution number as:

$$s \sim Levy: s = \frac{u}{|v|^{1/\lambda}} \ni u \sim N(0, \sigma^2)\ and\ v \sim N(0,1) \quad (16)$$

Where σ is obtained as:

$$\sigma = \left[\Gamma(1+\lambda) sin(\pi\lambda/2) / \left(\Gamma((1+\lambda)/2)\lambda 2^{((\lambda-1)/2)}\right)\right]^{1/\lambda} \quad (17)$$

In order to apply cuckoo search for blockmodeling problem, each nest/cuckoo corresponds to a partition vector. In fact in cuckoo search, nest/egg corresponds to chromosome/gen in genetic algorithm. In order to achieve a hybrid cuckoo search algorithm, we incorporate a local search procedure in the discovery of foreign eggs section. In fact, as perceived by figure 4, in line 18, for each solution being checked to be replaced by new randomly created solution, if the quality of new solution is worse than current under check solution, we perform a local search around this solution. In this way, the quality of solutions is not deteriorated and we implemented a modified cuckoo search algorithm for blockmodeling problem. The input parameter neighbourSearch is used to decide whether the local search is performed or not. That is if this parameter is set to zero the local search procedure of line 18, without any process, will keep the current cuckoo and BMCS will be a simple cuckoo search algorithm. The local search simply, searches for the best fitness among the first neighbors of a solution. To construct the first neighborhood for a partition vector, one point (position) randomly is selected and its value is changed. To prepare more exploration, more than one point (say two) can be used to be changed

CUCKOO SEARCH ALGORITHM FOR BLOCKMODEL PROBLEM: **BMCS**

Data: *network*,*nSize*,*pCount*,α,λ,p_a,*maxGenerations*,*neighbourSearch*
Result: The best solution

1 $n \leftarrow |network|$ // NETWORK SIZE
2 $\sigma \leftarrow \frac{\Gamma(\lambda+1)\sin(\frac{\pi\lambda}{2})}{\Gamma(\frac{\lambda+1}{2})\lambda 2^{\frac{\lambda-1}{2}}}$ // COMPUTATION OF σ
3 $\langle nests, fitness\rangle \leftarrow random\ Initialize(nSize, pCount)$
4 $\langle best, bestFitness\rangle \leftarrow bestFinding(nests, fitness)$
5 **while** $(t \leq maxGenerations)$ **do**
6 **for** $j \leftarrow 1$ **to** $nSize$ **do**
7 $u_a \leftarrow generate\ Random\ Uniform\ ()$
8 $\langle u, v, s\rangle \leftarrow generate\ Random\ Normal\ (n)$
9 $u \leftarrow \sigma u$
10 $C_j \leftarrow bound(nests[j] + \alpha s \frac{u}{|v|^{\frac{1}{\lambda}}}(nests[j] - best))$
11 $F_j \leftarrow evaluate(C_j)$
12 **if** F_j *is better than* $fitness[j]$ **then**
13 $\langle nests[j], fitness[j]$,neighbourSearch[j]$\rangle \leftarrow \langle C_j, F_j, 0\rangle$
14 **if** $u_a \leq p_a$ **then**
15 $\langle C_j, F_j\rangle \leftarrow random\ Initialize(1, pCount)$
16 **if** F_j *is better than* $fitness[j]$ **then**
17 $\langle nests[j], fitness[j]$,neighbourSearch[j]$\rangle \leftarrow \langle C_j, F_j, 0\rangle$
18 $\langle nests[j], fitness[j]\rangle \leftarrow localSearch(nests[j], fitness[j]$,neighbourSearch[j]$)$
19 $\langle best, bestFitness\rangle \leftarrow bestFinding(nests, fitness)$
20 $return(best, bestFitness)$

Figure 4. Cuckoo search algorithm for blockmodel problem

4. Experiments

In this section, the performance of the proposed hybrid cuckoo search algorithm in comparison with genetic algorithm/ greedy discrete PSO, for blockmodel/ community detection problem using some famous examples in social network analysis literature, is examined.

In this regard, we use three famous samples including Kapferer's Tailor Shop sample in [20], aggregated Sampson's data discussed by [5], and finally world trade in miscellaneous manufactures of metal 1994 discussed by [21] as a case of interval valued relation.

Now, in the next subsection the performance of BMCS against BMGA is investigated and then the capability of the proposed hybrid cuckoo search for community detection problem is compared with the greedy discrete particle swarm optimization and finally the effect of parameters such as iteration, nest size and incorporating the proposed local search are studied.

4.1 The comparison of BMCS and BMGA

Since BMCS with "neighbourSearch" greater than zero, is converted to a hybrid cuckoo search algorithm (denoted by BMHCS hereafter) which employs a local search procedure in addition to conventional update process, it is obvious that, in each update process, the execution time of this hybrid version is greater than execution time of the simple cuckoo search. Therefore it is fair that execution time of each update/recombination process of simple cuckoo search/BMGA, is restricted by corresponding update process of BMHCS. That is in each update process of BMHCS the elapsed time is measured as Thcs and then the update/recombination process of simple cuckoo search/BMGA is run until the execution time does not exceed this Thcs. Even though the total execution time of BMHCS, eventually is smaller than the total execution time of BMCS/BMGA, this is indispensable and in favor of BMGA/BMCS and if BMHCS is demonstrated to be outperformed BMCS/BMGA this favoritism will be completely insignificant. In all experiments the parameters of cuckoo search algorithm according to implemented MATLAB code proposed by Yang [19] were set to $\langle \alpha = 0.1 | \lambda = 1.5 | p_a = 0.25 \rangle$.

The local search of BMHCS were applied by setting neighbourSearch parameter to non-zero value which means that in each update process, if the fitness of a cuckoo is not improved the first neighborhood of that cuckoo will be sought. As mentioned before, this neighborhood is constructed by randomly selecting some eggs/gens and changing their value to all possible value.

Now the results of experiments in each sample are presented separately:

1) **Sampson Monastery Data.**

This sample is about the relations measured by Sampson [22] between monks. These relational data consist of four signed relations: like, esteem, influence and praise. In the literature, traditionally, positive and negative ties are recorded with separate matrices for each signed relation; specifically these signed relations are converted such that: like⟶(liking, disliking), esteem⟶ (esteem, disesteem), influence⟶ (positive influence, negative influence) and praise⟶(praise, blame). Doreian and Mrvar [5] summed the like, esteem and influence relations to create a valued signed relation which is called as Doreian- Sampson. This data is ordinal and valued in range of [-9, 9]. Since Doreian- Sampson data is a singed ordinal valued relation, experiments are done using inconsistency as fitness function.

For comparison purpose, the experiments were set as follows: for nest/population size two levels of 30 and 50, and for maxGens three levels of 50, 100, and 200, were considered and for each pair of (nest size, maxGens), BMGA and BMHCS were run 15 times and results were summarized in table 1 and were shown in figure 5, where box plot of results of BMHCS/BMGA with color of green/purple through maxGen of 50, 100, and 200 was drawn respectively.

The local search of BMHCS, for each cuckoo which is not improved by usual update process, selects randomly one egg of that cuckoo and change its value to all possible values and then among these values, the value which prepares the best fitness, is chosen for that egg.

In the table 1, the third column represents the p-value of a hypothesis test of superiority of genetic algorithm over proposed hybrid cuckoo search algorithm, in terms of fitness function and convergence time, using the nonparametric Wilcoxon rank sum test. This superiority, means that fitness function/ convergence time of BMGA is better/ greater than BMHCS. The forth column prepares a confidence interval, which was computed using the nonparametric "Sign test", at the level of 95% of results produced by BMGA / BMHCS.

nSize	maxGen	H_0: *BMGA ≽ BMHCS*		95% *Confidence Interval*	
		Inconsistency	Time	BMGA	BMHCS
30	50	0.1831	0.1065	(10.5, 14.41)	(10.5,13.82)
30	100	0.2417	0.03723	(10.5 12.23)	(10.5, 11.0)
30	200	0.3388	0.7332	(10.5, 10.5)	(10.5, 10.5)
50	50	0.9406	0.00052	(10.5, 11)	(10.5,13.82)
50	100	0.03276	0.003499	(10.5, 11)	(10.5, 10.5)
50	200	0.008987	0.06237	(10.5, 13.88)	(10.5, 10.5)

Table 1. The results of comparison between BMGA and BMCS for Sampson-Doreian Data

According to results of table 1, while there is no enough strong evidence for the superiority of BMGA/BMHCS over BMHCS/BMGA for the nest size equal to 30, there is strong evidence for superiority of BMGA/BMHCS over BMHCS/BMGA for nest size equals to 50; so that genetic algorithm outperform the proposed hybrid cuckoo search at the level of 50 of maxGen; but for maxGen larger than 50, ie 100 and 200, the BMHCS clearly outperforms the BMGA. Therefore, running with the more iteration, makes BMHCS more effective than BMGA and so the possibility of achieving the better solution is increased by the large maxGens for BMHCS. However except for nest size of 30 with maxGen of 200, the convergence time of BMGA is significantly lower than that of BMHCS

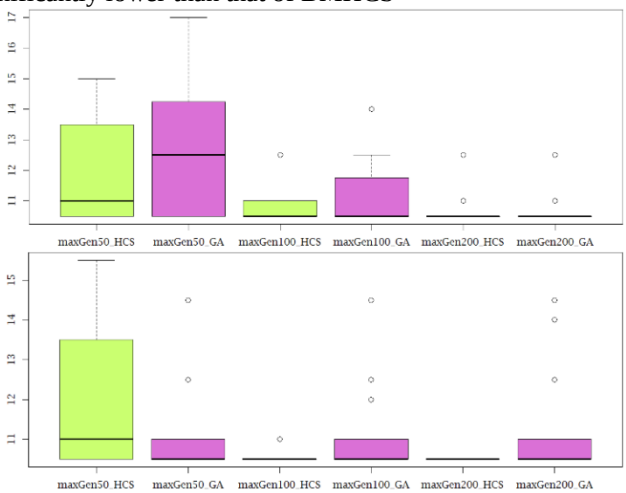

Figure 5. The boxplots of results produced by BMGA and BMHCS; Upper/Lower: the results of experiments with nest Size=30/50

Although, at the level of 200 for maxGen, it seems that the confidence interval of inconsistency index,

produced by BMGA, for nest Size of 50 is greater than for nest Size of 30, statistically there is no significant differences between results produced by BMGA for maxGen of 200 at two levels of 30 and 50 for nest size.

2) **Kapferer's Tailor Shop**

The second sample is Kapferer's Tailor shop, discussed by [20]. This network has a size of 39×39 and two/four actors with indegree/outdegree equal to zero. Since this relational data is dichotomous, all mentioned indices, except for inconsistency, are applicable. Among them, SAE and G^2 as objective functions to minimize lack of fitness of the blockmodel problem were chosen.

The experiments and the local search were set as previous sample and results for G^2 and SAE were presented in table 2/ figure 6 and table 3/figure 7 respectively.

nSize	maxGen	$H_0: BMGA \succcurlyeq BMHCS$		95% *Confidence Interval*	
		G^2	Time	BMGA	BMHCS
30	50	1.00	0.2528	(572.25,577.91)	(588.47,593.5)
30	100	0.7558	0.000695	(572.25,579.06)	(572.62, 576.3)
30	200	0.01233	1.67e-05	(572.25,575.97)	(572.25,572.25)
50	50	1.00	0.009771	(572.25,575.97)	(585.38,595.21)
50	100	0.8696	3.39e-05	(572.25,575.31)	(572.25,576.24)
50	200	0.0398	2.85e-05	(572.25,572.25)	(572.25,572.25)

Table 2. The results of comparison between BMGA and BMCS for Kapferer Tailor's shop data in terms of G^2

In table 2, in third column the p-value of hypothesis test of the superiority of the genetic algorithm over the proposed hybrid cuckoo search, in terms of fitness function and convergence time, was computed. According to the table 2, as perceived from figure 6, while the superiority of BMGA over BMHCS for maxGen of 50 and for maxGen of 100 with nest size of 50, is significant, for maxGen equals to 200, the BMHCS clearly outperforms BMGA.

On the other hand, the convergence time of BMGA is significantly less than that of BMHCS, which makes BMGA be advantageous over BMHCS. However the performance of BMHCS, in finding high quality solutions for large maxGen justifies the high convergence time

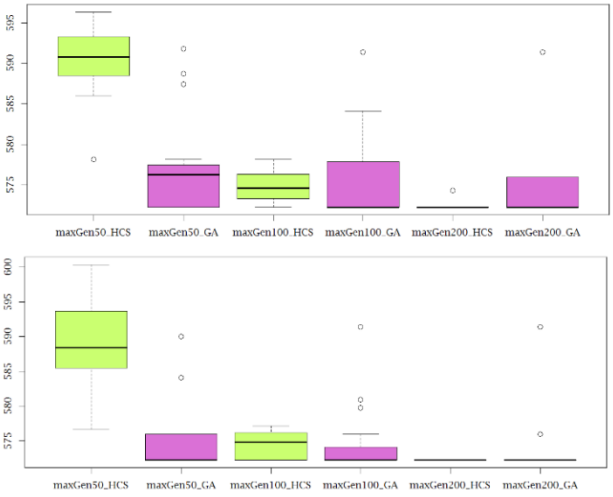

Figure 6. The boxplots of resulted G^2 produced by BMGA and BMHCS; Upper/Lower: the results of experiments with nest Size=30/50

The results of experiments in table 3, show that the genetic algorithm is not dominated by hybrid cuckoo search algorithm in minimizing SAE function. In addition, for each size of 30 and 50, as the maxGen increases, the quality of results found by BMHCS, is improved and eventually BMHCS finds the best solution which is obtained by BMGA. This means that the solutions found by BMHCS has the same quality as the solution obtained by BMGA. The quality of solutions of two algorithm can be compared from the boxplot presented in figure 7. In figure 7, it is obvious that the quality of solutions found by BMHCS, is improved by increasing maxGen so that there are no clear differences between BMHCS and BMGA for maxGen of 200. However as mentioned for experiments of G^2, the convergence time is the significant advantage of BMGA over BMHCS for experiments which use SAE as fitness function.

nSize	maxGen	$H_0: BMGA \succcurlyeq BMHCS$		95% *Confidence Interval*	
		Inconsistency	Time	BMGA	BMHCS
30	50	1.00	0.8779	(205.14,209.11)	(213.7, 217.85)
30	100	1.00	0.00052	(205.14,205.14)	(206.82,209.10)
30	200	0.7114	2.39e-05	(205.14,205.14)	(205.14,205.14)
50	50	1.00	0.8779	(205.14,209.11)	(213.7, 217.85)
50	100	1.00	1.67e-06	(205.14,205.14)	(206.37,207.91)
50	200	1.00	1.67e-06	(205.14,205.14)	(205.14,205.14)

Table 3. The results of comparison between BMGA and BMCS for Kapferer Tailor's shop data in terms of SAE

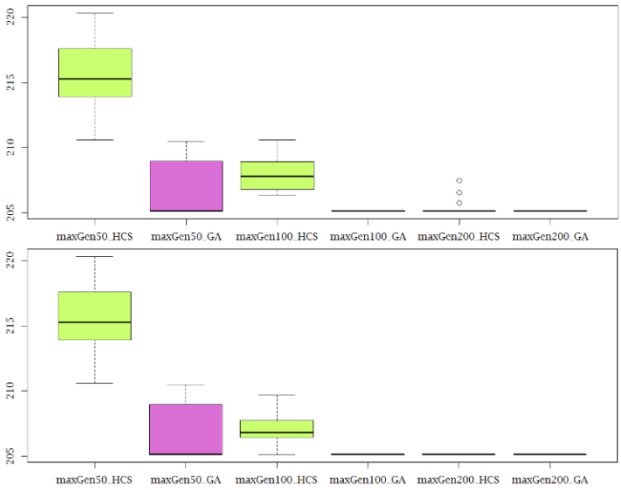

Figure 7.The boxplots of resulted SAE produced by BMGA and BMHCS; Upper/Lower: the results of experiments with nest Size=30/50

3) **World trade in miscellaneous manufactures of metal**

This data include miscellaneous manufactures of metal trade data among 80 countries in 1994. All countries with entries in the paper version of the Commodity Trade Statistics published by the United Nations were included, but for some countries, the 1993 data (Austria, Seychelles, Bangladesh, Croatia, and Barbados) or 1995 data (South Africa and Ecuador) were used because they were not available for 1994. Countries which are not sovereign are excluded because additional economic data were not available: Faeroe Islands and Greenland, which belong to Denmark and Macau (Portugal). Most missing countries are located in central

Africa and the Middle East, or belong to the former USSR. The arcs represent imports by one country from another for the class of commodities designated as '*miscellaneous manufactures of metal*', which represents high technology products or heavy manufacture. The absolute value of imports (in 1,000 US$) is used, but imports with values less than 1% of the country's total imports were excluded.

The data were used as a sample for the blockmodeling case in [21], and a core- peripheral structure as a result of conventional blockmodeling was demonstrated.

Since this relational data is interval valued, the application of G^2, as a measure of lack of fit, is neither appropriate nor practical; thus, in this case, the other indices are practical. In order to find the partition vector of most fitness with original data, matrix correlation, □, was used, and for this function, experiments were done separately.

In order to compare the performance of two algorithms, the configuration of experiments were set as follows: three levels of 20, 30, and 50 for nest/population size, and three levels of 40, 200, and 1000 for iteration or maxGen, were allocated. The local search of BMHCS as previous sample were set by neighbourSearch equals to 1, which constructs the first neighbor of current unimproved cuckoo by changing the value of one randomly selected egg of that cuckoo to all possible value and then adopts the best neighbor to be replaced by that cuckoo. All experiments were run 15 times and the results were summarized in table 4.

nSize	maxGen	H_0: $BMGA \geqslant BMHCS$		95% *Confidence Interval*	
		Correlation:ρ	Time	BMGA	BMHCS
20	40	1.00	1.00	(0.472,0.592)	(0.319, 0.368)
20	200	1.00	0.000923	(0.645, 0.645)	(0.620, 0.6426)
20	1000	0.0189	8.01e-06	(0.645, 0.645)	(0.645, 0.686)
30	40	1.00	1.00	(0.613, 0.64)	(0.345, 0.383)
30	200	0.9994	1.7e-06	(0.645, 0.645)	(0.638, 0.645)
30	1000	0.001627	1.67e-06	(0.645, 0.645)	(0.645, 0.695)
50	40	1.00	0.9166	(0.636, 0.645)	(0.377, 0.417)
50	200	0.5191	1.66e-06	(0.645, 0.645)	(0.645, 0.645)
50	1000	0.0006402	1.69e-06	(0.645, 0.645)	(0.645, 0.695)

Table 4. The results of comparison between BMGA and BMCS for metal trade network data in terms of matrix correlation

While, for maxGen of 40 regardless of nest size, the quality of results returned by BMGA is better than those of BMHCS, the convergence time of the genetic algorithm is larger than that of the hybrid cuckoo search algorithm; that is for small iteration, such as 40, the dominance of BMGA over BMHCS coincides with the larger convergence time of BMGA than that of BMHCS. On the other hand, for the maxGen of 200 and 1000, with regard to the convergence time, the superiority of BMGA over BMHCS is significant. However, as perceived from figure 8, this superiority for maxGen of 1000 concurs with its inferiority to BMHCS with respect to the quality of solutions. An important note is that by increasing the number of iterations, BMGA falls into local optima and premature convergence.

4.2 The Hybrid Cuckoo Search vs GDPSO

In addition to blockmodel problem, the proposed hybrid cuckoo search (HCS) of figure 5, using modularity index as fitness function can be used for community detection problem. Therefore the performance of the hybrid cuckoo search can be compared with the greedy discrete PSO (GDPSO). Since GDPSO is a time consuming algorithm, the hybrid cuckoo search was run in the time restriction equal to execution time of GDPSO; that is in order to make fair comparison of the hybrid cuckoo search with GDPSO, in each iteration, the time of update process of GDPSO is saved as TGDPSO and then the update process of the hybrid cuckoo search is run until its execution time does not exceed TGDPSO. Thus is in all experiments, instead of setting iterations number, the execution time threshold equals to GDPSO running time, for comparison of HCS with GDPSO, were used. The experiments for all three samples of karate, dolphins, and football, which are discussed by the authors of GDPSO, were set as follows:

$\langle c_1 = c_2 = 1.4961 | \omega = 0.7298 | popsize = 50 | gmax = 50 \rangle$

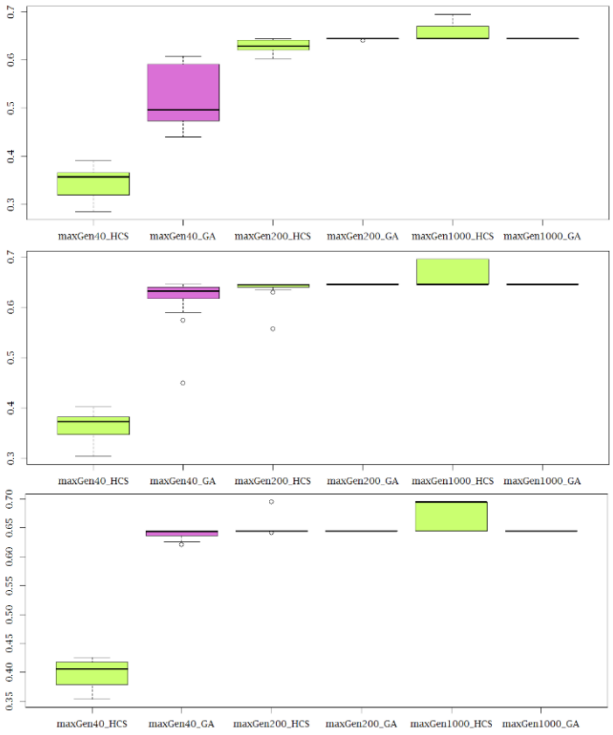

Figure 8. The box plot of results emerged from running BMHCS and BMGA respectively from up to down: for nest size of 20, 30, and 50

This configuration for c_1, c_2 and ω are the same as those used by the authors of GDPSO and the level of 50 for population size and gmax has been used by authors too. The values parameters of the HCS were equal to: $\langle \alpha = 0.1 | \lambda = 1.5 | p_a = 0.25 | \text{neighbourSearch} = 2 \rangle$. The value of 2 for neighbourSearch parameter means that for unimproved cuckoo during usual update process of cuckoo search, randomly two eggs are selected and then in the neighborhood emerged from changing the value of these two eggs to all possible values, the egg with the best fitness is selected. For the evaluation of the performance

differences between two algorithms, the p- values of the superiority of GDPSO over HCS using Wilcoxson rank sum, based on 30 times running of two algorithms were computed. The results of this comparison for three samples, were summarized in table 5 and illustrated by box plots in figure 9.

#	Sample Name	Network size	nSize	maxGen	Q_{Avg}^{MCS}	Q_{Avg}^{GDPSO}	$H_0: GDPSO \geq HCS$ $p-value:$
1.	Karate	34×34	50	50	0.4198	0.4168	0.005515
2.	Dolphins	62×62	50	50	0.5279	0.525	3.4e-06
3.	Football	115×115	50	50	0.5830	0.5689	6.4e-07

Table 5. The comparison of the hybrid cuckoo search with GDPSO

As perceived from figure 9, the superiority of GDPSO over the hybrid cuckoo search (HCS) is clearly rejected in all three samples and thus results of the proposed hybrid cuckoo search algorithm is not dominated by results of GDPSO in community detection problem. Therefore the hybrid cuckoo search has enough quality to search the best solution in comparison with the GDPSO, so that the adoption of HCS to search the best partition vector for community detection problem as well as blockmodel problem, is reasonable and tenable.

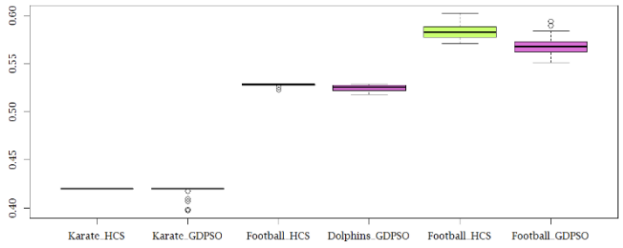

Figure 9. The boxplot of modularity index returned by HCS and GDPSO

4.3 The Effect of Parameters: maxGen, nestSize and algorithm

In all of the experiments mentioned before, the values of parameters used to run BMCS were not constant and for nestSize and maxGen several levels were considered. In addition to these parameters, whether the local search procedure is incorporated or not, must be investigated. For the study of effect of local search procedure, for all experiments reported in subsection 4-1, the results of running simple cuckoo search, denoted by CS, along with the results of the hybrid cuckoo search, denoted by HCS, were considered as a variable called algorithm. Therefor three factor of maxGen, nestSize and algorithm are studied for finding the important parameter set of BMCS. In order to study the effects of these parameters, for each sample of 4-1, interaction plot of factors was drawn and then three factor robust ANOVA test of Wilcox was performed separately.

According to interaction plot of figure 10 for Sampson-Doreian drawn for inconsistency index, it seems that the larger values of maxGen and nestSize, produces the lower inconsistency and in comparison with CS, HCS prepares the lower inconsistency. Furthermore, parallel/nonparallel curve in interaction plot of nestSize:maxGen/ nestSize:algorithm and maxGen:algorithm, seems to suggest that there are interaction effect between nestSize/ maxGen and algorithm and no interaction effect between nestSize and maxGen. This suggestion are corroborated with three-way robust ANOVA on the trimmed means ([23]), computed by t3way command of "WRS2" R package version: 0.9-1 and reported in table 6.

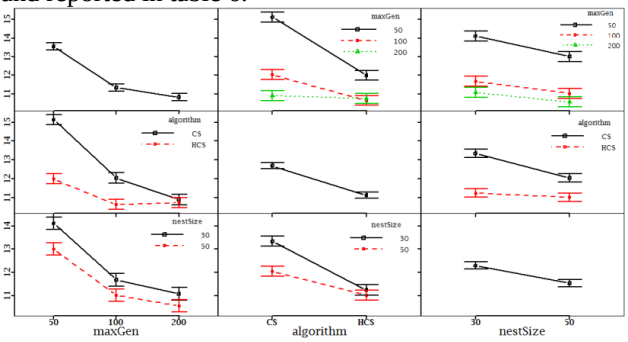

Figure 10. Interaction plot of three factor for Doreian-Sampson data in terms of Inconsistency index

The interaction plot of parameters for Kapferer's Tailor shop samples in terms of G^2 and SAE were drawn in figure 11 and 12, respectively. According to these figures, it seems that there are the main effects corresponding to maxGen and nestSize and the interaction effects between algorithm and maxGen/nestSize. This can be examined by three factor robust ANOVA test summarized in table 7.

Effect	Value	p-value
maxGen	73.150	0.0001
algorithm	33.916	0.0001
nestSize	7.210	0.01
maxGen:algorithm	29.587	0.001
maxGen:nestSize	3.147	0.23
algorithm:nestSize	6.130	0.017
maxGen:algorithm:nestSize	4.703	0.117

Table 6. The results of three factor robust ANOVA test for Inconsistency as response variable in Sampson-Doreian sample

The results of table 7, reveals relatively different behavior of parameters for G^2 and SAE. While maxGen and nestSize are significant factors for both fitness function of G^2 and SAE, the algorithm is the main effect only for SAE. This indicates that CS and HCS are totally different/indifferent in minimizing SAE/G^2 so that CS produces better/ not better solutions than HCS in decreasing SAE/G^2. The interaction of maxGen and algorithm/nestSize is clearly significant for SAE (p-value=0.047/0.001), but relatively significant for G^2 (p-value=0.116/0.126). This makes both fitness functions be better improved by HCS rather than CS in maxGen of 200. Furthermore the interaction of three factors is significant only for SAE. Even though the effect of algorithm and its interaction with the other factors is not clearly significant for G^2, it is not reasonable that the interaction of algorithm with maxGen/nestSize be considered completely insignificant.

The final sample, was studied at the two levels of 20 and 30 for nestSize, and at the four levels of 40,200, 1000, and 1500 for maxGen. The interaction plot of figure

13, proposes the clear improvement in high levels of maxGen/nestSize and relatively indifferent behavior between CS and HCS. In addition the interaction/no interaction effect between algorithm and maxGen/nestSize is perceived. The results of three factor robust ANOVA test in table 8, reports the significant main effects of maxGen, algorithm, and nestSize. In addition the interaction effect between maxGen and algorithm along with interaction effect of maxGen, algorithm and nestSize, are significant. Since maxGen and and nestSize have positive effects on matrix correlation, these significant interaction effects, make HCS outperforms CS in large maxGen of 1000 and 1500 and nestSize of 30.

In all experiments, except for one experiment for G^2, the main effects of maxGen, algorithm, and nestSize are considered significant. Among these effects the maxGen seems be more prominent; that is while nestSize and algorithm are important too, the clear significant improvement of fitness function in all samples is concurred with increasing the value of maxGen. In addition, interaction effect of maxGen with algorithm in all samples for each fitness function is significant. This interaction effect cause HCS to be superior to CS in large maxGen. In fact by increasing the maxGen, the possibility that HCS is dominated by CS is decreased and eventually the HCS dominates CS in a large maxGen. This large maxGen for Sampson-Doreian, Kapfere Tailor shop, and metal trade network equals to 50, 200, and 1000 respectively. However in small maxGen, HCS is not clear advantage over CS.

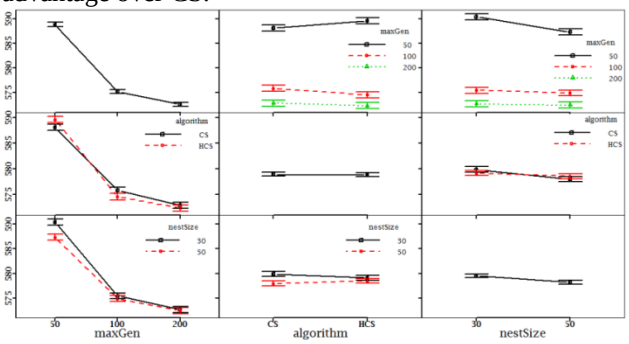

Figure 11. Interaction plot of three factor for Kapferer's Tailor shop data in terms of G^2

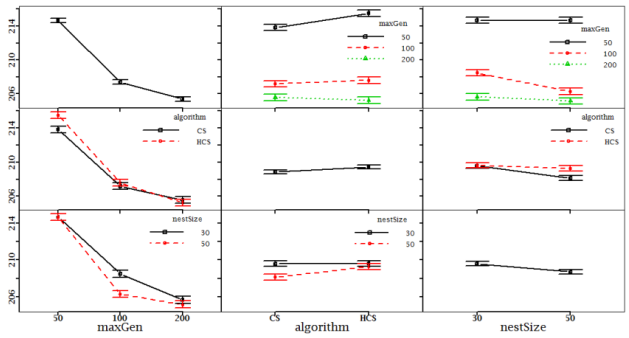

Figure 12. Interaction plot of three factor for Kapferer's Tailor shop data in terms of SAE

Effects	G^2		SAE	
	Value	p.value	Value	p.value
maxGen	579.148	0.000	525.020	0.000
algorithm	0.043	0.840	5.802	0.020
nestSize	5.026	0.031	5.377	0.025
maxGen:algorithm	4.639	0.116	6.736	0.047
maxGen:nestSize	4.444	0.126	17.070	0.001
algorithm:nestSize	0.347	0.560	1.992	0.165
maxGen:algorithm:nestSize	0.334	0.850	5.401	0.083

Table 7. The results of three factor robust ANOVA test for G^2/SAE as response variable in Kapferer Tailor shop sample

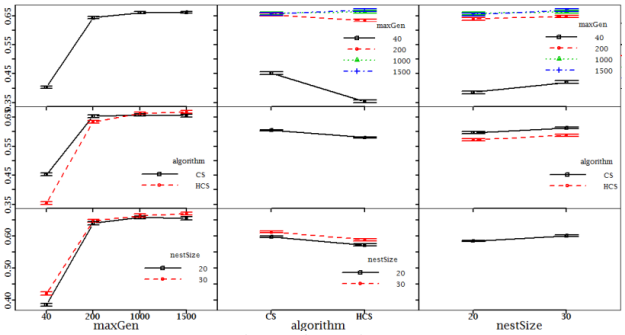

Figure 13. Interaction plot of three factor for metal trade network data in terms of Correlation

Effects	Value	p.value
maxGen	1849.138	0.0001
Algorithm	21.691	0.0001
nestSize	19.98	0.001
maxGen:algorithm	95.840	0.001
maxGen:nestSize	7.237	0.09
algorithm:nestSize	1.122	0.294
maxGen:algorithm:nestSize	10.194	0.031

Table 8. The results of three factor robust ANOVA test for matrix correlation as response variable in metal trade network

5. Conclusion

In this paper, we defined the blockmodel problem as an optimization problem and several fitness functions to measure how a given blockmodel presents a social structure agree with the original network data, were considered. Then we proposed a hybrid cuckoo search algorithm for solving blockmodel problem. This algorithm in comparison with an elitist genetic algorithm, through several samples, was not dominated and specifically for relatively large iteration, the proposed cuckoo search outperforms genetic algorithm. In addition to blockmodel problem, the performance of algorithm was studied for community detection problem and the quality of solutions produced by the algorithm clearly dominates the quality of those returned by its rival greedy discrete PSO algorithm. The effects of parameters were examined using non-parametric statistical tests and the results of these tests indicate that the large iteration plays important role for making clear improvement in fitness function for cuckoo search algorithm.

In addition significant interaction effect between iteration and incorporating the local search procedure, makes the proposed hybrid cuckoo search be advantageous over the simple cuckoo search algorithm. In fact for a large iteration the hybrid cuckoo search improves the fitness function better than the simple cuckoo search algorithm.

However the value of this large iteration was not known as a fixed and constant number and it must be found for each network data separately.

Although the role of local search was known significant for large iterations in this study, it is important to incorporate more efficient local search approach to achieve better results in relatively low execution time. This efficient hybridization of local search and cuckoo search algorithm is the main issue to be followed in future works.

References

[1] L. C. Freeman, "The development of social network analysis-With an emphasis on recent events," The sage handbook of social network analysis, vol. 21, pp. 26-39, 2011.

[2] F. Lorrain and H. C. White, "Structural equivalence of individuals in social networks," The Journal of mathematical sociology, vol. 1, pp. 49-80, 1971.

[3] P. Doreian, V. Batagelj, and A. Ferligoj, Generalized blockmodeling vol. 25: Cambridge university press, 2005.

[4] P. Doreian, V. Batagelj, and A. Ferligoj, "Generalized blockmodeling of two-mode network data," Social networks, vol. 26, pp. 29-53, 2004.

[5] P. Doreian and A. Mrvar, "Partitioning signed social networks," Social Networks, vol. 31, pp. 1-11, 2009.

[6] A. Žiberna, "Generalized blockmodeling of sparse networks," Metodoloski zvezki, vol. 10, p. 99, 2013.

[7] A. Žiberna, "Blockmodeling of multilevel networks," Social Networks, vol. 39, pp. 46-61, 2014.

[8] A. Žiberna, "Generalized blockmodeling of valued networks," Social networks, vol. 29, pp. 105-126, 2007.

[9] T. James, E. Brown, and C. T. Ragsdale, "Grouping genetic algorithm for the blockmodel problem," IEEE Transactions on Evolutionary Computation, vol. 14, pp. 103-111, 2010.

[10] O. C. Herfindahl, "Concentration in the steel industry," Columbia University., 1950.

[11] A. O. Hirschman, "The paternity of an index," The American Economic Review, vol. 54, pp. 761-762, 1964.

[12] M. Brusco and D. Steinley, "A tabu-search heuristic for deterministic two-mode blockmodeling of binary network matrices," Psychometrika, vol. 76, pp. 612-633, 2011.

[13] M. Brusco, P. Doreian, P. Lloyd, and D. Steinley, "A variable neighborhood search method for a two-mode blockmodeling problem in social network analysis," Network Science, vol. 1, pp. 191-212, 2013.

[14] Q. Cai, M. Gong, L. Ma, S. Ruan, F. Yuan, and L. Jiao, "Greedy discrete particle swarm optimization for large-scale social network clustering," Information Sciences, vol. 316, pp. 503-516, 2015.

[15] M. Girvan and M. E. Newman, "Community structure in social and biological networks," Proceedings of the national academy of sciences, vol. 99, pp. 7821-7826, 2002.

[16] I. Fister, D. Strnad, X.-S. Yang, and I. Fister Jr, "Adaptation and hybridization in nature-inspired algorithms," in Adaptation and Hybridization in Computational Intelligence, ed: Springer, 2015, pp. 3-50.

[17] X.-S. Yang and S. Deb, "Cuckoo search via Lévy flights," in Nature & Biologically Inspired Computing, 2009. NaBIC 2009. World Congress on, 2009, pp. 210-214.

[18] S. Wasserman and K. Faust, Social network analysis: Methods and applications vol. 8: Cambridge university press, 1994.

[19] X.-S. Yang, Nature-inspired metaheuristic algorithms: Luniver press, 2010.

[20] K. Nowicki and T. A. B. Snijders, "Estimation and prediction for stochastic blockstructures," Journal of the American Statistical Association, vol. 96, pp. 1077-1087, 2001.

[21] W. de Nooy, A. Mrvar, and V. Batagelj, Exploratory Social Network Analysis with Pajek vol. 27: Cambridge University Press, 2005.

[22] S. Sampson, "Crisis in a cloister, unpublished Ph. D," Dissertation, Dept. of Sociology, Cornell University, USA, 1969.

[23] R. R. Wilcox, Introduction to robust estimation and hypothesis testing: Academic Press, 2011.

Saeed Nasehimoghaddam graduated at BSc and MSc levels from faculty of industrial engineering, in Iran University of Science and Technology (IUST) respectively in 2005 and 2010. His focus during graduate studies was on socio economic systems engineering. After graduation from IUST at MSc level he followed his scientific interest in the University of Zanjan as a lecturer at engineering faculty and taught some relevant courses: such as Layout Planning, Engineering Economy, Engineering Statistics, Social Network Analysis, Project Planning and Control. His main research area is related to Data Mining and Social Network Analysis, and Computational Intelligence.

Mehdi Ghazanfari He received the BSc degree in industrial engineering from Iran University of Science and Technology (IUST), Iran, in 1986, and the MSc degree in system engineering from the Amirkabir University of Technology (AUT) Tehran, Iran, in 1989 and the PhD degree in industrial engineering from the University of New South Wales (UNSW), Sydney, Australia in 1994, respectively. he was an Assistant Professor, became an Associate Professor in 2000, and a Professor in 2003 and so far he has held lecturing position at the faculty of industrial engineering of IUST

Babak Teimourpour *O*btained his MSc degree in Socio-Economic Systems Engineering from Institute for Research on Planning and Development, Tehran, and he received his PhD in Industrial Engineering from Department of Industrial Engineering, Tarbiat Modares University (TMU), Tehran. He teaches PhD and MS level courses. His teaching interests include 'Data Mining' and 'Social Network Analysis'.

Coreference Resolution Using Verbs Knowledge

Hasan Zafari *
Department of Information and Communication Technology (ICT), Malek-Ashtar University of Technology, Tehran, Iran
hasan_zafari@yahoo.com
Maryam Hourali
Department of Information and Communication Technology (ICT), Malek-Ashtar University of Technology, Tehran, Iran
mhourali@mut.ac.ir
Heshaam Faili
School of Computer and Electrical Engineering, College of Engineering, University of Tehran, Tehran, Iran
hfaili@ut.ac.ir

Received: 11/Feb/2015 Revised: 07/Jan/2017 Accepted: 07/Mar/2017

Abstract

Coreference resolution is the problem of clustering mentions in a text that refer to the same entities, and is a crucial and difficult step in every natural language processing task. Despite the efforts that have been made to solve this problem during the past, its performance still does not meet today's application requirements. Given the importance of the verbs in sentences, in this work, we tried to incorporate three types of their information on coreference resolution problem, namely, selectional restriction of verbs on their arguments, semantic relation between verb pairs, and the truth that arguments of a verb cannot be coreferent of each other. As a needed resource for supporting our model, we generate a repository of semantic relations between verb pairs automatically using Distributional Memory (DM), a state-of-the-art framework for distributional semantics. This resource consists of pairs of verbs associated with their probable arguments, their role mapping, and significance scores based on our measures. Our proposed model for coreference resolution encodes verb's knowledge with Markov logic network rules on top of the deterministic Stanford coreference resolution system. Experiment results show that this semantic layer can improve the recall of the Stanford system while preserves its precision and improves it slightly.

Keywords: Coreference resolution, anaphora resolution, semantically related verbs, text inference, NLP

1. Introduction

Coreference resolution (CR) is determining mentions in the text which denote the same entity. By mention, we mean all pronouns, named entities and noun phrases that can refer to an entity. For example, there are many mentions in the following text snippet from which more important ones are marked with brackets.

> [Mexican football]$_{m1}$ got [a boost]$_{m2}$ in [September]$_{m3}$ when [former Brazil and Barcelona star]$_{m4}$ [Ronaldinho]$_{m5}$, joined [modest local club [Queretaro]$_{m6}$]$_{m7}$. [Carlos Trevino]$_{m8}$, [a former official of the [Queretaro state government]$_{m9}$]$_{m10}$, launched [an attack]$_{m11}$ on [Ronaldinho]$_{m12}$ before [the Brazilian]$_{m13}$ had played [a single game]$_{m14}$.

Two coreferent chains in the above text snippet are:

{m4, m5, m12, m13}, {m8, m10}

CR is an important subtask in natural language processing systems. Although it has become one of the core research topics in past decades, the complete solutions are elusive because it needs various types of knowledge to be solved completely.

This paper explores whether CR can benefit from verb's knowledge, especially semantic relation between verbs. More specifically, if we know that two verbs are semantically related, can we conclude that their arguments are semantically related too, and this relatedness leads us to conclude that they are corefer. The motivation comes from the fact that current CR systems are mostly relying on rather shallow features, such as the distance between the coreferent expressions, string matching, and linguistic form. It is expected that incorporating background knowledge in the form of semantically motivated features, along with an inference model incorporating it can improve the results.

In this paper, we focus on verb's knowledge and try to leverage it in CR. Verbs are one of the most important constituents in a text, which convey the main parts of sentence meaning and give a lot of information about it to the reader. Human can understand the meaning of sentence easily, using verb frame and prior knowledge about it. In other words, when a human reads a sentence, the first step in understanding the meaning is finding its verb, then using the information provided by the verb, and matching them with her previous experiences, the probable arguments and consequent events can be guessed.

Recently, researchers tried to use verb knowledge in CR and related subjects [1] [2] [3], [4] but it seems this line of research has more potentials and needs more attention.

In general, verbs provide three pieces of information that could be used in CR. The first piece is concerned with selectional restriction, which helps us to guess argument's semantic type. In other words, each verb sense has some predefined frames, and each frame slot

* Corresponding Author

could be filled by some limited entity types. For example, the verb overlook has two main senses, restricting subject and object to be a place (e.g. "The villa overlooks the town") or subject to be a person and object an abstract (e.g. "Nobody could overlook the fact"). The second piece has to do with the relationship between verbs in a text. That is, the verbs in a coherent text are related to each other semantically, creating a network of related arguments. These relationships could be used to detect coreferent mentions. For example, it may be useful to know that if someone joins a team, he may play for the team. This knowledge could be used to corefer [Ronaldinho]m5 to [the Brazilian]m13 in the above text snippet.

The third piece of information that we utilized in our model is the truth that arguments of a verb cannot be coreferent of each other. For example, in the sentence Carlos attacked he, we should have Carlos ≠ he.

The rest of the paper is organized as follows. We review related work in section 2, and propose our approach in section 3, including semantically related verbs acquisition, Predicate-Argument Structure and the model to applying this information to CR. Finally section 4 reports experiment results.

2. Related Work

Due to the importance of leveraging knowledge in natural language processing, many works have been developed to use them in CR.

Like us [5] extended the Stanford deterministic coreference system by linking mentions to Wikipedia. This process improved mention-detection and enabled new semantic attributes to be incorporated from Freebase. They tried to solve the named entity linking and coreference resolution, jointly.

In [6] YAGO is used to extract type relations for all mentions. These methods incorporated knowledge about all possible meanings of a mention. If a mention has multiple meanings, extraneous information might be associated with it.

Using named-entity linking in coreference resolution [7] extracted attributes from Wikipedia categories and used them as features in a mention-pair model. They reported 2 point improvements in B3 metric F1 points on non-transcript portion of the ACE 2004 dataset over their baseline system [8].

Caseframe network is proposed in [1] which is a kind of verbs knowledge for CR. A caseframe encodes two types of verb knowledge, including semantic category of verb's arguments and relationships between events. They extracted related verb's knowledge using easy to detect coreferent mentions. This approach requires a huge data to overcome the problem of extracting related verbs without sparsity. Our work, on the other hand, circumvents this problem by a novel idea (section 4).

In [3], [4] the authors tried to extract chains of events sharing a common participant. Again, because finding two verbs having coreferent arguments leads to likely sparse data of related verbs, their repository of related verb should be sparse relative to of our method. In order to estimate strength of pairwise relation, they used a distributional score based on how often two events share grammatical arguments, using pointwise mutual information (PMI). They predicted the next likely event involving the protagonist. They used narrative cloze to evaluate event relatedness, and an order coherence task to evaluate narrative order and reported improvement in both tasks.

As a powerful inference method MLN has been employed as a common inference paradigm in many recent works. MLN can represent a probabilistic distribution over all possible configurations of the relations in an application, which is the case in NLP applications including CR. This key advantage of Markov logic causes its widespread use in CR.

In [9] the author encoded some basic knowledge about CR like appositive, mentions surface overlap, distance and so on in MLN rules and used Alchemy Toolkit for training and testing with Markov logic networks.

In [10] MLN is used in a pairwise coreference resolution model. They stated that their system gives a better performance than all the learning-based systems from the CoNLL-2011 shared task, and shows competitive performance compared with the best system from CoNLL-2011, which employs a rule-based method, on the same dataset.

Proposing a joint entity mention model for CR using MLN [11] used an anaphoricity classifier to discriminatively cluster mention with discourse entities. They reported a performance of 63.56% (gold mentions) on the official CoNLL 2012 data set.

A joint unsupervised approach using Markov logic is proposed in [12]. They offered a restricted set of entity level features. Clustering of mentions is driven by head features, and few semantic type and morphological features are used to assign further mentions to these clusters.

Recently [13] proposed a joint model, which despite other coreference models considers the mention head and boundary detection and coreference resolution jointly. Their main contribution is improving mention head and mention boundary detection, through which they improved end-to-end coreference decision. The only similarity between our method and this work is using head word of the mentions in both of the methods. We used head words of the mentions to determine their semantic category, while they proposed an ILP based method to determine head words more exactly that what is proposed by parsers and (without generalizing it) incorporating its knowledge in coreference decision. The main difference between our method and [13] is that our method is a knowledge based method which aims at resolving coreference decision that can be solved just

using semantic knowledge of the verbs, while it tried to improve mention head and boundary detection that is useful in both coreference decision and final evaluation.

3. Proposed Approach

Our method aims at modelling CR using mention-pair approach, which uses knowledge of verbs in the form of a semantic layer on top of Stanford's deterministic coreference system [14]. This architecture is formulated as a joint inference problem using Markov Logic Networks [15]. It combines first-order logic formulas with probabilistic theory. This allows for transparent formalization of the method and flexibility of incorporating constraints and the feature set. Given the importance of the verbs in sentences, we tried to incorporate three types of their information on CR problem, namely, selectional restriction of verbs, semantic relation between verb pairs, and the truth that arguments of a verb cannot be coreferent of each other.

The main hypothesis of this paper is that the verbs which are semantically related to each other could have coreferent arguments. For example, it may be useful to know if someone has exploded, they may apologize at a later time.

Ronaldinho *had only just arrived in town when* ***Trevino*** *was exploded. Following a wave of criticism,* ***he*** *apologized to the club and player.*

Given the fact that ***explode*** and ***apologize*** are semantically related, the pronoun *he* can be resolved to *Trevino* rather Ronaldinho which is not its correct antecedent. In order to enable the system to do such inference, some types of information about verbs and their relationships should be provided, including:

- In this context the verb "*explode"* has a patient (object) of type *person* and means "*show a violent emotional reaction*".
- Considering the meaning of context of "*explode"*, it is semantically related to "*apologize".*
- The object (patient) of "*explode"* is the subject (agent) of "*apologize"*.

This relationship can be of the different types such as causality, antonym, temporal and so on. Some example sentences containing coreferent mentions that could be understood using these relations are:

CASUAL: The police **shoot** the theft in the chest. He **died** immediately.

TEMPORAL: Firstly **defrost** the meat in the worm water. Then you can **cook** it.

ANTONYM: The teen **climbed up** the tree. He **climbed down** after retrieving his kite.

In the past, some efforts have been done to construct semantically related verbs repositories. For example, [16] tried to use some patterns to extract semantically related verbs from the web. Despite the value of these efforts, due to very low coverage and lack of required information such as semantic role mapping between verbs' arguments, the source could not be used in our method. WordNet [17] includes sematic relations such as cause, troponym and antonym for some verbs but this source also has both abovementioned problems (low coverage and lack of role mapping between verbs' arguments). The low coverage of WordNet relation is because of the fact that this resource does not include semantic relations those are plausible but not guaranteed. For example, it may be valuable to know that if someone has *shot* to a person, they may *kill* him. WordNet does not include the relation (shot $\rightarrow$ kill) since the event *shot* would not always cause *kill*. In [1] the author tried to find semantically related verbs by targeting verb pairs that have easy-to-find coreferent argument. It is a useful and accurate method, but could not lead to a comprehensive enough repository.

3.1 Semantically Related Verbs

Because of low coverage of available repositories of related verbs and lacking of needed information about related verbs such as probable common arguments and role mapping of common argument, they do not meet requirement of our method. As a result, we decided to create such a repository ourselves. For this purpose, we used Distributional Memory (DM) [18], a state-of-the-art framework for distributional semantics. We called this repository semantically related verbs repository (SRVR). It contains about 1M semantically related pairs of verbs associated with their probable arguments and significant scores denoting the relation strength, along with role mapping of their common argument.

The overall steps to creating this repository are as follows. Firstly, candidate tuples are extracted from DM. We assume that a verb-noun pair can be a candidate tuple if they are connected through a preposition. Next, tuples that do not contain event pairs are deleted. That is, tuples where w1+link are phrasal verbs and tuples where w2 is non-action nominal. Then, after converting action nominals to their corresponding verbs, and aggregating verb pairs, some metrics of relations strength are introduced. Then using subject and object links in DM, common arguments of semantically related verbs are extracted, which beside common argument weight (CAW), a measure of relations strength, can help to find mapping of verb pairs thematic roles. This process is depicted in figure 1 Part A.

3.1.1 Extraction of Potential Relations

The DM tensor contains about 130M tuples automatically extracted from the corpora of about 2.83 billion tokens. In order to get initial tuples that could denote pairs of related events, we have firstly selected 24 links from 25,336 direct and inverse link types formed by syntactic dependencies and patterns. These links are composed of 22 prepositions plus coordination and its invers direction. We extracted all tuples of these 24 links from DM as initial tuples (*InitTuples*).

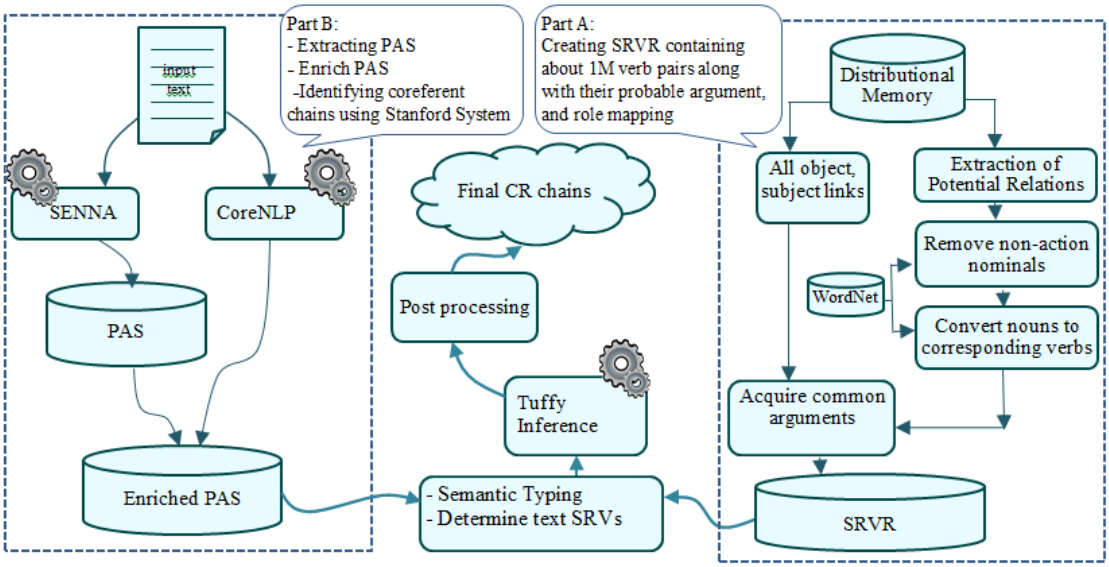

Fig 1. Proposed coreference resolution system

InitTuples totally include about 23M tuples in form of ⟨⟨w1, L, w2⟩, λ⟩. In these tuples w1 is mostly a verb (except coordination link) and w2 is always a noun. Table 1 shows these links along with their example tuples. For instance, in ⟨accuse, of, murder⟩, the preposition *of* is a sign of semantic relation between *accuse* and *murder*.

3.1.2 Removing Non -Action Nominals

Having extracted InitTuples from DM, the next step is to remove the tuples which do not contain event pairs from it. In a natural language, an event can be encoded using a verb or a noun. In all tuples ⟨⟨w1, link, w2⟩, λ⟩ extracted in previous subsection, w2 is a noun. Obviously, not all these nouns are event or action nominals. Following [19], action nominals are defined as "nouns derived from verbs (verbal nouns) with the general meaning of an action or a process". Also, according to [20], "an event is a situation that occurs or happens, and can be expressed by verbs, nominal or some other linguistic units". So, we have to identify action nominals (event nouns) from non-action ones in InitTuples.We have intended to remove two types of tuples that do not contain event pairs, including (i) Tuples where w1 together with *preposition* create phrasal verbs like *account for*, and (ii) Tuples where based on WordNet event denoting synsets w2 is not event at all, like *day*

In order to remove phrasal verbs from the InitTuples, we used a predefined list of phrasal verbs to remove such tuples from InitTuples.

For detecting and removing tuples where w2 is not an event at all, we used the WordNet hypernymy structure. For this purpose we have chosen five WordNet synsets including {event, process, state, message, symptom} so that their hyponym (children) are mostly action nominals. For example, "event" is such a synset and has many action nominals as its hyponym (children) e.g. *attack*, *discovery*, *strike*, *escape*. Beside *event*, there are other synsets that can denote an event like *process*. We have chosen these five synsets from WordNet by examining about 500 event nouns. Indeed, not all nouns under these synsets are action nominals. However, as our first goal is identifying and discarding tuples containing non-event nouns, this method works well at present.

Table 1. List of links used to extract potentially related event pairs.

Link	Example tuple	link	Example tuple
after	⟨divorce, after, marriage⟩	since	⟨revise, since, publish⟩
at	⟨win, at, match⟩	through	⟨gain, through, study⟩
because	⟨suffer, because, illness⟩	under	⟨purchase, under, agreement⟩
before	⟨defrost, before, cooking⟩	until	⟨teach, until, retirement⟩
by	⟨learn, by, experiment⟩	upon	⟨renew, upon, expiration⟩
despite	⟨fail, despite, effort⟩	via	⟨melt, via, heating⟩
during	⟨kill, during, raid⟩	while	⟨suffocate, while, feeding⟩
for	⟨marry, for, love⟩	whilst	⟨suspend, whilst, investigation⟩
from	⟨absolve, from, blame⟩	with	⟨charge, with, murder⟩
of	⟨accuse, of, murder⟩	without	⟨capture, without, fight⟩
on	⟨attract, on, offer⟩	coordination	⟨fight, coord , die⟩
over	⟨argue, over, deal⟩	coordination	⟨discount, coord-1, price⟩

3.1.3 Common Arguments

Considering the fact that semantically related verbs should have common arguments, we believe that the more two verbs are semantically related, the more words they will have as their common arguments (subject or object). For instance, *plant* and *harvest* which are semantically related verbs, have many words that can be their common arguments, but *plant* and *crash*, which are not semantically related, have almost no word as their common arguments:

Argument (plant) ∩ Argument (harvest) =
{crop, plant, tree, grape, seed, potato, grain, fruit, wheat }

Argument (plant) ∩ Argument (crash) = ∅

We call these words that can be arguments of both verbs as common arguments. Common arguments can be found in *subject* and *object* links in DM. There are more than 10M such links in DM. We define Common Argument Weight (CAW) as the relative measure of the strength between two verbs. Algorithm 1 has three outputs, including CAW, common arguments and role mapping. Common arguments can be acquired by selecting common arguments (CA) of top n tuples from *sortedTuples*, sorted tuples of `jointTuples` having the highest value of f (λ1, λ2). Role mapping maps the thematic roles of related verbs (e.g., the Agent of kill is mapped to the Patient of *arrest*). This is very useful information about semantically related verbs that can be used in many NLP applications, like Coreference Resolution.

In order to get this mapping, we have heuristically chosen the rel1 and rel2 of the top 1 tuple from *sortedTuples*. Although this is only a heuristic, but in most of the cases it works properly. The rationale behind it is that the common argument that comes with both verbs most of the times has a certain role with each verb. Hence, choosing the top one tuple of the *sortedTuples* which has the highest value of λc is a simple and acceptable solution for this problem. The verb pair (escape, arrest), for instance, has nouns like {prisoner, criminal, man} as their common arguments which are *subject* of *escape* and *object* of *arrest* most of the times. So, the mapping *escape* (sbj) = arrest (obj) is obtained for this verb pair.

Although gathered from large parsed corpora and not necessarily co-occurring in the same document, the acquired common arguments are so accurate. Beside a metric for relations strength measurement, common arguments can act as a means to disambiguate polysemous verb with respect to another verb.

Input: verb1, verb2
Outputs: sbj, obj mapping, CAW, common arguments
/*`tuples schema:⟨verb,link,arg,λ⟩` */
1: V1Links ← sbj, obj links of verb1 in DM
2: V2Links ← sbj, obj links of verb2 in DM
3: jointTuples ← empty
4: **for** t1∈ V1Links **do**
5: **for** t2∈ V2Links **do**
6: **if** t1.arg = t2.arg **then**
9: CA ← t1.arg1
10: λ1 ← t1.λ
11: λ2 ← t2.λ
12: rel1 ← t1.rel
13: rel2 ← t2.rel
14: λc ← f(λ1, λ2)
15: jointTuples.add (CA, λ1, λ2, λc, rel1, rel2)
16: **end if**
17: **end for**
18: **end for**
19: sortedTuples ← jointTuples.sortDescending(λc)
20: CAW ← $\pi_{\lambda c}(\sigma_{top1}$ sortedTuples)
21: RoleMapping ← $\pi_{rel1, rel2}(\sigma_{top1}$ sortedTuples)
22: commonArgs ← $\pi_{CA}(\sigma_{top\ n}$ sortedTuples)

Algorithm 1. Extracting CAW, Common Arguments and Role Mapping.

For instance, in pair (install, execute), common arguments are words denoting a program or script, which indicates execute means run a program, but in pair (arrest, execute) common arguments denote a prisoner or criminal, which indicates execute means put to death. Table 2 shows some examples of CAW, common arguments and role mapping.

To acquire this information for two given verbs verb1 and verb2, we have firstly chosen *subject* and *object* links (tuples) of DM for them, namely `V1Links` and `V2Links`, respectively. There are about a few thousands of such links for each verb in DM. Then we joined the tuples of `V1Links` and `V2Links` based on their common arguments to get joint tuples `jointTuples`. That is, for each tuple of `V1Links` × `V2Links` if `V1Links.arg` = `V2Links.arg`, we keep (join) them, otherwise discard them. Then, we calculate f (λ1, λ2) as a function of λ1 and λ2 of the joint tuple, where λ1 is the weight of verb1 tuple and λ2 is the weight of verb2 tuple.

Table 2. some examples of SRVR record data

Verb pair	Common arguments	Role mapping	CAW
design- print	page, poster, card, form, leaflet, book, work, logo, character, map, stamp	obj-obj	685.7961
sow- harvest	crop, seed, field, grain, plant, corn, wheat, bean, barley, onion	obj-obj	651.5708
rob-arrest	man, gang, thief, youth, pirate, bandit, criminal, robber, soldier, guy, burglar	sbj-obj	258.8246
Try-succeed	government, man, company, party, student, team, child	sbj- sbj	396.6854
own-manage	Business, company, property, site, estate, asset, land, team, farm	obj-obj	1227.6482

Lastly, by sorting the joint tuples based on f ($\lambda1$, $\lambda2$) in descending order and picking the highest one, CAW can be calculated as a function of $\lambda1$, $\lambda1$ of this tuple. See algorithm 1 for more details.

3.2 Predicate Argument Structure (PAS)

PAS is a concise notation for representing a text document, since it constitutes events within the text and their participants. Understanding events and their participants is crucial in order to semantically analyze the natural language text. The event is usually described by a verb. The participants in this event are noun phrases or pronouns, each of which has a specific role in the event. Semantic roles are representations that express the abstract role that arguments of a predicate can take in the event. These roles are diverse but in this article, we are only interested in agent and patient who are usually equivalent to the syntactic role of subject and object, respectively.

The relationship between the verb and its arguments is important to us for two reasons. First, by knowing the verb and the syntactic (or semantic) relation of its argument, we can usually determine the semantic categories of the argument. On the other hand, to properly map the common argument of two related verbs, we need to know what relation (agent or patient) each argument has with its corresponding verb. It helps us identify the coreferent argument of two related verbs. As a result, it is necessary to process the input text and extract all of its predicate-argument structures. We used an open-source SRL tool SENNA [21] to convert input text to PAS.

3.2.1 Enriching PAS

Extracting PAS from text accounts for mention extraction of the text because mentions are actually arguments in the PAS. The predicates and the semantic relationship of arguments with them are some features of our model. Nevertheless, in our CR model, we need another information of the mentions that are not provided in PAS now, such as the exact boundaries of the mentions, head noun of the noun-phrase mentions, semantic category of the mentions, and coreferent mentions that can be detected using a state of the art CR system. We intended to enrich PAS with this information.

We used Stanford CoreNLP [22] to extract our needed information from the input text. Stanford CoreNLP is an NLP package which processes the input text. It provides a set of natural language analysis, including noun phrase extractor, head finder, named entity extractor and deterministic Coreference resolution. We used Stanford deterministic CR tool [14] to determine currently known coreferent mention of the text. Actually, in this article we are trying to add a semantic layer to this layered CR system. Then, in PASs, every mention is replaced with its representative (if any). Stanford deterministic CR tool was the top-ranked system at the CoNLL-2011 shared task. However, this system cannot find all coreferent mentions, and not all of its output is correct. Yet, it is useful in our method because it could resolve easy-to-find coreferent mentions almost correctly, which is very valuable for us. At the end of this step, all named entities of the input text are extracted to be consulted with output of SENNA named entity extractions, as explained in the next section.

3.2.2 Semantic Typing

Semantic typing is to accurately determine the conceptual categories of mentions, which we call Semantic Category (SC). SC has an important role in our method. First, it is one of the mentions features in CR model that prevents linking non-coreferent mentions. If the SC of the mention is known, most of the non-coreferent antecedents can be ruled out. Secondly, it helps us select just those related verbs from SRVR that are consistent with the given verb in the text. In other words, two verbs may be related with respect to some of their meanings and not related considering their other meanings. One such example is pair (charge – disconnect) that is semantically related if their common argument is *a devise or battery* (i.e. charge means to *energize a battery*) and (charge- arrest) that are semantically related if their common argument is a *person* (i.e. charge means *blame for*).

In an ideal case, SC would be able to discriminate between different types of mentions, while not considering similar (coreferent) mentions different (overfitting). SC is a set of predefined categories that determines the general type of a mention. It is like categories in NER with the difference that it tries to solve its shortcomings. One shortcoming of NER is its over-simplified ontological model, leaving instances of other potentially informative categories unidentified. Hence, the utility of named entity information is limited. In addition, instances to be detected are mainly restricted to proper nouns, while we are mainly facing with common nouns in text.

SC can be fine or coarse-grained. In general, coarse-grain SC can be like categories that are used in NER, such as the persons, organizations, locations, etc. fine-grain SC can be the head word of the mention (noun phrase) or its hypernym (parent) in the WordNet (any synset in the WordNet). In this study, we are looking for SCs that are neither too coarse nor too fine-grained. That is, the set of categories used in semantic typing must be adequate enough to serve the tasks. Too coarse-grained SC may not be able to distinguish different mentions very well. Too fined-grained SC, on the other hand, could introduce different categories for coreferent mentions.

Table 3: selected semantic categories from WordNet

SC	Nouns denoting	SC	Nouns denoting
Animal	animals	object	natural objects (not man-made)
Artifact	man-made objects	quantity	quantities and units of measure
Attribute	attributes of people and objects	phenomenon	natural phenomena
Body	body parts	plant	plants
Cognition	cognitive processes and contents	possession	possession and transfer of possession
communication	communicative processes	process	natural processes
Event	natural events	person	people
Feeling	feelings and emotions	relation	relations between people or things
Food	foods and drinks	shape	two and three dimensional shapes
Group	groupings of people or objects	state	stable states of affairs
Location	spatial position	substance	substances
Motive	goals	time	time and temporal relations

In this paper, we adapted SC introduced in [23] which extended the named-entity recognition approach to the classification of common nouns into 26 different supersenses. Rather defining these categories manually, they adopted the "lexicographer class" labels used in WordNet, which include labels such as person, location, event, quantity, etc. Table 3 shows these categories.

3.2.3 Assigning SC to the Mentions

There are various sources to assign SC to a mention but usually none of these sources are able to determine SC solely. That's why we tried to combine them to determine SC. These resources include:

- **Mentions head word**: the head word of a noun phrase can be obtained using Stanford's dependency parser. The head words itself can be considered as a fine-grain SC. However, by generalizing it using WordNet hypernym structure, it can be converted into coarser grained SC. In *former Barcelona player*,

for instance, the head word is *player*, which yields *person* after generalizing using WordNet hypernym structure with respect to table 3 categories.

- **Pronoun**: For many pronouns, SC is known. For personal pronouns (he, she, her, you, and so on) for example, the SC is *person* and for the locative pronoun (here, there, somewhere) is *place*, and for temporal (now, then, sometimes) is *time*.
- **Coreference chains** acquired from Stanford deterministic system: Since all of the mentions in a coreference chain refer to same entity, they should have the same SC. Therefore, given a coreference chain, if the SC of one of its mention is known, we can assign it to all other mentions in that chain. For example, in a chain like {x, he}, knowing the SC of the pronoun *he* is *person*, the SC of mention x will be *person* too.
- **Selectional restriction**: The predicate selectional restriction on its argument is a good source to determine SC of the arguments. Given the predicate and semantic (or syntactic) relation of its argument, we can use DM to determine the arguments SC. For example, in *eat (obj: x)* the SC of x is likely *food*.
- **NER**: Named Entity Recognition tools map named entity to one of the predefined categories like person, location, etc. we used NER of the SENNA and Stanford CoreNLP as one of the sources in determining mentions SC.

Due to the different accuracy of any of the resources listed above, the order of applying them should be so that the more precise ones are examined before the less precise resources. This order is as follows:

1. For an unambiguous pronoun the SC is assigned according to its category.
2. For mentions x that their head word has just one sense, the SC (x) assigned using hypernym structure of WordNet (algorithm 2). Otherwise, CatsHead (x), list of all probable SCs of x along with their weights using algorithm 2 is created.
3. If the mention x is a member of a coreference chain $\{m_1, \ldots, m_n\}$, and the SC of one of the m_i is y then the SC of x will be y.
4. For the named entities that NER of SENNA and Stanford CoreNLP are unanimous for, the SC equals to the NER category. Why not being limited to only one of these sources is because these tools usually have errors (especially between *person* and *organization*).
5. For the mention x that selectional restriction introduces just one SC, calculate and assign SC. Otherwise, create CatsPred (x), list of all probable SCs of x with respect to selectional restriction of its predicate using DM.

For the mentions that SC is not determined using the above steps, combine SCs introduced by CatsHead and CatsPred. CatsHead and CatsPred include all probable SCs for a mention along with the weight of each SC. The weight of each SC in CatsHead is calculated and accumulated based on the order of senses in WordNet. That is, for each sense with sense-number i a coefficient, z (i), is used to calculate its weight. For CatsPred, the weight is calculated using the tuple weight, λ. Then by merging these two lists and choosing the most likely SC, the mention's SC will be determined.

In the merging process, the lists join together with respect to their SC, and the weights are multiplied. Then

the multiplied weights are sorted and the SC that has the highest value is selected as the mentions SC.

Input: Noun
Outputs: CatsHead
1: SCs ← all SCs in the table 3
2: **for each** sc **in** SCs **do**
3: w (sc) ← 0
4: maxSense ← number of noun Senses (Noun)
5: **for** s# =1 to maxSense **do**
6: **for each** sc **in** SC **do**
7: **if** sc ∈ hypernym (s#) **then**
8: w (sc) +=z (s#)
9: **for each** sc **in** SCs **do**
10: **if** w (sc) >0 **then**
11: append (CatHead, sc, ″/″, w (sc))
12: **return** CatHead

Algorithm 2. Extracting mention category based on WordNet hypernym structure.

For example, suppose we want to calculate SC for the mention *his first match* in the sentence, *he played his first match*. The head word of this mention is *match.* Its SC is not calculable by none of the 1 to 5 items listed above. Therefore, we have to calculate its SC by merging its CatsHead and CatsPred. Figure 2 shows the value of these lists.

Input text: He played his first match
Target mention: his first match
PAS: play (A1: his first match)
Head word: match
CatHead:
artifact/13-event/5-person/4-amount/2-cognition/2 -group/1
CatsPred:
event/7.8-artifact/1.7 -attribute/8.5 - animal/6.8- state/2.7
Results: SC (match) = *event*

Fig 2. Calculating SC by merging CatsHead and CatsPred

3.2.4 Related Verbs and Meaning in Context

SC has another usage in our method, i.e. identifying the correct sense of two verbs in the input text that deemed related with respect to the SRVR. In fact, a verb in the input text could have supposed to be related to many other verbs in that text. On the other hand, these relations may hold with respect to some senses of those verbs but not hold with respect to other senses of them. For instance, the pair *arrest-execute* is semantically related if *execute* means *put to death*, but not related to each other if *execute* means *run a program*. We used SC of the common arguments of two related verbs in the SRVR to determine if they are really related in the input text or not. Figure 3 shows a text contains two verbs, *execute* and *test*.

This pair is deemed semantically related according to SRVR, but is not related based on their meaning in the context. The common arguments of this verb pair according to SRVR are program, code, procedure, process, and function with SC of communication. On the other hand, the argument of execute in the text is prisoner with SC of person. Since person and communication are not compatible, we conclude that execute and test are not related here.

Input text:
The prisoner was executed …. We have tested all the doors' locks.
KB: execute→test
Common arguments:
program, code, procedure, process, function
SC(Common arguments) = *communication*
Results:
Execute (*person*) ≠ execute (*communication*)

Fig 3. Using Common arguments of the related verbs to prevent incorporating a pair of related verbs from SRVR that is not related considering their meaning in the context

3.3 Applying Verb Knowledge to CR

In this section, we propose our unsupervised model for CR. The model is a knowledge-based model which incorporates verb knowledge into a CR system. We incorporated three types of verb's information on CR problem. The model is based on Markov Logic Networks [24] which combines first-order logic rules with probabilistic theory. This allows encoding different types of features and constraint in CR easily and in a way that can be understood by people.

3.3.1 Markov Logic Network

Markov Logic Network (MLN) is a probabilistic extension of first-order logic, which becomes one of the most powerful tools for joint inference. MLN specifies what data (evidence) is available, what predictions to make (query), and what constraints and correlations exist (rules). The process of computing predictions given an MLN is called inference. In MLN, one can write first-order logic rules with weights. The weight of a rule specifies its confidence. This allows one to capture rules that are likely, but not certain, to be correct. This is the case for most of the constrains and rules that hold between mentions' features and their coreference status

3.3.2 Coreference Model

In this section, we explain details of the MLN based model for CR. Specifically, we express rules of our method in terms of query and evidence predicates.

The evident predicates which provide information for the rules include extracted predicate from the text, related verbs from SRVR, and semantic type of mentions. These predicates are expressed in the following schema.

```
1:  vA0(verb,mention)
2:  vA1(verb, mention)
3: *relatedA0A0(verb,verb,float wgt)
4: *relatedA0A1(verb,verb,float wgt)
5: *relatedA1A0(verb,verb,float wgt)
6: *relatedA1A1(verb,verb,float wgt)
7: *vA0A1(verb,mention,mention)
8: *Type(mention,type)
9:  coref(mention,mention)
```

The main query predicate is `coref(x,y)` which is true if x is corefer with y.

MLN rules specify the relationship between evidence features and the query predicate.

The following rule reflects the fact that if according to the evidence, two predicates of the input text are related, and the mapping between their common arguments is A0A0 (i.e. the agent of the first verbs is mapped to the agent of the second verb), then the agent argument of them could be coreferent to each other.

```
10: wgt:vA0(v1,m1),vA0(v2,m2),
relatedA0A0(v1,v2,wgt)=> coref(m1,m2)
```

There are three rules corresponding to the other three possible mappings,:

```
11: wgt:vA0(v1,m1),vA1(v2,m2),
relatedA0A1(v1,v2,wgt)=> coref(m1,m2)

12: wgt:vA1(v1,m1),vA0(v2,m2),
relatedA1A0(v1,v2,wgt)=> coref(m1,m2)

13: wgt:vA1(v1,m1),vA1(v2,m2),
relatedA1A1(v1,v2,wgt)=> coref(m1,m2)
```

The weight of these rules is equal to the value of relation strength between the verb pair in SRVR.

Another knowledge that verbs provide to us is that if two mentions have the same arguments, they should not be coreferent. This is ensured by the hard rule (which has infinite weight and must be satisfied)

```
14: vA0A1(v1,m1,m2)=>!coref(m1,m2).
```

Mentions with different SC cannot be coreferent. This is ensured by the hard rule (which has infinite weight and must be satisfied)

```
15: Type(m1,t1),Type(m2,t2),[t1<>t2]
  =>!coref(m1,m2).
```

General rules of reflexivity, symmetry, and transitivity of the model are:

```
16: coref(x,x).
17: coref(x,y)=> coref(y,x).
18: coref(x,y),coref(y,z)=>coref(x,z).
```

3.4 Implementation and Post Processing

We used a state-of-the-art MLN systems, namely Tuffy [25] in order to implement MLN rules. It is implemented in Java and used PostgreSQL as the underlying database system. Tuffy processes the evidence, program, and query files, and produces output links along with their probabilities. In order to make Tuffy to include probabilities of the output, we set the marginal inference. Then we have to merge these links to get final coreference chains.

It should be noted that the evidence that provides information for inference is not free of errors. Rather, there are errors in almost all the past steps that have been done to provide evidence. Hence, the inference results may contain mistaken output links. The post processing step aims at concatenating the output links to get coreference chains while tries to reduce (eliminate) mistaken links. For this purpose, a greedy algorithm is employed, which looks like the maximum spanning forest algorithm.

The algorithm receives weighted output links of the inference as input and produces coreference chains. To do so, a graph G (V, E) is created; where V represents all the mentions in the input text, and E determines the mention pairs that are coreferent. E is initially empty (the graph has no edge at first). The following loop examines inference output (L) one-by-one and adds them to the set E of the graph G (V, E) if they do not have conflict with the existing rules.

At the termination of the algorithm, the forest forms coreference chains of the document mentions.

While L is not empty

1. *Remove an edge with maximum weight from L*
2. *If the removed edge connects two trees which do not contains mention(s) that conflict with rules 14 and 15,*
    a. *Add it to the graph G.*
    b. *Combine two trees into a single tree.*

4. Experiments

In this section, the results of the proposed coreference system will be evaluated with respect to the baseline, i.e. Stanford's deterministic coreference system. For this purpose, two separate test data are used. The first is CoNLL 2012 coreference data. The second test set is about odd news of Yahoo News (www.yahoo.com/news/odd/). The reason for selecting odd Yahoo News is that this news is mainly about the strange happenings which contain many events. Hence the proposed method can be better evaluated on this data.

4.1 Experimental Setup

Datasets: since the aim of our approach is to resolve CR on the text that needs semantic knowledge of related verbs, we have to evaluate our method on the data that need such knowledge. As the standard test data for CR, like CoNLL 2012 data, may not include such text, we collected news wire documents that talk about news containing events. Odd news of the Yahoo site has such a property. Hence, we collected 20 news documents from this site to create second test data. Two human annotators were asked to manually annotate this data set. The human inter-annotator agreement achieved on this test set is 93%.

Baseline System: We choose two publicly available state-of-the-art end-to-end coreference systems as our baselines: *Stanford* coreference resolution system [14], winner of the shared task 2011, and *Illinois* coreference system [13]. The first which our method is implemented on top of it, is a rule based system implemented as part of Stanford CoreNLP toolkit [22]. It comprises a pipeline of "sieves" that merge coreferent mentions according to deterministic rules. Higher precision sieves are applied earlier in the pipeline according to the following order, looking at different aspects of the text, including: (1) speaker identification, (2-3) exact and relaxed string matches between mentions, (4) precise constructs, including appositives, acronyms and demonyms, (5-9) different notions of strict and relaxed head matches between mentions, and finally (10) a number of syntactic and distance cues for pronoun resolution.

Table 4: Performance of coreference resolution for all systems on the test set 1

	MUC			B^3			BLANC		
System	R	P	F1	R	P	F1	R	P	F1
Stanford	59.66	61.54	60.6	55.09	49.2	51.97	55.14	48.11	51.34
Illinois	52.33	57.25	54.68	45.33	60.52	51.83	52.00	68.42	59.09
Our system	61.25	62.08	61.66	55.73	49.03	52.16	56.29	48.08	51.86

Table 5: Performance of coreference resolution for all systems on the test set 2

	MUC			B^3			BLANC		
System	R	P	F1	R	P	F1	R	P	F1
Stanford	50.0	83.33	62.5	38.09	90.0	53.53	25.0	88.88	39.02
Illinois	42.06	65.51	51.23	34.89	69.78	46.52	27.08	81.21	40.62
Our system	65.41	81.25	72.47	45.81	82.06	58.80	31.54	90.9	46.83

Evaluation Metrics: we used widely recognized metrics MUC, B3, and BLANC.

MUC [26] Link-based metric which measures how many predicted and gold clusters need to be merged to cover the gold and predicted clusters, respectively.

B3 [27] Mention-based metric which measures the proportion of overlap between predicted and gold clusters for a given mention.

BLANC [28] Metric based on the Rand index [29] that considers both coreference and non-coreference links to address the imbalance between singleton and coreferent mentions.

It should be noted that we used system mention to evaluate our method; that is, the detection of the mention boundaries has been done using the system.

Results:

Table 4 and 5 compare the performance of our system against the baseline systems with respect to Test-set 1 and 2, respectively. As expected, the performance of the proposed system on the Test-set 2 which contains more events is more evident. The reason is that the baseline systems just uses shallow features, which are not sufficient to identify coreferent mentions in such documents. Practically, coreferent mentions in such documents has a different surface, implying different aspects of referring entity. For person entity, for example, referring expressions may refer to its name, nationality, job, role within the story (victim, criminal, passenger, etc.), and so on. Hence resolving such a different surface mentions need more semantically motivated features like what we utilized.

References

[1] D. Bean and E. Riloff, "Unsupervised Learning of Contextual Role Knowledge for Coreference Resolution," Proc. Hum. Lang. Technol. Conf. North Am. Chapter Assoc. Comput. Linguist. (HLT-NAACL 2004), pp. 297–304, 2004.

[2] H. Lee, M. Recasens, A. Chang, and M. Surdeanu, "Joint entity and event coreference resolution across documents," in Association for Computational Linguistics, 2012.

[3] N. Chambers and D. Jurafsky, "Unsupervised Learning of Narrative Schemas and their Participants," Proc. Jt. Conf. 47th Annu. Meet. ACL-IJCNLP 4th Int. Jt. Conf. Nat. Lang. Process. AFNLP, vol. 2, no. August, p. 602, 2009.

[4] N. Chambers and D. Jurafsky, "Unsupervised learning of narrative event chains," Proc. Assoc. Comput. Linguist., vol. 31, no. 14, pp. 789–797, 2008.

[5] L. Zilles and D. S. Weld, "Joint Coreference Resolution and Named-Entity Linking with Multi-pass Sieves," Emnlp, no. October, pp. 289–299, 2013.

[6] A. Rahman and V. Ng, "Coreference Resolution with World Knowledge," Acl, no. June, pp. 814–824, 2011.

[7] L. Ratinov and D. Roth, "Learning-based multi-sieve co-reference resolution with knowledge," Proc. 2012 Jt. Conf. Empir. Methods Nat. Lang. Process. Comput. Nat. Lang. Learn., no. 1, pp. 1234–1244, 2012.

[8] E. Bengtson and D. Roth, "Understanding the value of features for coreference resolution," Proc. Conf. Empir. Methods Nat. Lang. Process. - EMNLP '08, vol. 51, no. October, p. 294, 2008.
[9] S. Huang, Y. Zhang, J. Zhou, and J. Chen, "Coreference Resolution using Markov Logic Network," Science (80-.)., pp. 157–168, 2009.
[10] Y. Song, J. Jiang, W. X. Zhao, S. Li, H. Wang, and 王厚峰, "Joint learning for coreference resolution with Markov logic," Proc. 2012 Jt. Conf. Empir. Methods Nat. Lang. Process. Comput. Nat. Lang. Learn., no. July, pp. 1245–1254, 2012.
[11] T. Bögel and A. Frank, "A joint inference architecture for global coreference clustering with anaphoricity," Lect. Notes Comput. Sci. (including Subser. Lect. Notes Artif. Intell. Lect. Notes Bioinformatics), vol. 8105 LNAI, pp. 35–46, 2013.
[12] H. Poon and P. Domingos, "Joint Unsupervised Coreference Resolution with Markov logic," Proc. Conf. Empir. Methods Nat. Lang. Process., no. October, p. 650, 2008.
[13] H. Peng, K.-W. Chang, and D. Roth, "A Joint Framework for Coreference Resolution and Mention Head Detection," CoNLL, pp. 12–21, 2015.
[14] H. Lee, Y. Peirsman, A. Chang, N. Chambers, M. Surdeanu, and D. Jurafsky, "Stanford ' s Multi-Pass Sieve Coreference Resolution System at the CoNLL-2011 Shared Task," Proc. Fifteenth Conf. Comput. Nat. Lang. Learn. Shar. Task. Assoc. Comput. Linguist., pp. 28–34, 2011.
[15] M. Richardson and P. Domingos, "Markov logic networks," Mach. Learn., vol. 62, no. 1–2 SPEC. ISS., pp. 107–136, 2006.
[16] T. Chklovski and P. Pantel, "VerbOcean: Mining the Web for Fine-Grained Semantic Verb Relations.," EMNLP, no. Lin 1997, 2004.
[17] G. A. Miller, "WordNet: a lexical database for English," Commun. ACM 38.11 39-41., 1995.
[18] M. Baroni and A. Lenci, "Distributional Memory: A General Framework for Corpus-Based Semantics," Comput. Linguist., vol. 36, no. 4, pp. 673–721, 2010.
[19] B. Comrie, "The syntax of action nominals: A cross-language study," Lingua, vol. 40, no. 2–3, pp. 177–201, 1976.
[20] M. Pustejovsky, J., Hanks, P., Sauri, R., See, A., Gaizauskas, R., Setzer, A., Radev, D., Sundheim, B., Day, D., Ferro, L. and Lazo, "The timebank corpus," Corpus Linguist., vol. 40, pp. 647–656, 2003.
[21] R. Collobert, J. Weston, L. Bottou, M. Karlen, K. Kavukcuoglu, and P. Kuksa, "Natural Language Processing (almost) from Scratch," J. Mach. Learn. Res., vol. 12, pp. 2493–2537, 2011.
[22] C. D. Manning, J. Bauer, J. Finkel, S. J. Bethard, M. Surdeanu, and D. McClosky, "The Stanford CoreNLP Natural Language Processing Toolkit," Proc. 52nd Annu. Meet. Assoc. Comput. Linguist. Syst. Demonstr., pp. 55–60, 2014.
[23] M. Ciaramita and Y. Altun, "Broad-coverage sense disambiguation and information extraction with a supersense sequence tagger," Proc. 2006 Conf. Empir. Methods Nat. Lang. Process. - EMNLP '06, no. July, pp. 594–602, 2006.
[24] M. Richardson and P. Domingos, "Markov logic networks," Mach. Learn., vol. 62, no. 1–2, pp. 107–136, 2006.
[25] F. Niu, C. Ré, A. Doan, and J. Shavlik, "Tuffy: Scaling up Statistical Inference in Markov Logic Networks using an RDBMS," Proc. VLDB Endow., vol. 4, no. 6, pp. 373–384, 2011.
[26] M. Vilain, J. Burger, J. Aberdeen, D. Connolly, and L. Hirschman, "A Model-Theoretic Coreference Scoring Scheme," Messag. Underst. Conf., no. 1, pp. 45–52, 1995.
[27] A. Bagga and B. Baldwin, "Algorithms for scoring coreference chains," in The First International Con-ference on Language Resources and Evaluation Work-shop on Linguistics Coreference, 1998, pp. 563–566.
[28] Marta Recasens and Eduard Hovy, "BLANC: Implementing the Rand index for coreference evaluation," Nat. Lang. Eng., vol. 17(4), pp. 485–510, 2011.
[29] W. M. Rand, "Objective criteria for the evaluation of clustering methods," J. Am. Stat. Assoc., vol. 66(336), pp. 846–850, 1971.

Hasan Zafari received his B.Sc. degree in Software Engineering from University of Kerman, Iran. He received his M.Sc. degree in Software Engineering from Islamic Azad university of Arak, Iran. He is currently a Ph.D. student at the Department of Information and Communication Technology (ICT), Malek-Ashtar University of Technology, Tehran, Iran.

Maryam Hourali is an Assistant Professor at Malek-Ashtar University of Technology, Iran. She received her B.Sc. in Applied Mathematics in university of Tehran, Iran, and her M.Sc. in Information Technology from the Iran University of Science and Technology (IUST), and her Ph.D. in Industrial Engineering-Information Technology from Tarbiat -Modares University, Iran.

Heshaam Faili is an Associate Professor at School of Electrical and Computer Engineering, university of Tehran, Iran. He received his B.Sc. and M.Sc. in Software Engineering, from Sharif University of Technology and his Ph.D. in Artificial Intelligence, from Sharif University of Technology.

Mitosis Detection in Breast Cancer Histological Images Based On Texture Features Using AdaBoost

Sooshiant Zakariapour
Department of Computer Engineering, Babol Noshirvan University of Technology, Babol, Iran
sooshiant@stu.nit.ac.ir
Hamid Jazayeriy*
Department of Computer Engineering, Babol Noshirvan University of Technology, Babol, Iran
jhamid@nit.ac.ir
Mehdi Ezoji
Department of Electrical Engineering, Babol Noshirvan University of Technology, Babol, Iran
m.ezoji@nit.ac.ir

Received: 03/Jan/2017 Revised: 29/May/2017 Accepted: 03/Jun/2017

Abstract

Counting mitotic figures present in tissue samples from a patient with cancer, plays a crucial role in assessing the patient's survival chances. In clinical practice, mitotic cells are counted manually by pathologists in order to grade the proliferative activity of breast tumors. However, detecting mitoses under a microscope is a labourious, time-consuming task which can benefit from computer aided diagnosis. In this research we aim to detect mitotic cells present in breast cancer tissue, using only texture and pattern features. To classify cells into mitotic and non-mitotic classes, we use an AdaBoost classifier, an ensemble learning method which uses other (weak) classifiers to construct a strong classifier. 11 different classifiers were used separately as base learners, and their classification performance was recorded. The proposed ensemble classifier is tested on the standard MITOS-ATYPIA-14 dataset, where a 64×64 pixel window around each cells center was extracted to be used as training data. It was observed that an AdaBoost that used Logistic Regression as its base learner achieved a F1 Score of 0.85 using only texture features as input which shows a significant performance improvement over status quo. It is also observed that "Decision Trees" provides the best recall among base classifiers and "Random Forest" has the best Precision.

Keywords Breast cancer grading; Mitosis detection; Computer Aided Diagnosis; Texture Features; Ensemble learning; Pathology.

1. Introduction

Detecting dividing (ie. mitotic) cells is a challenging problem in the field of digital pathology. Mitotic cells are defined as cells that have basophilic cytoplasm and hairy extensions, while having no visible nucleus membrane. In clinical practice, mitotic cells are counted manually by pathologists in order to grade the proliferative activity of breast tumors[1]. However, this task is laborious, subjective and time-consuming. Using computer-based methods for recognizing and counting mitoses can reduce error rates and inter-observer variation. The challenging problem in classifing cells into mitotic and non-mitotic classes is that mitosis is a complex biological process in witch the cell undergoes various morphological transformations, apearing in a large variety of shape configurations[2]. Variation in appearances may also be caused by other factors like aberrant chromosomal makeup of tumors and imperfections of the tissue preparation process[3]. Figure 1 shows a mitotic cell and some non-mitotic cells as an example.

The World Health Oraganization has recommended the Nottingham Grading System for grading breast cancer (i.e malignant, benign or non-cancerous). This system relies on three factors to grade cancer stages: tubule formation, nuclear atypia and the number of mitotic cells present in the tissue, the latter being of significant importance. A simple way to detect or even grade breast cancer is by counting mitotic cells present in a pre-defined area of tissue samples; if the count of mitotic cells is greater than a specific number, it is possible that the tissue is cancerous . In this research we aim to detect mitotic cells present in breast tissue using their texture features. When classifiying cells into mitotic and non-mitotic cells it is important to select features that are available in mitotic cells throughout the mitotic transformation process. Our results show that, being a rotation-invariant feature, histogram and texture features are appropriate for classifying cells using a supervised learning method.

We use Adaptive Boosting[4] for classification of mitotic cells. Adaptive Boosting, also known as AdaBoost, is an algorithm for constructing a "strong" classifier as a linear combination of "weak" classifiers. Weak classifiers can be thought of as features that are weakly related to classes. AdaBoost tries to create a highly accurate prediction rule by combining many rules that are relatively weak or inaccurate.

There are many types of immunohistochemistry stains used forstaining tissues. Our proposed method only works

* Corresponding Author

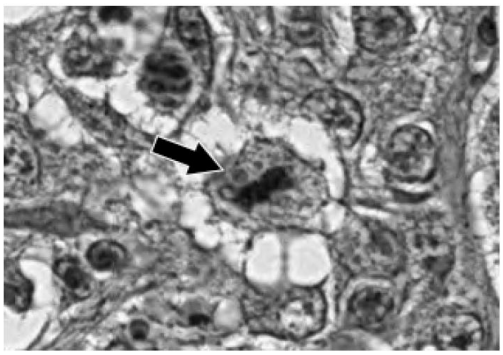

(a) Mitotic cell

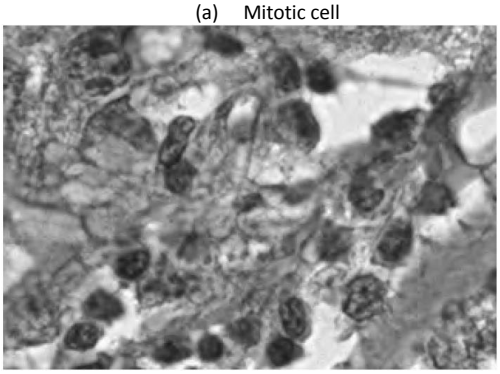

(b) Non-Mitotic cell

Fig. 1 Examples of mitotic and non-mitotic cells. In Fig. 1(a) the mitotic cell is located in the center of the image, surrounded by non-mitotic cells.

on biopsy images stained with H&E[1]. The input images should have a dimension of 1539×1376 pixels. Currently our mitosis detection method is limited to detecting mitotic cells in 3-channel RGB color images.

This paper also tries to address the problem of classifying highly-imbalanced data of mitotic and non mitotic cells using adaboost. Various weak learners can be used as base estimators in an AdaBoost classifier. We show that it is possible to classify highly imbalanced data of mitotic cells using AdaBoost with Logistic Regression as base estimator. The literature on mitosis detection in biopsy images is briefly reviewed in Section II. In Section III, the selected features used for classification are briefly discussed. In section IV, our results are presented. Our AdaBoost classifer achieves an F1 measure of 0.85, showing improvement over competing methods. Our results are compared with other detection methods in the last section.

2. Related Work

In histography of breast cancer, a paraffinized section of breast tissue is scanned under a microscope to detect the dividing cells. Mitoses are dark cells that have no visible nuclear membrane, and usually appear to have hairy extensions. To detect and count these cells, there are two main approaches. The first approach is to to detect mitotic cells straightly from the tissue image, usually using neural networks[5-8]. The second approach is segment all the cells that are found in the tissue image, and then classify these cells into mitotic and non-mitotic classes[3,9-13].

The first approach is somewhat straight-forward: pixel values are fed into the neural network; the neural network decides if the image belongs to a mitotic cell or not. Neural networks has been used in a number of studies as a means for achieving high detection performance. For example in [6], the authors used Deep Neural Networks to detect mitotic cells in a single step from the input image. Their performance on the standard AMIDA13 dataset was an F1 score of 0.61, the highest score in the 2013 contest of mitosis detection. Similarly, in [5], Wang et al. used a cascade of handcrafted features alongside convolutional neural network features in order to detect mitotic cells faster than the previously mentioned research. The reported training time for this method was 4 days, with yielded an F1 score of 0.734 on a dataset of 35 images. Both of these methods, however, suffer from high computational overhead and very long training/detection times.

The second approach requires several steps to be performed on the input image beore classifying cells, starting with separating cells from the background tissue, or cell segmentation. Before segmenting cells, it is common practice to pre-process the input images. Improper lighting and non-standard staining usually results in blurred images containing artifacts[2]. Gaussian filter has been used for reducing noise[14] and minimizing the effect of variations in tissue staining[15]. ROI[2] selection is sometimes performed on input images to remove unnecessary processing on input data[16]. Histogram equalization has been used to normalize color distribution to that of a chosen image[17]. Intensity stretching after converting color images to grayscale was done in [18].

The method proposed in [8] employs a morphological double threshold operation to segment candidate cells. It then uses rotation-invariant features such as color, binary shape-based, Laplacian and morphological features. For classification, the authors used a cascade ensemble of AdaBoost classifiers and a single AdaBoost classifier. Results favor cascaded ensemble of AdaBoost classifiers with F1 measure of 58% vs 39% for single AdaBoost classifier. Also, the authors concluded that a granular structure may be a strong evidence for mitosis appearance. In [3], the authors extracted histogram features from cells and used random forests with weighted voting to classify the candidates and reported an F1-score of 0.72. To minimize over-segmentation, the authors developed a method that maximizes gray-level scale-space, blurring images while conserving edges. Histogram and intensity features were selected as rotation-invariant features which are necessary for the problem of mitosis detection. Weighted voting discourages trees with poor classification performance during training.

[1] Hematoxylin and Eosin, fluorescent acidic compounds widely used for staining tissues

[2] Region of Interest

Fig 2. Our proposed method for classifying cells into mitotic and non-mitotic classes

Support Vector Machines has been used in order to detect mitotic cells based on objective and pixel-wise textural features in [12]. Regions of interest were selected using maximum likelihood classification and object-wise local binary pattern features were extracted from the input cells afterwards. The input cells were segmented using morphological operations. The result was a F1 score of 0.71. In another research, SVM was used to classify mitotic cells using a set of 1050 features extracted from grayscale input images[18].

Steps of our proposed method performed on a sample tissue image. The original image is shown in figure (a). In figure (b), pre-processing is performed on previous image. Following this, the blue-ratio image is calculated from the previous step; the image is blurred, then a morphological openning action is performed on the image, removing smaller blobs (figure (c)). The center point of each blob is then taken as the seed point (figure (d)), and a 64×64 window over each center point is extracted, which is shown in figure (e). The extracted cells are then fed to the classifier, classifying each cell as mitotic or non-mitotic, shown in figure (f).

Methods that rely on separating cells before training their classifier usually suffer from failures in their segmentation step. As performing morphological operations on histology images to separate cells often results in false cell boundaries and cells that are not segmented correctly, features extracted from them are not reliable. Thus, we do not segment cells from the background tissue. When segmenting cells, we select a 64×64 pixels window centering the cell, which holds the cell and the background image intact. Moreover, our AdaBoost classfier which uses Logistic Regression as its base estimator, does not need to assign weights to input data, to compensate for class imbalance between mitotic and non-mitotic cells. In the next section our proposed method is presented.

3. Methods

In this study, we use a fully-texture-based strategy for detecting mitoses in breast histopathology images stained with H&E, aiming to improve Precision and Recall of mitosis detection at the same time. Our emphasis is on extracting texture features as rotation-invariant features, while using a simple form of AdaBoost classifier that can classify unbalanced data. In the problem of detecting mitoses in histopathology images, class distribution for mitotic and non-mitotic cells is highly unbalanced, as there are usually very few mitoses against thousands of non-mitotic cells present in a sample tissue.

Mitotic cells usually appear as dark cells with hairy extentions and a granular texture in biopsy images. These cells do not have a specific orientation in the tissue when the cross section of breast tissue is being imaged. Thus, our classification method should be based on rotation invariant features which tend to remain almost unchanged throughout cell division phases. The pipeline diagram of our proposed method is shown in Fig. 2.

3.1 Pre-Processing

The slides from different patients's tissue samples differ in staining conditions and tissue appearance. Non-standard staining leads to unwanted artifacts in the images. Moreover, each batch of slides appears with a different lighting and contrast when scanned under a microscope[2], sometimes leading to noisy, blurred images. Adaptive Histogram Equalization[19] is employed to imporve contrast of the input images. Adaptive histogram equalization is a contrast enhancement method that works by applying to each pixel, the histogram equalization mapping regarding the pixels in a region around it.

Afterwards, the blue ratio image is calculated from each input image. Hematoxylin, which is a dark blue-purple substance, has more concenteration in cell nuclei. Eosin, on the other hand, stains proteins with a pink color. In a stained tissue sample, sometimes the tissue is not stained homogenously, so using blue channel The contrast between mitotic cells and background tissue is enhanced in the blue ratio image. Blue ratio image is defined in equation 1:

$$\text{BRatio} = \frac{B}{1+R+G} \times \frac{256}{1+R+G+B} \qquad (1)$$

where R, G and B are values from Red, Blue and Green channels, for each pixel of the image. This transformation converts an RGB image to a single channel image. Fig. 3(b) shows the effect of pre-processing on a sample image.

3.2 Segmentation

Adaptive thresholding[20] is used for cell segmentation. Biopsy images from batches of biopsy samples from different patients can have a wide range of luminance and appear with variable color intensities. It is not feasible to find a single threshold value to separate (darker) cells from

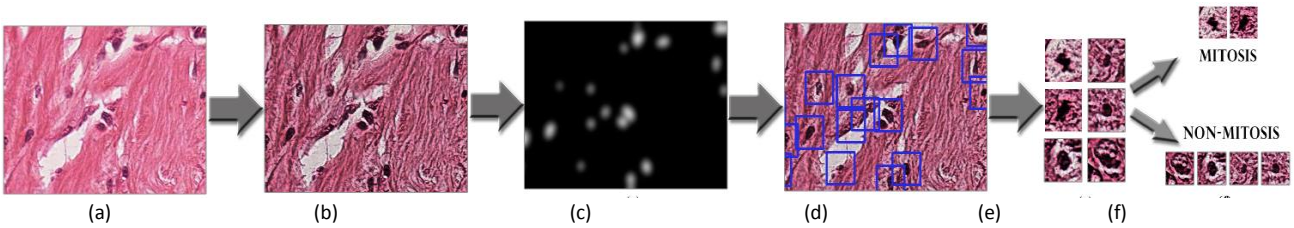

Fig 3. Steps of our proposed method performed on a sample tissue image. The original image is shown in figure (a). In figure (b), pre-processing is performed on previous image. Following this, the blue-ratio image is calculated from the previous step; the image is blurred, then a morphological openning action is performed on the image, removing smaller blobs (figure (c)). The center point of each blob is then taken as the seed point (figure (d)), and a 64×64 window over each center point is extracted, which is shown in figure (e). The extracted cells are then fed to the classifier, classifying each cell as mitotic or non-mitotic, shown in figure (f).

the rest of the tissue. Adoptive thresholding with a block size of 100 pixels and a threshold value of local neighbourhood's mean value was used. The resulting image is noisy, so we perform a morphological openning action on it, removing all blobs smaller than a disk of radius 4 pixels. Seed points located in the center of weight of each cell was then extracted from the resulting binary image. To choose a seed point for each cell, we applied a Gaussian filter so that a dark to bright gradient forms in each blob. Afterwards, center points were detected using regional maximum detection.

Lastly, a 64×64 pixel window around each cells center was extracted to be used as training data. Mitotic and non-mitotic cell nuclei closer than 8μm (approximately 32 pixels) are treated as a single instance, as required by mitosis counting protocol. Thus, if a non-mitotic cells is present in a window containing a mitotic cell, they are treated as a single mitotic cell. Ground truth mitotic cells (annotated by the dataset) were separated from non mitotic cells to be fed to the AdaBoost classifier in the supervised training step. Fig 3(d) shows this step performed on a sample image.

After separating the positive and negative classes, it was observed that there is a high imbalance in the number of two classes. There were about 800 mitotic figures present in the positive class, compared to at least 300,000 non-mitotic cells or dark objects in the negative class. For input images, 60,000 of non-mitotic cell samples where randomly selected to train our classifier. Still, the count of mitotic cells versus non-mitotic cells shows a very high imbalance between the two classes. To mitigate this problem, we rotated each positive class sample that was not located near the edges of the image in 30 degree steps, saving each sample as a new sample. Using this method, the count of positive class was increased to around 9,000, versus 60,000 for negative class. Our data still remained imbalanced, but new instances of positive class result in improved classification performance.

In breast tissue, cells do not have a specific orientation. In other words, a mitotic cell is still counted as a mitotic cell when veiwed from another angle. This idea suggests that features that are rotation-invariant should be selected Performance comparison of AdaBoost classifiers using various base-learners on our un-balanced data.

3.3 Features and Feature Extraction

Mitotic cells are often darker than other cells and appear to have hair like extensions. Mitoses do not take a specific orientation in the tissue, so their shape is captured from various angles in each instance. For features, a total of 112 features that distinguish intensity variations or texture pattern of each cell were selected. To include texture features, Local Binary Patterns, Haralick features and Entropy were selected. Local binary patterns assigns a binary number to each pixel by comparing its neighbour pixels to it[21]. Local binary patterns of input images were calculated. Histograms from the resulting images were calculated over 27 bins. Assuming most cell center points would be located in the center of the 64x64 pixel window. Moreover, another histogram from 32x32 pixel windows centered on each cell seed point was calculated. A vector of 54 float values was created from this feature.

Haralick features[22] was used as a feature that captures texture and tone. Haralick Features First transforms image pixels into a co-occurrence matrix. This matrix is built according to approximity of each pixel with a certain intensity, with pixels that have other intensities. It then calculates a number of statistical features from the matrix. A vector of 56 float values was created from this feature.

Lastly, eight samples from the positive class (mitotic cells) were selected. We selected these cells on the account that their shape represented what a normal mitosis would look like. Similarity to each of these samples was calculated for all training data using template matching method. In template matching, a template image T is slid in over a search image S while its sum of products between coefficients in pixels S(x, y) and T(x, y) is calculated for all pixels of the template image. If the two images were of equal dimentions, a higher sum simply means there two images have more smilarity. Eight float values were extracted as features using template matching with eight representative mitotic cells.

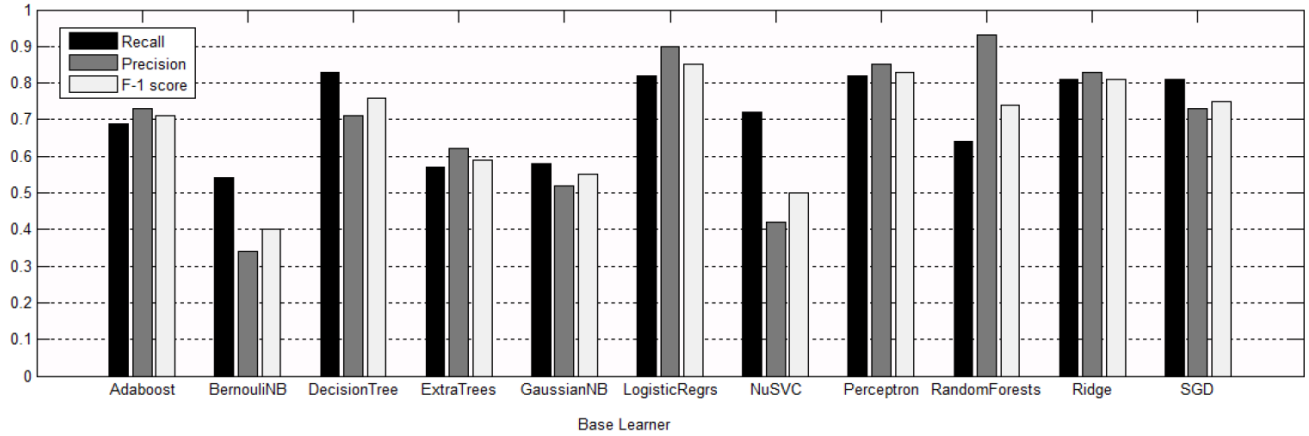

Fig 4. Performance comparison of AdaBoost classifiers using various base-learners on our un-balanced data

3.4 Classification

For classification, every learning algorithm will tend to suit we used AdaBoost[4], an ensemble learning method that combines the performance of many "weak" classifiers, to produce a powerful "commitee" out of them. For mitotic cell classification, various learning algorithms such as Random Forests[3], Cascaded AdaBoost[8] and SVM[18] have been used. AdaBoost's ability to use various weak learners as its base learner makes it a good choice for classifer. An adaboost classifier can also rapidly tweak it's base learners' parameters to fit the dataset, usually without overfitting in practice. For the case of two-class classification with AdaBoost, suppose we have a pool of $n = 2k - 1,\ k \in N$ weak classifiers, each being an expert when classifying a subset of the input data. For a given input xi each classifier kj votes for its opinion $K_j(x_i) \in \{-1,1\}$. The final class decided by this ensemble learning method for xi will be $\mathrm{Sign}(C(x_i))$ where the cost function $C(x_i)$ is defined as [23]:

$$c(x_i) = \alpha_1 K_1(x_i) + \alpha_2(x_i) + \cdots + \alpha_n K_n(x_i) \quad (2)$$

where α denotes the weights that we assign to the opinion of each classifier K. The classifiers K_i -also known as base estimators or weak learners- can be a combination of any types of classifiers. The AdaBoost classifier used in this research, uses only a single type of classifier as the base estimator in each test.

The pseudocode for AdaBoost algorithm is as follows[23]:

For a two-class classification problem, we have T input points x_i and T labels yi taking values of {-1, 1} for the two classes respectively.

Initial weights w_i are assigned to all data points x_i. Let W be the sum of weights wi of all data points and Let W_e be the sum of weights of mis-classified inputs for the considered classifier.

To choose M classifiers from a pool of classifiers, we perform M iterations:

At the m-th iteration, the classifier with the lowest rate of weighted error We is chosen and added to the list of chosen classifiers. In each iteration, AdaBoost systematically extracts a classifier from the pool of classifiers by recording how many of the multidimentional xi points it succeeds to classify. At the beginning, all of the base estimators have the same weight. After each iteration, the more difficult xi's remain to be classified correctly, so AdaBoost's algorithm assigns a larger weight to them. The process of drafting classifiers, tries to add new classifiers to the selected classifiers at each iteration, so that the overall performance improves.

for $m = 1$ *to* M

1. *Choose a classifier km from the pool of classifiers, which would minimize*
$$W_e = \sum_{y_i \neq K_m(x_i)} W_i(m)$$
2. *Set* α_m *,the weight of the classifier* k_m *to*
$$\alpha_m = \frac{1}{2} ln(\frac{1 - e_m}{e_m})$$
where $e_m = \frac{W_e}{W}$
3. *Update the weights of each xi for the next iteration. If classifier km successfully classifies* x_i*, set*
$$w_i^{m+1} = w_i^m e^{\alpha_m} = w_i^m \sqrt{\frac{1 - e_m}{e_m}}$$
otherwise set
$$w_i^{m+1} = w_i^m e^{-\alpha_m} = w_i^m \sqrt{\frac{e_m}{1 - e_m}}$$

4. Implementation and Evaluation

A series of tests were performed on 11 AdaBoost classifiers which had various classifiers as their base learner. In each test a different base estimator was used and the classification performance was measured with 5-fold cross-validation tests. The measures evaluated in our tests were Recall, Percision and F1 score. There has been a few mitos detection contests to date, namely ICPR 2012, AMIDA-13 and Mitos-Atypia-2014. Being a weighted average of Percision and Recall, F1 score was used as the main measuring criteria for comparison in

these contests; Accordingly, we too used F1 score to rank our classifiers' performance.

4.1 Dataset

The dataset used in this research is MITOS-ATYPIA-14. This dataset contains a set of breast cancer biopsy slides taken from 16 patients and prepared according to standard laboratory protocols. The images are scanned using two WSI devices: Aperio Scanscope XT and Hamamatsu Nanozoomer 2.0-HT. In this research we only use the 1,136 frames that have X40 magnification, provided from the Aperio device, and stored as 24 bit RGB bitmap images in TIFF format. The slides are stained with standard H&E dyes which stain cell nuclei with a purple-blue hue while staining underlying tissue with a pink color. The slides are from different batches, scanned under various lighting conditions and are not stained uniformly, to be as realistic as possible.

4.2 Implementation and Parameters

Our classifer was implemented in Python 2.7 on a 64-bit Intel(R) Core(TM) i7-4700MQ processor setup with 8GBytes of RAM. The AdaBoost classifier was provided by the Open-Source Scikit-learn library[24].

We use a number of classifiers as base learners for our main AdaBoost classifier. Some of these classifiers are weak classifiers (for this particular problem), others being strong component classifiers. The authors in [25] suggested that using strong component classifiers in AdaBoost is not viable and most likely will result in overfitting. However, findings in [26] show that when SVM (usually considered a strong classifier) is used as a base estimator with only a small subset of training data fed to it, it can act as a weak classifier; The resulting classification performance may even be greater than that of a SVM classifier or an AdaBoost with other component classifiers.

Classifiers that can be used in an AdaBoost are those that can assign weights to their input data, as this function is essential to AdaBoost's boosting algorithm. The classifiers that were used as base learners are:

1. AdaBoost (as base-learner)
2. Bernouli Naive Bayes
3. Decision Trees
4. Extra Trees
5. Gaussian Naive Bayes
6. Logistic Regression
7. NuSVC
8. Perceptron
9. RandomForest (as base-learner)
10. RidgeClassifier
11. SGDclassifier

The main AdaBoost classifier used 400 base estimators; i.e the main AdaBoost classifier used 400 Perceptrons when using Perceptrons as base estimators. Classifying performance of each resulting classifier was measured and compared, which is presented in TABLE 1. Of the mentioned classifiers, some are based on decision trees, some on neural networks and some others are regressors which can be used as classifiers.

4.3 Evaluation

When test cells are classified into mitotic (positive) or non-mitotic (negative) classes, we can evaluate our classifier's performance. To evaluate the problem of two-class classification, we use three evaluation criteria:

- Precision: The fraction of instances detected by the classifier to those that are relavant. Precision is defined as:
$$\mathrm{Pr} = \frac{\mathrm{TP}}{\mathrm{TP+FP}} \quad (3)$$
- Recall: The fraction of relavant instances to those that are detected by the classifier. Recall is defined as:
$$\mathrm{Re} = \frac{\mathrm{TP}}{\mathrm{TP+FN}} \quad (4)$$
- F1 Score: harmonic mean of Recall and Precision. F1 score is defined as:
$$\mathrm{F}_1 = \frac{2\,\mathrm{Pr.\,Re}}{\mathrm{Pr+Re}} \quad (5)$$

where TP (True Positives) is the count of cells correctly classified as mitotic. Respectively, FP (False Positives) is the count of cells that are wrongly classified as mitotic. True Negatives (TN) are cells correctly classified as non-mitotic. False Negatives (FN) are in fact mitotic cells, but are wrongly classified as non-mitotic.

The performance of our main AdaBoost classifiers varied based on the type of base estimators the main classifier used. It was observed that, without tweaking parameters or assigning any weights to classes, an AdaBoost classifier that used Logistic Regression as its base estimator had the best performance when classifying highly imbalanced data of mitotic cells. The mentioned classifier achieved an F1 score of 0.85, Recall of 0.82 and Precision of 0.90.

The best recall among our classifiers belongs to an AdaBoost that uses Decision trees as its base estimator, with a recall score of 0.83. The best precision belongs to an AdaBoost that uses Random forests as its base estimator, with a precision score of 0.93. We compared the peformance of our classifier with the reported F1 scores from a number of competing methods. The results are shown in Fig. 5, 6 and 7. We compared our average F1Score from 5-fold cross-validation on the input images. Using cross-validation, we ensure that the test data used for measuring performance is not known to our classifier beforehand, thus, measuring the accuracy of our perdictive model in practice.

An AdaBoost classifier using Logistic Regression as base estimator achieved the highest performance when classifying highly imbalanced data of mitotic cells, without tweaking parameters. It was also observed that tweaking parameters, i.e changing estimators count, tweaking class weights or running iteration had little influence (less than 5%) on classification performance.

Table 1: Performance measures showing Recall, Precision and F1 Score for AdaBoost classifers with various base learners

Base Learner	Recall	Precision	F1Score
AdaBoost	0.69	0.73	0.71
Bernouli Naive Bayes	0.54	0.34	0.40
Decision Trees	**0.83**	0.71	0.76
Extra Trees	0.57	0.62	0.59
Gaussian Naive Bayes	0.58	0.52	0.55
Logistic Regression	0.82	0.90	**0.85**
NuSVC	0.72	0.42	0.50
Perceptron	0.82	0.85	0.83
Random Forest	0.64	**0.93**	0.74
Ridge Classifier	0.81	0.83	0.81
SGD Classifier	0.81	0.73	0.75

5. Conclusion and Future Work

Using adaptive thresholding on blue-ratio images of H&E stained breast tissue scanned images, candidate cells were segmented from underlying background tissue. A feature vector of length 144 was then extracted from each input cell image. The extracted features were a number of texture and pattern features. Finally, the input cells were classified using AdaBoost, an ensemble learning method based on boosting. Input data formed two classes: Mitotic and Non-mitotic. There was a high imbalance between the number of the two classes in our training data. To mitigate class unbalance, rotated versions of mitotic cells were also added to the positive class. We tested a number of classifiers as base learners for our main AdaBoost classifier and compared their performance. It was observed that, an AdaBoost classifier that used Logistic Regression as base learner had the best performance when classifying our highly imbalanced set of data. Our results show a significant improvement over similar existing methods.

In future, we plan to employ neural networks to add more features to our classifier. We are also considering using neural networks as a filter applied to the input images, for the task of segmenting cells from background tissue. Classic methods such as thresholding or morphological operations tend to miss some cells when the H&E staining process is not performed uniformly on the tissue, or when lighting conditions are not the same when biopsy slides are scanned.

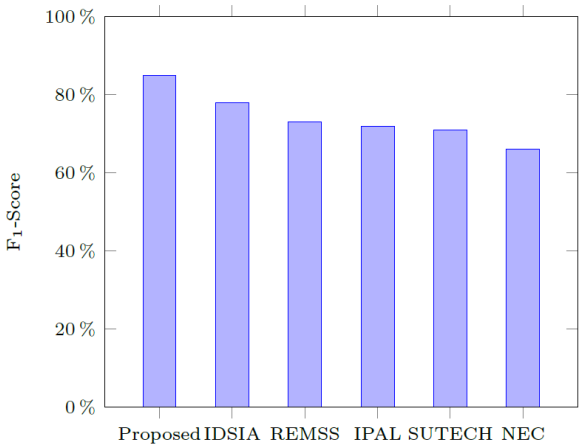

Fig 5. Performance results: F1-Score of our method compared with competing methods from MITOS-14, ICPR2012, AMIDIA-13 contests. IDSIA[6], REMSS[3], IPAL[27], SUTECH[12], NEC[7].

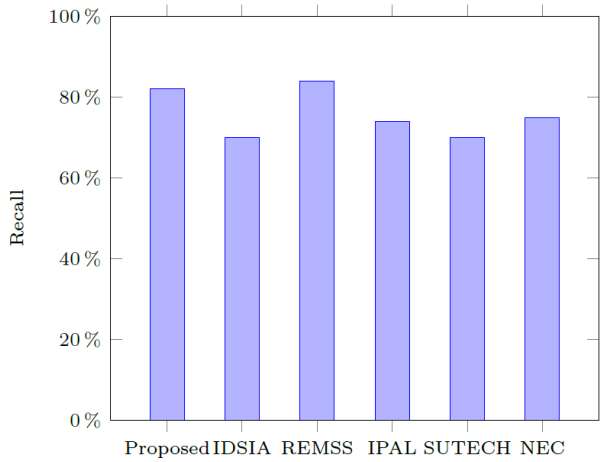

Fig 6. Performance results: Recall of our method compared with competing methods from MITOS-14, ICPR2012, AMIDIA-13 contests. IDSIA[6], REMSS[3], IPAL[27], SUTECH[12], NEC[7].

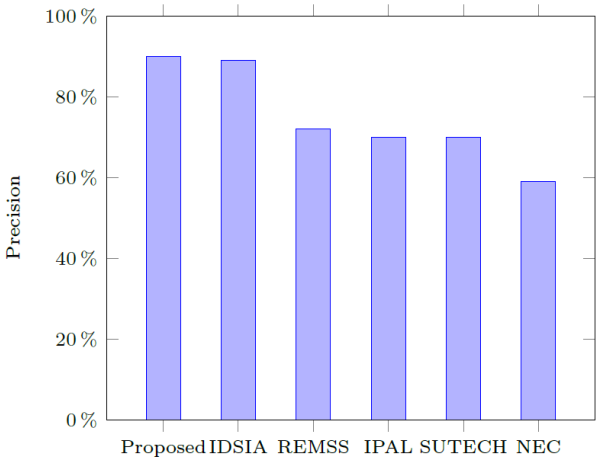

Fig 7. Performance results: Precision of our method compared with competing methods from MITOS-14, ICPR2012, AMIDIA-13 contests. IDSIA[6], REMSS[3], IPAL[27], SUTECH[12], NEC[7].

References

[1] L. Roux, D. Racoceanu, N. Loménie, M. Kulikova, H. Irshad, J. Klossa, F. Capron, C. Genestie, G. Le Naour, and M. N. Gurcan, "Mitosis detection in breast cancer histological images an icpr 2012 contest," Journal of pathology informatics, vol. 4, 2013.

[2] J. A. A. Jothi and V. M. A. Rajam, "A survey on automated cancer diagnosis from histopathology images," Artificial Intelligence Review, pp. 1–51, 2016.

[3] A. Paul and D. P. Mukherjee, "Mitosis detection for invasive breast cancer grading in histopathological images," Image Processing, IEEE Transactions on, vol. 24, no. 11, pp. 4041–4054, 2015.

[4] Y. Freund and R. E. Schapire, "A desicion-theoretic generalization of on-line learning and an application to boosting," in European conference on computational learning theory. Springer, 1995, pp. 23–37.

[5] H. Wang, A. Cruz-Roa, A. Basavanhally, H. Gilmore, N. Shih, M. Feldman, J. Tomaszewski, F. Gonzalez, and A. Madabhushi, "Cascaded ensemble of convolutional neural networks and handcrafted features for mitosis detection," in SPIE Medical Imaging. International Society for Optics and Photonics, 2014, pp. 90 410B–90 410B.

[6] D. C. Cireşan, A. Giusti, L. M. Gambardella, and J. Schmidhuber, "Mitosis detection in breast cancer histology images with deep neural networks," in Medical Image Computing and Computer-Assisted Intervention–MICCAI 2013. Springer, 2013, pp. 411–418.

[7] C. D. Malon, E. Cosatto et al., "Classification of mitotic figures with convolutional neural networks and seeded blob features," Journal of pathology informatics, vol. 4, no. 1, p. 9, 2013.

[8] F. B. Tek et al., "Mitosis detection using generic features and an ensemble of cascade adaboosts," Journal of pathology informatics, vol. 4, no. 1, p. 12, 2013.

[9] J. A. A. Jothi and V. M. A. Rajam, "Segmentation of nuclei from breast histopathology images using pso-based otsus multilevel thresholding," in Artificial Intelligence and Evolutionary Algorithms in Engineering Systems. Springer, 2015, pp. 835–843.

[10] A. Paul, A. Dey, D. P. Mukherjee, J. Sivaswamy, and V. Tourani, "Regenerative random forest with automatic feature selection to detect mitosis in histopathological breast cancer images," in Medical Image Computing and Computer-Assisted Intervention–MICCAI 2015. Springer, 2015, pp. 94–102.

[11] H. Irshad et al., "Automated mitosis detection in histopathology using morphological and multi-channel statistics features," Journal of pathology informatics, vol. 4, no. 1, p. 10, 2013.

[12] A. Tashk, M. S. Helfroush, H. Danyali, and M. Akbarzadeh, "An automatic mitosis detection method for breast cancer histopathology slide images based on objective and pixel wise textural features classification," in Information and Knowledge Technology (IKT), 2013 5th Conference on. IEEE, 2013, pp. 406–410.

[13] J. Monaco, J. Hipp, D. Lucas, S. Smith, U. Balis, and A. Madabhushi, "Image segmentation with implicit color standardization using spatially constrained expectation maximization: Detection of nuclei," in Medical Image Computing and Computer-Assisted Intervention–MICCAI 2012. Springer, 2012, pp. 365–372.

[14] K. Nandy, P. R. Gudla, R. Amundsen, K. J. Meaburn, T. Misteli, and S. J. Lockett, "Automatic segmentation and supervised learning-based selection of nuclei in cancer tissue images," Cytometry Part A, vol. 81, no. 9, pp. 743 – 754, 2012.

[15] S. Waheed, R. A. Moffitt, Q. Chaudry, A. N. Young, and M. D. Wang, "Computer aided histopathological classification of cancer subtypes," in 2007 IEEE 7th International Symposium on BioInformatics and BioEngineering. IEEE, 2007, pp. 503 – 508.

[16] M. N. Gurcan, L. E. Boucheron, A. Can, A. Madabhushi, N. M. Rajpoot, and B. Yener, "Histopathological image analysis: A review," IEEE reviews in biomedical engineering, vol. 2, pp. 147 – 171, 2009.

[17] O. Sertel, U. V. Catalyurek, H. Shimada, and M. Guican, "Computer-aided prognosis of neuroblastoma: Detection of mitosis and karyorrhexis cells in digitized histological images," in Engineering in Medicine and Biology Society, 2009. EMBC 2009. Annual International Conference of the IEEE. IEEE, 2009, pp. 1433 – 1436.

[18] A. Brook, R. El-Yaniv, E. Isler, R. Kimmel, R. Meir, and D. Peleg, "Breast cancer diagnosis from biopsy images using generic features and svms," IEEE Transactions on Information Technology in Biomedicine, 2006.

[19] S. M. Pizer, E. P. Amburn, J. D. Austin, R. Cromartie, A. Geselowitz, T. Greer, B. ter Haar Romeny, J. B. Zimmerman, and K. Zuiderveld, "Adaptive histogram equalization and its variations," Computer vision, graphics, and image processing, vol. 39, no. 3, pp. 355 – 368, 1987.

[20] F. Chan, F. Lam, and H. Zhu, "Adaptive thresholding by variational method," IEEE Transactions on Image Processing, vol. 7, no. 3, pp. 468 – 473, 1998.

[21] T. Ojala, M. Pietikainen, and T. Maenpaa, "Multiresolution gray-scale and rotation invariant texture classification with local binary patterns," IEEE Transactions on pattern analysis and machine intelligence, vol. 24, no. 7, pp. 971 – 987, 2002.

[22] R. M. Haralick, K. Shanmugam et al., "Textural features for image classification," IEEE Transactions on systems, man, and cybernetics, no. 6, pp. 610 – 621, 1973. [23] R. Rojas, "Adaboost and the super bowl of classifiers a tutorial introduction to adaptive boosting," Freie University, Berlin, Tech. Rep, 2009.

[24] F. Pedregosa, G. Varoquaux, A. Gramfort, V. Michel, B. Thirion, O. Grisel, M. Blondel, P. Prettenhofer, R.Weiss, V. Dubourg, J. Vanderplas, A. Passos, D. Cournapeau, M. Brucher, M. Perrot, and E. Duchesnay, "Scikit-learn: Machine learning in Python," Journal of Machine Learning Research, vol. 12, pp. 2825 – 2830, 2011.

[25] J. Wickramaratna, S. Holden, and B. Buxton, "Performance degradation in boosting," in International Workshop on Multiple Classifier Systems. Springer, 2001, pp. 11 – 21.

[26] X. Li, L. Wang, and E. Sung, "Adaboost with svm-based component classifiers," Engineering Applications of Artificial Intelligence, vol. 21, no. 5, pp. 785 – 795, 2008.

[27] H. Irshad et al., "Automated mitosis detection in histopathology using morphological and multi-channel statistics features," Journal of pathology informatics, vol. 4, no. 1, p. 10, 2013.

Sooshiant Zakariapour received his B.Sc degree in electrical engineering from Sharif University of Technology, Iran, in 2013. He is currently a M.Sc student of computer engineering in Babol Noshirvani University of Technology, Iran. His current research interest include medical image analysis, machine learning and application of neural networks in computer vision.

Hamid Jazayeriy received the B.Sc. and M.Sc degrees from University of Tehran and University of Isfahan, Iran, in 1996 and 2000 respectively. He received his PhD degree in software engineering in 2011 from University Putra Malaysia. He is currently an assistant professor at Babol Noshirvani University of Technology. His current research interests include distributed systems, machine learning and optimization

Mehdi Ezoji received the B.Sc. degree from Sharif University of Technology, Iran, and the M.Sc. and Ph.D. degrees from Amirkabir University of Technology, Iran. Since 2011 he has been a member of the Electrical and Computer Engineering Faculty of Babol Noshirvani University of Technology, Iran. His research interests are machine vision, pattern recognition and machine learning.

Crisis Management using Spatial Query Processing in Wireless Sensor Networks

Mohammad Shakeri*
Department of Computer, Neyshabur Branch, Islamic Azad university, Khorasan Razavi, Iran
alborz.corp@gmail.com
Seyed Majid Mazinani
Department of Electrical Engineering, Imamreza International University, Mashhad, Iran
smajidmazinani@imamreza.ac.ir

Received: 04/Jan/2017 Revised: 11/Jun/2017 Accepted: 12/Jul/2017

Abstract

Natural disasters are an inevitable part of the world that we inhabit. Human casualties and financial losses are concomitants of these natural disasters. However, by an efficient crisis management program, we can minimize their physical and social damages. The real challenge in crisis management is the inability to timely receive the information from the stricken areas. Technology has come to the aid of crisis management programs to help find an answer to the problem. One of these technologies is wireless sensor network. With recent advances in this field, sensor nodes can independently respond to the queries from the users. This has transformed the processing of the queries into one of the most useful chapters in sensor networks. Without requiring any infrastructure, the sensor network can easily be deployed in the stricken area. And with the help of spatial query processing, it can easily provide managers with the latest information. The main problem, however, is the irregular shape of the area. Since these areas require many points to present them, the transmission of the coordinates by sensor nodes necessitates an increase in the number of data packet transmissions in the sensor network. The high number of packets considerably increases energy consumption. In related previous works, to solve this problem, line simplification algorithm s, such as Ramer-Douglas-Peucker (RDP), were used. These algorithms could lessen energy consumption by reducing the number of points in the shape of the area. In this article, we present a new algorithm to simplify packet shapes which can reduce more points with more accuracy. This results in decreasing the number of transmitted packets in the network, the concomitant reduction of energy consumption, and, finally, increasing network lifetime. Our proposed method was implemented in different scenarios and could on average reduce network's energy consumption by 72.3%, while it caused only 4.5% carelessness which, when compared to previous methods, showed a far better performance.

Keywords: Wireless Sensor Network; Query Processing; Spatial Query; Crisis Management; Image Processing.

1. Introduction

The world that we inhabit constantly witnesses the occurrence of unfortunate events, affecting countless people who are desperate to receive help. However, the measures taken immediately after these events are vital and play a determining role in the amount of fatalities and financial losses. One of these measures is crisis management. Crisis management refers to all the actions taken to minimize the physical and social impacts of an event. Moreover, latest information on disaster-stricken areas is necessary for decision-making processes and all the institutions involved in crisis management procedures. In disaster-stricken areas network and communication infrastructures are destroyed while normal social and economic interactions are impossible. As mentioned earlier, a proper understanding of the stricken area is necessary. At present, GPS, maps, and satellite images are used [1]. However, creating a sensing structure with high capabilities to predict dangers can prove very effective.

This structure must be quick and easy to launch, independent, and should not require any particular infrastructure. What is more, it should be adaptable to different conditions [2]. We propose using wireless sensor network which has all these features, and can fly over the stricken region and collect the latest information and transmit it to base station [3, 4]. Wireless sensor network consists of many small devices which sense, process, and save the environmental data [5]. These devices have limited power supplies and usually battery replacement is infeasible since the sensor network may be set to watch over rough regions [6]. As a mature technology, wireless sensor network has evolved into an alternate data gathering device. Currently, these devices are able to answer to query requests from users [7]. Some sensor network models work as distributed data station such as TinyDB. They process query requests similar to SQL which is an easy way for users to receive data from the region in which the network is installed [8].

With respect to the fact that Iran is in a very seismic area, conducting research in this field and dealing with natural disasters, especially crisis management, is of great import. A real challenge in crisis management is the immediate access to information related to the stricken area. This is the motivation behind the present article: to collate information from across the stricken area during the early hours by means of wireless sensor networks. Regarding the features of sensor networks, this network

* Corresponding Author

can be installed in the area during the early hours and provide involved institutions with valuable information.

When we intend to implement wireless sensor networks in disaster-stricken areas to collect a region's data to assist crisis management, we encounter a challenge. This challenge takes the form of the topology of the affected area. If the topological shape is a regular quadrilateral (Fig.2), then, using two points, the affected area can easily be specified for the sensor nodes. However, the topology of these areas is seldom regular; therefore, these irregular areas require a lot of points to be presented (Fig.3). Transmitting the coordinates of these points to sensor nodes necessitates increasing transmitted packets in the sensor network. The high rate of sending packets increases network's energy dissipation, particularly in multiple transmissions. Benefiting from line simplification algorithms, previous researchers were able to reduce the number of necessary points for the presentation of the region while at the same time they manages to reduce sensor network's energy consumption. In this article, we try to present a new simplification algorithm which reduces the points of the topology of the area more than previous works so as to have lesser energy consumption and carelessness.

The main objective of this article is to present an efficient algorithm to simplify packet irregular shapes so that it will be able to improve its capacity to function well in usages where either the communicative costs to determine irregular shapes are high or there is a severe communicative limitation (such as the one in wireless sensor networks). Inspired by regular shapes which require two points to be presented, the proposed algorithm puts forward a shape similar to the original one by using fewer points. These points demand less memory, less time, and fewer communicative packets to carry out transmission. In almost all former researches, line simplification algorithms were used to carry out shape simplification. However, our proposed algorithm is specifically designed for packet shapes and achieved better results than former algorithms.

In sections 2 and 3, processing spatial query requests and the topology of the affected area are investigated. In section 4, the review of related works will be presented. In section 5, we will explain the proposed algorithm. The implementation and the analysis of the results are included in section 6. Finally, part 7 deals with conclusion and suggestions for further research.

2. Spatial Query Processing in WSN

The wireless sensor network is installed and we intend to use the data collected by the network. We send our request for data to the sensor network, and the network responds to it through a procedure. This procedure is referred to as processing the queries (Fig. 1).

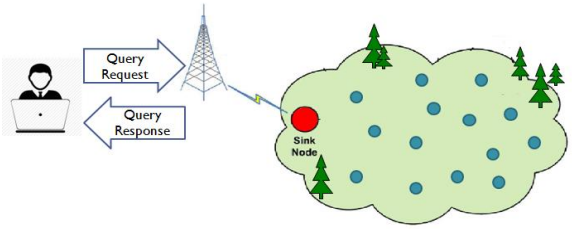

Fig. 1: Query processing in wireless sensor networks.[5]

The user requests his needed information in the form of some query requests from the base station. Queries will reach the nodes from the base station by means of a path which is calculated by a routing protocol, while processing will be carried out on queries and the intended data will be collected by the sensor nodes. Finally, query results will return to the base station via a return path [9]. The structure of a query may resemble SQL query with the following blocks [10]:

SELECT - FROM - WHERE - GROUPBY-HAVING

For example:

SELECT *temperature FROM sensors WHERE location = (x , y)*

If in a query a certain region or certain coordinates are specified for the nodes of the sensor network, and if the nodes can respond to the queries with regard to that region, then the query is an spatial one [11]. In this query, the user needs the information of only a certain part of the region in which the network is installed and tries to introduce the intended region to the sensor nodes by benefiting from such methods as specifying the list of nodes' coordinate, specifying the geometrical shapes such as circle, quadrilateral, polygon, and, finally, by specifying the trajectory path. The majority of mechanisms prepare a window for the nodes and only the nodes inside the windows respond to them. In some mechanisms a node is specified while the neighbouring nodes engage in responding to the queries. These sorts of queries are widely used in real situations [2].

3. Examining the Topology of Affected Area

Firstly, we should notify the nodes of the topology of the affected area. As it was mentioned earlier, we can easily specify the intended area by means of only two points for regular shapes such as squares and rectangles, meaning that only by sending one packet to sensor nodes, it is possible to introduce the area in the queries. As shown in Fig. 2, by sending a point with the lowest x,y as point A, and by sending another point with the highest x, y as point B, we can specify the entire intended area.

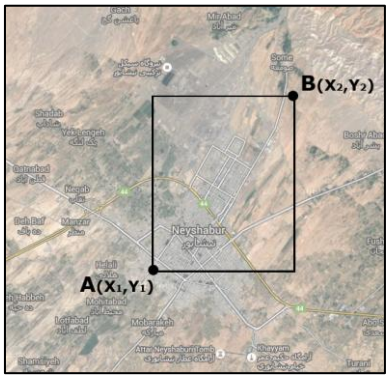

Fig. 2: Affected area with a regular shape [12]

As Fig. 2 illustrates, a sensor node whose coordinates are between the two points, is positioned within the intended area. Otherwise, it is situated beyond that area and should not respond to the queries. If a sensor node meets the following two conditions, it can respond to the queries:

$X_1 \leq \text{Node.x} \geq X_1$, $Y_1 \leq \text{Node.y} \geq Y_1$

However, this is quite unlike the irregular shapes where it is impossible to determine them with only two points since they require many. This is illustrated in Fig. 3.

Fig. 3: Affected area with irregular shape

In Fig. 3, the specified area is the city of Neyshabur. As shown in Fig. 3, the intended area is of an irregular shape and it is not possible to determine the shape of this area for the sensor nodes with only two points. For example, to determine the shape of this area we need 251 points. If each point requires two bytes, then we need 502 bytes of free memory space. And if the network packets are 28 bytes, then we need 18 packets to transfer the points which determine the shape of the area. Because of high energy consumption in wireless communications between the nodes of sensor networks, and multiple transmissions, this is very costly.

4. Related Works

Simplification algorithms are used to solve the problem of the number of points in irregular shapes. In older researches the Nth point method was used in such a way that the value of N is chosen by the user and the algorithm eliminates N points [13]. Or N points will be randomly eliminated [14]. But these methods are not accurate since they eliminate the points irrespective of their coordinates in the shape [15], and in the majority of cases the shape loses its essence after simplification.

One of the optimized algorithms that simplifies the lines logically is the Ramer-Douglas-Peucker algorithm which was presented by David Douglas and Thomas Peucker [16], and is the continuation of Urs Ramer's work [17]. This algorithm is tasked with finding a line segment which resembles the main line segment but with fewer points. By taking into account the beginning and the end of the line segment, this algorithm determines the farthest point from the line and divides it into two new line segments: one line segment from the starting point to the farthest point and one from the farthest point to the line end point. This operation is carried out for these two line segments separately.

A threshold is considered for this algorithm. If the distance of the farthest point from the line is more that the threshold, the line breaks into two line segments. But if it is less than the threshold value, that point can be eliminated. Consequently, it is possible to reduce the number of line points. Obviously, the threshold determines precision. The larger the threshold is, the more the eliminated points are. However, the line segment obtained from the algorithm bears little resemblance to the main line segment. If the threshold is small, line segment bears more resemblance but fewer points are eliminated. In the following, we will explicate the algorithm by providing an example. Take Fig. 4 as an example. We apply RDP algorithm to two AZB and AWB lines. For AZB line, the beginning and the end of the line segment, that is, line AB, are connected by a straight line. Now, we should calculate the distance from point Z to the line. The distance of point $Z = (x_z, y_z)$ and line AB by $(x_A, y_A), (x_B, y_B)$ is obtained from the following formula

$$d(Z, AB) = \sqrt{\left(x_z - x_A - \lambda_q(x_B - x_A)\right)^2 + \left(y_z - y_A - \lambda_q(y_B - y_A)\right)^2}$$

where λ_q is equal to

$$\lambda_q = \frac{(x_B - x_A)(x_z - x_A) + \left(y_B - y_A\right)\left(y_z - y_A\right)}{(x_B - x_A)^2 + \left(y_B - y_A\right)^2}$$

Considering the threshold value, we can observe that the distance $d(Z, AB)$ of point $Z = (x_z, y_z)$ is above the threshold. Therefore we cannot eliminate the Z point and no simplification takes place.

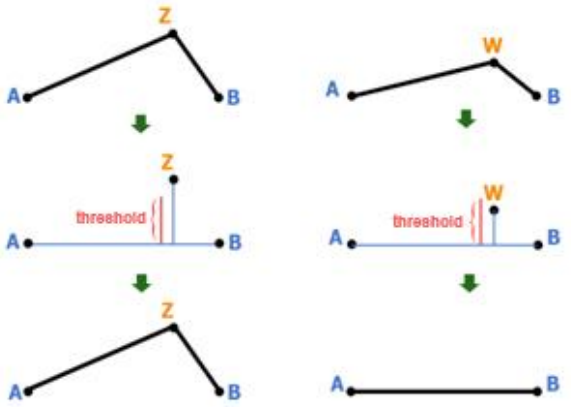

Fig. 4: RDP algorithm performance

Now we apply the algorithm to AWB line. First, the AB line is considered and then the distance from W to this line is calculated. This distance is below the threshold so it can be eliminated based on the algorithm's principles. The result is the AB line and simplification took place.

This algorithm can examine irregular shapes in a linear fashion and reduce its points. In the following, we will present some researches in which RDP algorithm was employed.

In [18] RDP algorithm is used in the fields of meteorology and geography in order to simulate the current of rivers and lakes and to draw the geographical maps.

In [19], the RDP simplification algorithm is utilised in navigation and routing systems so that they can carry out the best planning for linear paths with respect to optimum decision-making processes for telephone communication in navigation systems.

In [20], RDP has come to the aid of cultural heritage and architecture and has been able to classify Iberian ceramics with the help of simplified curves.

In [21], RDP has been used in image processing, and the utilised maps were drawn in robotic and industrial machines.

In [22], da Silva et al., used RDP algorithm in sensor networks and were able to simplify the area under examination to be used in Duty cycle mechanism in wireless sensor networks.

In [23], RDP simplification algorithm has been used in modelling and simulation, and a model to simulate evacuation in areas with complex paths is presented.

In [24], the researchers used RDP algorithm to simplify the queried area to reduce the points of the shape of the area. In this research, the output parameters of wireless sensor network simulation are presented using RDP simplification algorithm.

In [25], RDP algorithm is used to process images to automatically produce similar polygamies by specifying the threshold.

The researchers in [26], who deal with introducing and examining spatial query processing mechanisms, use RDP algorithm in pre-processing phase to simplify the queried area.

In [27], with regard to Douglas algorithm, large data collected across the route by position-based systems are reduced by simplification algorithms, and processing volume in position-based systems is considerably improved and optimized.

In [28], with the help of genetic and Douglas simplification algorithms, 3D printing programs are optimized.

5. The Proposed Algorithm to Simplify the Shape of the Area

The idea for this algorithm is derived the regular quadrilateral and rectangular shapes. The fact that we require two points to present regular shapes led us into using an algorithm which benefits from this feature. In this method, as opposed to other algorithms to which the irregular shape appears as a line and try to simplify the points on the line.

Points forming the shape of the irregular area is defined by *IMG*: $IMG = \{PI_1, PI_2, PI_3, \dots, PI_n\}$

where PI_1 is one of the points forming the shape of the area and $PI_i = \left(x_{PI_i}, y_{PI_i}\right)$.

we have processed the irregular shapes as closed ones. With respect to the nature of quadrilateral shapes which require two points to be presented, the proposed method divides the whole area into equal smaller quadrilaterals. To do this, first we need to determine the entire quadrilateral span of the irregular shape.

In order to do this, we should find the leftmost, rightmost, topmost, and bottommost point of the irregular shape. In other words, we look for two points which have the smallest and the biggest x, and two points which have the smallest and the biggest y, similar to Fig. 5.

Determining the leftmost and rightmost, the topmost and bottommost point in the shape of the area to form the regular frame of the shape:

a is the leftmost, b is the rightmost, c is the bottommost, and d is the topmost point

$\{a, b, c, d\} \in IMG$

$$a = (x_a, y_a) = \{PI_i | PI_i \in IMG\ , x_{PI_i} = \min(x_{PI_i} \in IMG)\}$$
$$b = (x_b, y_b) = \{PI_i | PI_i \in IMG\ , x_{PI_i} = \max(x_{PI_i} \in IMG)\}$$
$$c = (x_c, y_c) = \{PI_i | PI_i \in IMG\ , y_{PI_i} = \min(y_{PI_i} \in IMG)\}$$
$$d = (x_d, y_d) = \{PI_i | PI_i \in IMG\ , y_{PI_i} = \max(y_{PI_i} \in IMG)\}$$

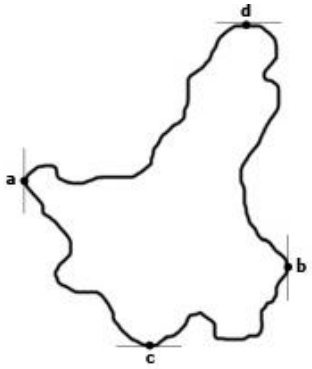

Fig. 5: Identifying determining points of the area

Using these four points, the bottom right and top left corners can be calculated. To calculate the x,y of point A, which is situated at the bottom left corner, we should use the x of point a and the y of point c, and to identify the x,y of point B, which is located at the top right corner, we need to use the x of point b and the y of point d. This is illustrated in Fig. 6.

A is the smallest point of the span and $A = (x_a, y_c)$

B is the biggest point of the span and $B = (x_b, y_d)$

The size of two horizontal sides is shown by *LX* and

$LX = x_b - x_a$

The size of two horizontal sides is shown by *LY* and

$LY = y_b - y_a$

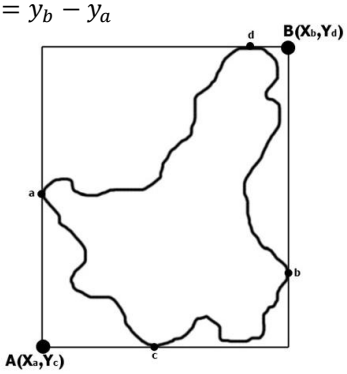

Fig. 6: Determining the span of the shape of the area

Now, by calculating points A and B, we can proceed with dividing the quadrilaterals. We should divide the entire area covered by the quadrilateral extending from point A to point B into quadrilaterals with equal length. Fig. 7 illustrates this point.{Tobler, 1964 #39}

The size of the threshold is shown by *t* which is equal to the size of quadrilaterals' sides, but must be adjusted according to the size of the frame so that quadrilaterals can cover the entire span. Determining *tx* which shows the size of horizontal and parallel sides to *x* axis $tx = \frac{LX}{[LX/t]}$

Determining *ty* which shows the size of horizontal and parallel sides to *y* axis $ty = \frac{LY}{[LY/t]}$

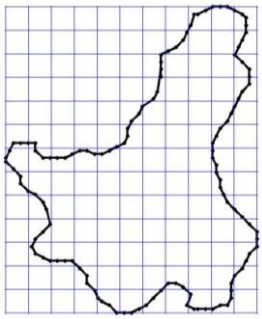

Fig. 7: Quadrilateral divisions in the proposed algorithm

After the division, the coordinates of the four corners of each quadrilateral is recorded.

Each quadrilateral is shown by determining each of its four corners $QL_i = \{Pdl_i, Pdr_i, Pul_i, Pur_i\}$

Pdl is the bottom-left corner of the quadrilateral

$$Pdl_i = \{\, Pdl_i = \left(x_{Pdl_i}, y_{Pdl_i}\right) | x_{Pdl_i} = x_{Pdl_i} + (hx \times tx) \\ , \; y_{Pdl_i} = y_{Pdl_i} + (hy \times ty) \,, \\ hx \in \{1,2,\dots,([LX/t] - 1)\}, \\ hy \in \{1,2,\dots,([LY/t] - 1\}\,)\}$$

The total number of quadrilaterals within the area A and B reaches 143. Some of these are situated within the shape, and some are situated outside the shape. Then, the quadrilaterals which are inside the shape must be determined. Even if only center of quadrilateral fall inside the shape, we should consider that quadrilateral as entirely falling within the shape.

To determine whether a point is inside or outside of the shape, we used a simple method: we move in four directions: right, left, top, and bottom. If in all these four directions we come across a point in the irregular shape, that point is very probably inside the irregular shape. However, if we do not come across in any of these four directions, the intended point is outside the shape. In other words, between the points of the irregular shape there must be four other points two of which must have an ***x*** equal to that of the intended point; and one of their ***y***s must be smaller and the other must be greater than the *y* of the intended point. The other two points of the irregular shape must have a ***y*** equal to that of the intended point, while one of their ***x***s must be smaller and the other must be greater than the intended ***x***. if these four points with these features are found among the points of the irregular shape, the point is very probably inside the shape. This means that given the ***x*** and ***y*** of the intended point, it must be looked for among the points of the irregular shape so that we can find four points possessing the previously mentioned features. The condition for being inside is that the center of the quadrilateral must lie inside shape.

First, we define an entire set of points on or inside the shape as *Pin* The four intended points are defined as $\{P_j, P_k, P_t, P_r\} \subset IMG$

and

$$Pin = \{P_i | A \le P_i \le B \,, x_{P_i} = x_{P_j} = x_{P_k} \,, \\ y_{P_i} \ge y_{P_j}, y_{P_i} \le y_{P_k} \,, y_{P_i} = y_{P_t} = y_{P_r} \,, \\ x_{P_i} \ge x_{P_t}, x_{P_i} \le x_{P_r} \;|\; \{P_j, P_k, P_t, P_r\} \subset IMG \,\}$$

Now we should say that if the center of the quadrilateral is either inside or on the shape, it is determined as being inside. In other words, the center of the quadrilateral must be a member of the set *Pin*.
The quadrilateral which lies inside the shape is defined by *QLin* set:

$$Qlin = \{QL_i | (\left[QL_{\substack{x \\ Pdl \\ i}} + \frac{tx}{2}\right], \left[QL_{\substack{y \\ Pdl \\ i}} + \frac{ty}{2}\right]) \in Pin\}$$

For example, in Fig. 8 we can observe the quadrilaterals which are considered as falling within the shape. Out of 143 quadrilaterals, only 83 fall within the shape. Accordingly, we could manage to turn irregular shapes into regular quadrilateral shapes.

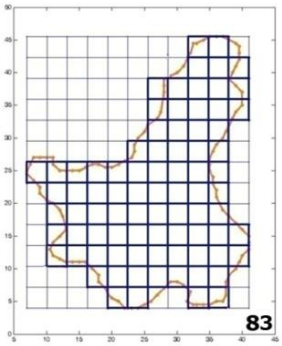

Fig. 8: Determining the quadrilaterals inside the shape using the proposed algorithm

As illustrated in the above Figure, the smaller the quadrilaterals become, the more their presenting accuracy increases. Therefore, the size of these quadrilaterals can act as the threshold that determines accuracy. The smaller the size of the threshold becomes, the more accuracy and the number of quadrilaterals increase. And to the extent the threshold gets bigger, both accuracy and the number of quadrilaterals decrease.

As it was mentioned before, to specify each quadrilateral, we require two points. As Figure 8 illustrated, 83 quadrilaterals are inside the shape; consequently, the total number of points which indicate the irregular shape are 164. If the quadrilaterals shrink in size, then certainly the number of points will increase. The points required to present the unsimplified irregular shape is 251. As a result, we could considerably reduce the number of points necessary to present the irregular shape. It should be noted, however, that, as with other simplification algorithms, the reduction in the number of points is inaccurate, meaning that some parts from the original shape are eliminated while a part is annexed to it which did not previously belong.

In the following, by merging the quadrilaterals which are inside the shape, we try to reduce the number of points even more that in simplification algorithm. The strategy of the merge algorithm is to merge the quadrilaterals that are inside the shape, and whose points have been discretely presented, into a bigger one so that all these quadrilaterals and their points change into one quadrilateral with only one point.

$$Qlmerg = \{\sum_{i=i+tx}^{LX} QLin_i \mid QLin_{\substack{x \\ Pdl \\ i}} = QLin_{\substack{x \\ Pdl \\ i+1}}\}$$

As it is obvious from Fig. 9, several of the quadrilaterals that are inside the shape and are attached to one another can be specified as a bigger quadrilateral. Thus, any number of quadrilaterals which are merged are possible to be presented by two points only. The more quadrilaterals we are able to merge, therefore, the more we reduce the number of points of a shape.

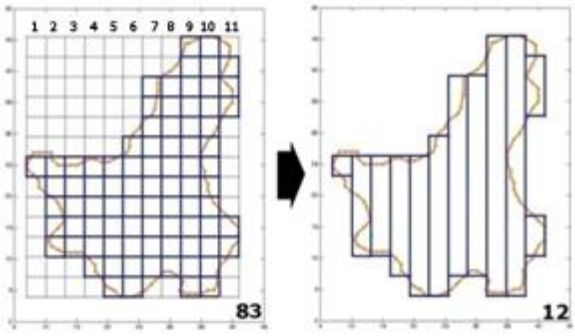

Fig. 9: Columnar merge in the proposed algorithm

The proposed algorithm merges quadrilaterals in a column. As the Figure clearly shows, we merge quadrilaterals which are inside the shape and are in the same column. In other words, it is possible to present the quadrilaterals which enjoy equal x and are situated in one column with two points. The most desirable condition occurred in column 9 where 13 quadrilaterals were merged and formed a bigger one. In place of transmitting 26 points to present 13 quadrilaterals, now it is possible to transmit only two points. However, the worst condition occurred in column 1. Apparently, we did not manage to merge any quadrilaterals in this column and, therefore, we did not experience any reduction in the number of points. If all the quadrilaterals are attached to one another in one column, then we only need two points for the entire column. But it is possible, as in the last column, that after merging we might have a multi-piece column, and that for each piece we need to specify two separate points.

As shown before, to present an unsimplified shape, we needed 251 points. After simplification, however, this amount shrank to 164. But after operating the merge algorithm, these points decreased considerably and reached 12 quadrilaterals with 24 points. This points to more than one-tenth reduction in the original number of points. This considerable reduction in points from 164 to 24 had no effect of the degree of accuracy.

In the next phase, we will re-merge the bigger quadrilaterals. If the obtained quadrilaterals are the same size and are next to one another, they can merge and form a bigger one as in Fig. 10.

The bigger quadrilaterals obtained from the first phase merge, which were equal in size and situated next to one another, were merged again.

$$Qlmerg2 = \left\{ \sum_{i=i+1}^{|Qlmerg|} QLmerg_i \mid (QLmerg_{\substack{x \\ Pdl \\ i}} = QLmerg_{\substack{x \\ Pdl \\ i+1}}) \right\} = \left\{ , \left(\left(QLmerg_{\substack{x \\ Pul \\ i}} - QLmerg_{\substack{x \\ Pdl \\ i}} \right) = \left(QLmerg_{\substack{x \\ Pul \\ i+1}} - QLmerg_{\substack{x \\ Pdl \\ i+1}} \right) \right) \right\}$$

We could thereby once again reduce the number of quadrilaterals and the points required to present them.

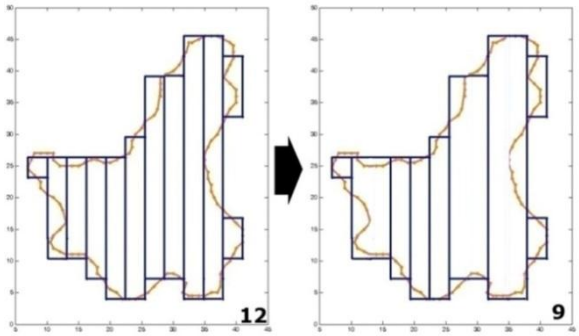

Fig. 10: Merging in the second phase in the proposed algorithm

The number of quadrilaterals decreased from 12 to 9 and required only 18 points for their presentation. It is important to note that the merging activities in the first and second phases had no impact on accuracy while the number of necessary points decreased considerably.

Apparently, the merge algorithm, which attaches quadrilaterals in columnar manner, is suitable for shapes whose heights are more than their widths. But in shapes whose widths are more than their heights, merging activity could be carried out differently. In place of merging the quadrilaterals in columnar fashion, it is possible to carry out the merging process in rows. In other words, we need to merge the quadrilaterals which are in one row and form a bigger one.

$$Qlmerg = \left\{ \sum_{i=i+ty}^{LY} QLin_i \mid QLin_{\substack{y \\ Pdl \\ i}} = QLin_{\substack{y \\ Pdl \\ i+1}} \right\}$$

The effect of this change could be observed in Fig. 11.The width of the shape that is employed here, as it is shown in the above figure, is more than its height. After exerting the columnar algorithm, the number of quadrilaterals reached 14. But after linear merge, this number decreased to 5, which is almost one-third of the former merge algorithm. In columnar merge we require 28 points while in linear merge only 10 points are required. Therefore, merge algorithm must take into consideration both the width and the height of the shapes, meaning that it should benefit from columnar merge in shapes whose heights are more than their widths, while it should exploit linear merge in shapes whose widths are more than their heights so that we can have the least possible number of points.

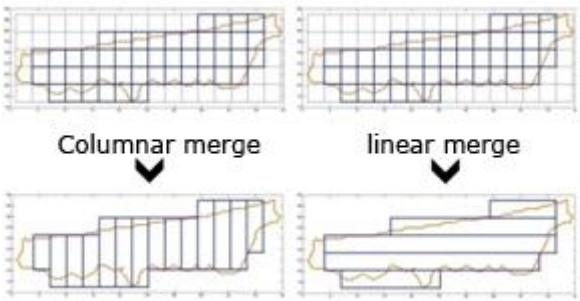

Fig. 11: Columnar and linear merge in the proposed algorithm

Our approach formulation model can be presented using the following flow chart.(Chart1)

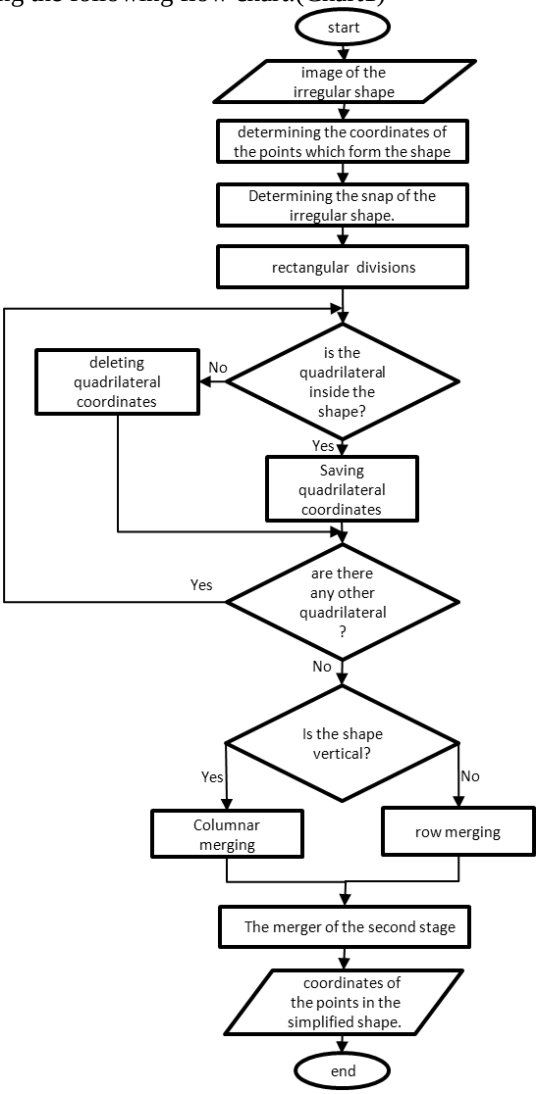

Chart. 1: Our approach formulation model

6. Implementing and Assessing the Proposed Algorithm and RDP

In this part, we have planted various sensor networks in different scenarios, simplified several different shapes with the proposed algorithm and RDP, and have sent them to the network as spatial queries. We will finally analyze the results of the queries so that it is possible for

us to compare the proposed algorithm with RDP in terms of energy consumption and accuracy in responding to the queries. To carry out the plantation of sensor networks, we first need to select areas with irregular and different shapes.

We have selected three different cities as examples. We have specified the examined areas in the shapes: the first is the residential area of the city of Neyshabur (Fig. 12), next is the residential area of the city of Mashad (Fig. 13), and the third is the residential area of the city of Nur (14).

Fig. 12: Neyshabur scenario

Fig. 13: Mashad scenario

Fig. 14: Nur scenario

In this article, we implemented and tested the three scenarios using MATLAB software [29], in order to assess the obtained results.

First, we specify the constitutive points of the shape of each scenario (Fig. 15).

Fig.15:Scenarios' shapes

Then, we calculated the points and the coordinates of the shapes of the scenarios. The number of points of irregular shapes is presented in Table 1 without simplification.

Table 1: The number of points in the original shapes of scenarios

Scenario	Neyshabur	Mashad	Nur
The number of points in the original shape	251	241	207

After extracting the list of point coordinates from the scenarios, we can implement the simplification algorithm and decrease the number of points. They can now be compared with respect to the reduction of the number of points and accuracy. We first implement the RDP and then the proposed algorithm.

6.1. Implementing RDP Simplification Algorithm

The RDP algorithm was implemented on the scenarios. The number of points of irregular shapes after being simplified by RDP method in three scenarios is presented in Table 2.

Table 2: The number of points resulting from RDP algorithm

Scenario	Neyshabur	Mashad	Nur
The number of points of unsimplified shape	251	241	207
The number of points of the shape simplified with RDP	99	102	94

Using RDP algorithm, we could reduce the number of points to more than half the original number. However, after planting the sensor network, it has to be compared with the proposed algorithm in terms of accuracy and the number of points.

6.2. Implementing the Proposed Simplification Algorithm

In this section, we implemented the proposed algorithm and the merge function on the three scenarios.

First, we carried out quadrilateral divisions according to what was previously mentioned, and presented the results in Fig. 16. The coordinates of each corner of the quadrilateral were recorded in a matrix. In Table 3, we can observe the number of quadrilaterals formed for each scenario.

Table 3: The number of quadrilaterals resulting from rectangular formations in the scenarios

Scenario	Neyshabur	Mashad	Nur
Number of quadrilaterals	1394 (41×34)	1610 (35×46)	644 (14×46)

Now, we should see which quadrilaterals fall within the shapes. The results obtained from the examination are presented in the following. As presented in Fig. 16, the quadrilaterals whose two corners are inside the shape are considered as being entirely inside, and their sides are highlighted. The number of quadrilaterals together with the number of the ones which are considered as inside the shape are presented in Table 4.

According to Table 4 and Fig. 16, the number of the quadrilaterals is relatively large. Also, many of these quadrilaterals are close to one another and are capable of forming a bigger quadrilateral.

In the following, we will implement the merge algorithm of the first phase on these quadrilaterals. The results obtained from the operation of merging the quadrilaterals are presented in Fig.16. In the second phase, bigger and equal quadrilaterals obtained from the merge algorithm of the first phase can be further merged. The merge algorithm of the second phase was implemented, and its results are presented in Fig. 16.

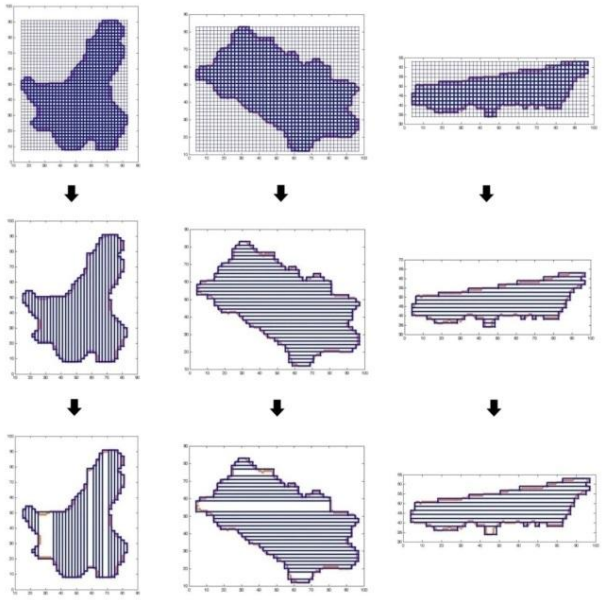

Fig. 16: The implementation of two merges phases on the scenario using the proposed algorithm.

According to Fig. 16, by merging quadrilaterals, we were able to considerably decrease their number. The number of quadrilaterals is presented in Table 4.

Table 4: The number of quadrilaterals obtained from implementing the proposed algorithm in different phases.

Scenario	Neyshabur	Mashad	Nur
Total number of quadrilaterals	1394	1610	644
Number of quadrilaterals inside the shape	758	830	355
Number of quadrilaterals after the first phase merge	43	38	19
Number of quadrilaterals after the second phase merge	37	34	18

It should be noted that scenarios are merged with respect to their width and height. For instance, Neyshabur scenario, whose height was more than its width, was merged in a columnar fashion. On the other hand, Mashad and Nur scenarios were merged in rows and horizontally, since their widths were more than their heights. Since for the presentation of each quadrilateral we require two points, the ultimate required points for the presentation of the scenarios with different algorithms are presented in Table 5.

Table 5: The number of points obtained from simplification using RDP and the proposed algorithms.

Scenario	Neyshabur	Mashad	Nur
Unsimplified number of points	251	241	207
Number of points obtained from RDP algorithm	99	102	94
Number of points obtained from the proposed algorithm	74	68	36

6.3. Calculating Carelessness

The simplification of the shape of the areas and the reduction in the number of points to present these areas caused a certain degree of carelessness. There is a difference between the shapes simplified with simplification algorithm and the original shapes. This is because after simplification, some parts which formerly fell inside the shape, would now fall outside it, while some parts which did not belong to the shape, were now annexed to it. These differences give rise to a certain degree of carelessness in responses to the queries because some of the nodes which in the original shape were inside the area now fall outside it. And some of the nodes which were outside the original shape are now inside it. These differences exist normally around the shape of the intended area. This carelessness explains the reason why some nodes that should not have responded to the queries transmit some responses, while the nodes that ought to have responded to the queries do not participate in sensing process. This degree of carelessness is calculated by the following formula.

Carelessness= the proportion of the number of wrong nodes to the total number of nodes in the area in the original shape.

The number of wrong nodes is equal to the total number of nodes that wrongly responded + the nodes that did not respond wrongly.

6.4. The Implementation of Sensor Network in the Scenarios

Now, we deploy the sensor network in three different scenarios so that we can compare them with respect to the maximum level of energy consumption and accuracy in different scenarios and in the simplification algorithm. To

make this comparison, we need to deploy the sensor network in the original shape with regard to which the two simplification algorithms can be compared.
-The dimensions of the deployment area are 100*100 m.
-The queries are broadcast through fullflooding method.
- Only the nodes inside the area respond to queries.
-Network packets are 28 bytes.
- Nodes are aware of their position (they are equipped with GPS).
-The energy of data transmission is 50nj/bit.
- We require two bytes of memory to send each point of the shape.
- Nodes are identical and stable.
- The radio range of each node is 15m.
- Nodes are always active and never change into sleep mode.
-Each node is identified from 1 to *n* with a unique identity information (n is the number of nodes of the network).
-The consumed energy is equal for both sending and receiving data.
Each scenario ought to be deployed with different number of nodes (500-1000-1500). To show the degree of carelessness, we benefit from presenting the percentage of wrong nodes to the total number of nodes of the area in the original shape. This means that we first should obtain the number of wrong nodes, and then express them as the percentage of the total number of nodes in the original shape.

6.5. The Implementation of Sensor Network in Neyshabur Scenario

First, we implement the sensor network in Neyshabur scenario with the original shape, simplified with RDP algorithm, and, finally, with the proposed algorithm. The results obtained from the implementation of the sensor network with different algorithm are available in Table 6. Based on Table 6, the level of energy consumption of the sensor network in Neyshabur scenario with RDP and our proposed algorithms, and the implementation without the simplification of the points (main shape) with different number of nodes (500-1000-1500) are presented in Fig. 17.

Table 6: The results of the sensor network implementation in Neyshabur scenario

Simplification by proposed algorithm			**Simplification by RDP algorithm**			**Main Shape**			**Neyshabur scenario Sink coordinates 29* 83**
1500	1000	500	1500	1000	500	1500	1000	500	**Number of nodes**
480	313	152	522	338	161	469	310	149	**Nodes inside the shape**
74	74	74	99	99	99	251	251	251	**Number of points**
6	6	6	7	7	7	18	18	18	**Number of packets**
9.3	4.1	1.0	10.9	4.8	1.2	28.1	12.5	3.2	**Energy consumption (Jules)**
7	6	0	4	3	2	**Nodes that should have responded**			
18	9	3	55	34	14	**Nodes that should not have responded**			
5.3	4.8	2	12.5	11.9	10.7	**Error percentage**			
66.6	66.6	66.5	61.6	61.0	60.9	**Percentage of energy consumption reduction**			

By decreasing the number of points of the original shape in Neyshabur scenario, and also by reducing network packets, the simplification algorithms could considerably decrease energy consumption. This reduction in energy consumption occurred in all three networks with different number of nodes (500-1000-1500).

As it is obvious from Fig. 17, our proposed algorithm outperformed RDP algorithm and could respond to the queries by consuming less energy. The amount of reduction in energy consumption in Neyshabur scenario for 500-1000-1500 number of nodes in RDP algorithm was 60.99, 61.04, and 61.06, respectively.
However, the energy reduction in our algorithm was 66.55, 66.60, and 66.62, respectively: 5% more reduction in energy consumption relative to other algorithms. This is due to the better performance of the proposed algorithm in reducing the number of points in the shape.

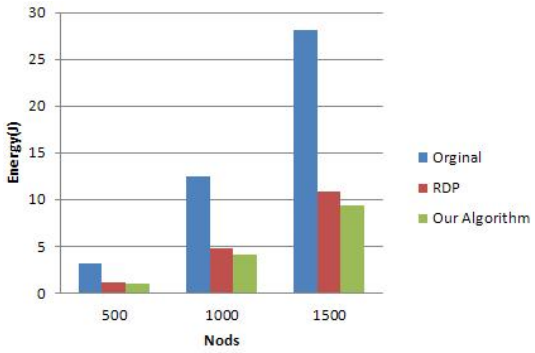

Fig. 17: Comparing algorithms in Neyshabur scenario with respect to energy consumption

The carelessness percentage of Neyshabur scenario is available in Fig. 18. This diagram illustrates the carelessness percentage in two RDP and the proposed algorithms in relation to the unsimplified original shape. In Neyshabur scenario, our proposed algorithm enjoyed lower carelessness percentage in relation to RDP algorithm. This degree of lower carelessness occurred in each mode of implementation of sensor network.

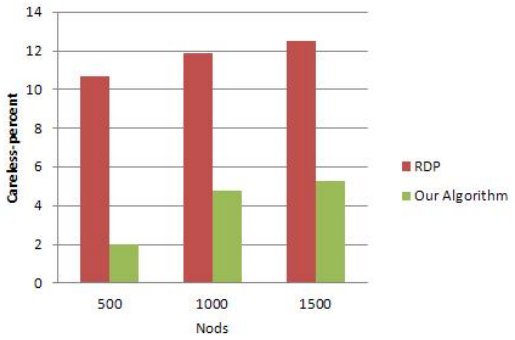

Fig. 18: Comparing algorithms in Neyshabur scenario with respect to carelessness

The RDP algorithm in the sensor network with different nodes (500-1000-1500) suffered from carelessness 10.7, 11.9, 12.5 respectively. In our proposed algorithm, carelessness was 2, 4.8, and 5.3 respectively. Consequently, in terms of accuracy, our proposed algorithm outperformed RDP algorithm. The lower carelessness is due to a more accurate simplification of our algorithm since fewer wrong areas were added and subtracted from the shape. These wrong areas will be explicated in section 6-3.

The carelessness of our algorithm in Neyshabur scenario was, in the worst possible state, was 5.3 per cent, while the carelessness of RDP algorithm, in the worst possible state, reached 12.5 per cent.

6.6. The Implementation of Sensor Network in Mashad Scenario

In this section, we first implement the sensor network in Mashad scenario with the original shape. Next, we will implement the simplified sensor network using RDP algorithm. And, finally, using our proposed algorithm, we will deploy it in the same scenario.

The results obtained from the implementation of the sensor networks with different algorithms are presented in Table 7.

Figure 19 presents the results of the implementation of Mashad scenario with regard to energy consumption. This implementation of the sensor network is achieved with 500-1000-1500 nodes. The following diagram illustrates the implementation of RDP simplification and our proposed algorithms on the original shape of Mashad scenario.

In this scenario, too, our algorithm outperformed RDP algorithm, while at same time, by a better simplification of the points, it could lessen energy consumed in responding to the queries. This reduction was even better than Neyshabur scenario, and as the results reveal, it could, in all the three sensor networks with different node numbers, have lesser energy consumption. The results reveal that reduction in energy consumption in RDP algorithm in sensor networks with 500-1000-1500 number of nodes was 52.78, 52.85, and 53.21 per cent respectively, while in our proposed algorithm this reduction for the same number of nodes was 70.43, 70.50, and 70.73 per cent respectively.

Table 7: Results of the implementation of sensor network in Mashad scenario

Simplification by the proposed algorithm			**Simplification by RDP algorithm**			**Original shape**			**Mashad scenario** Sink coordinates 48* 97
1500	1000	500	1500	1000	500	1500	1000	500	**Number of nodes**
480	313	152	573	391	184	514	345	158	**Nodes inside**
74	74	74	102	102	102	241	241	241	**Shape's number of nodes**
6	6	6	8	8	8	17	17	17	**Number of packerts**
9.3	4.1	1.0	12.5	5.5	1.4	26.7	11.8	3.0	**Energy consumption (Jules)**
7	6	0	2	1	0	**Nodes that should have responded**			
18	9	3	59	46	26	**Nodes that should not have responded**			
5.3	4.8	2	11.8	13.6	13.9	**Error percentage**			
66.6	66.6	66.5	52.8	52.8	52.7	**Energy consumption reduction**			

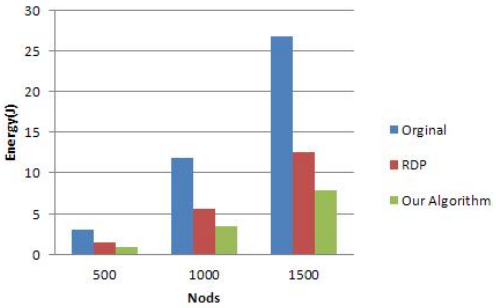

Fig.19:Comparing the algorithms in Mashad scenario in terms of energy consumption

Accordingly, our proposed algorithm could considerably optimise energy consumption by more than 17%. This reduction is due to the better performance of the proposed algorithm in reducing the number of points of the shape. The results also reveal that our proposed algorithm had a finer performance in Mashad scenario than in Neyshabur scenario, and reduction in energy consumption could reach from 5% to 17%. Fig. 20 illustrates the degree of carelessness in Mashad scenario. The degree of carelessness is calculated in percentage terms after the implementation of the sensor network with different number of nodes and the deployment of the algorithms.

Our algorithm in Mashad scenario had far lesser carelessness, such that it could even be ignored. This lesser degree of carelessness is down to a more accurate simplification of our algorithm because fewer wrong areas were added or subtracted from it. These wrong areas were explained in section 6-3. In the worst possible condition, RDP algorithm suffered from 14% error, while the error of our algorithm was, in the worst possible condition, only 4%.

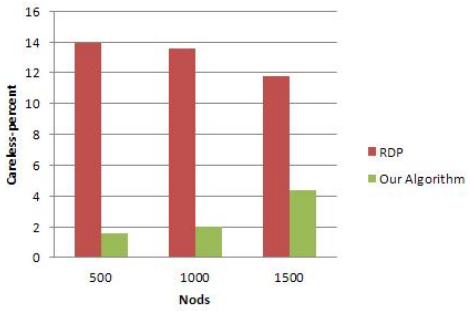

Fig.20:Comparing the algorithms in Mashad scenario in terms of carelessness

After deploying the sensor network with 500-1000-1500 nodes, the degree of carelessness of RDP in Mashad scenario was 13.9, 13.6, and 11.8 per cent respectively. This parameter for our proposed algorithm with the same number of nodes was 1.6, 2, and 4.4 per cent respectively. The error in the sensor network with 500 nodes was close to zero.

6.6.The Implementation of Sensor Network in Nur Scenario

In the following, we will implement the senor network in Nur scenario with the original shape, and after that with the shape simplified with RDP algorithm, and finally with our proposed algorithm. The results the implementation of the sensor network with different algorithms are presented in Table 8.

Table 8: Results of the implementation of sensor network in Nur scenario

Simplification by the proposed algorithm			**Simplification by RDP algorithm**			**Original Shape**			**Nur scenario Sink coordinates 58* 97**
1500	1000	500	1500	1000	500	1500	1000	500	**Number of nodes**
223	136	67	242	154	76	235	139	71	**Nodes inside**
36	36	36	94	94	94	207	207	207	**Shape's number of points**
3	3	3	7	7	7	15	15	15	**Number of packets**
4.6	2.0	0.5	10.9	4.80	1.2	23.4	10.4	2.6	**Energy consumption (Jules)**
13	6	5	8	3	1	**Nodes that should have responded**			
1	3	1	7	15	5	**Nodes that should not have responded**			
5.9	6.4	8.4	6.3	12.9	8.4	**Error percentage**			
79.9	79.9	79.9	53.3	53.2	53.2	**Energy reduction percentage**			

In Fig. 21 the results of the energy consumption of this implementation with RDP and our proposed algorithms are presented against the implementation on the original shape of Nur scenario.

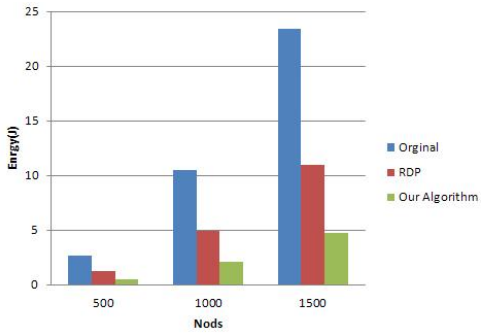

Fig. 21: Comparing the algorithms in Nur scenario in terms of energy consumption

As Fig. 21 shows, a better result was obtained by our algorithm. The results show that the sensor network with different node numbers implemented with our algorithm in Nur scenario had a far lesser energy consumption in relation to RDP algorithm. Based on implementation results, reduction in energy consumption in Nur scenario was even better than previous scenarios. Considering the results of the deployment of the sensor network with different number of nodes in Nur scenario, RDP algorithm with 500-1000-1500 nodes could enjoy 53.25, 53.29, and 53.30 per cent reduction in energy consumption respectively.

However, our algorithm has considerably decreased energy consumption by 79.92, 79.95, and 79.96 per cent respectively. This reduction in energy consumption is due to the better performance of the proposed algorithm in reducing the number of points in the shape. Energy reduction in Nur scenario was more than those of Neyshabur and Mashad, and our algorithm could reduce energy consumption by 80% in Nur scenario. It could respond to the queries consuming half the amount of the energy consumed in RDP algorithm. The results of carelessness obtained from the deployment of the sensor network in Nur scenario with different number of nodes are presented in Fig. 22.

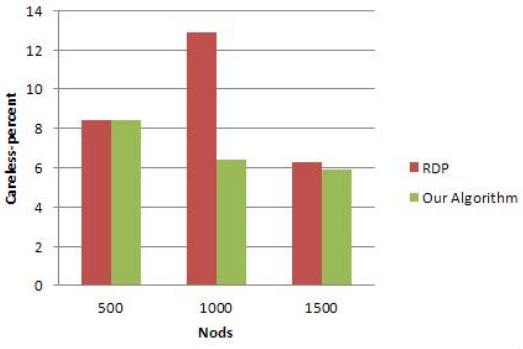

Fig.22:Comparing the algorithms in Nur scenario in terms of carelessness

In this scenario, the two RDP and proposed algorithms had similar performance with regard to carelessness, except when the number of nodes was 1000. The RDP algorithm in the sensor network with 500-1000-1500 nodes achieved 8.4, 12.9, and 6.3 per cent carelessness respectively. The proposed algorithm, too, achieved 8.4, 6.4, and 5.9 per cent carelessness respectively. This close

degree of carelessness is due to the formation of equal wrong areas by both of the algorithms. These wrong areas were explained in section 6-3. The consumed energy by the proposed algorithm in this scenario was half the amount consumed by RDP algorithm. But, as the diagram reveals, carelessness in both algorithms is more or less equal. it could be argued that as long as carelessness in both algorithms is equal, the energy consumed by our algorithm is half the RDP algorithm.

7. Conclusion

In this article we introduced the processing of spatial queries in sensor networks and analysed its function in crisis management and stricken areas. The problem with these areas was their irregular shape which required many points to be presented. This resulted in an increase in the sensor network's number of packets and higher energy consumption. By examining previous related works and benefiting from line simplification algorithms, we could reduce the points of the shape of the area and solve the problem. Then, we presented our algorithm and, as the results of implementation revealed, in all the scenarios the proposed algorithm manifested a better performance in reducing energy consumption. In the worst-case scenario, our proposed algorithm reduced energy consumption by 66%, while in the best-case scenario, it reduced energy consumption by 80% relative to the original shape of the area. This amount of reduction of energy consumption in the sensor network which has limited energy is a notable success. In order to draw a satisfactory conclusion from the results{Vieira, 2003 #1} of the implementations and include all the scenarios with their different shapes, we worked out an average of energy reduction for both the proposed and RDP algorithm which is presented in Fig. 23. According to this Figure, on average, RDP and our proposed algorithms reduced energy consumption by 55.7% and 72.3% respectively. This amount of energy reduction was due to the better performance of the proposed algorithm in reducing the number of points of the original shape. Our proposed algorithm, therefore, performed almost 17% better than the last solution in tackling the problem of irregular shapes.

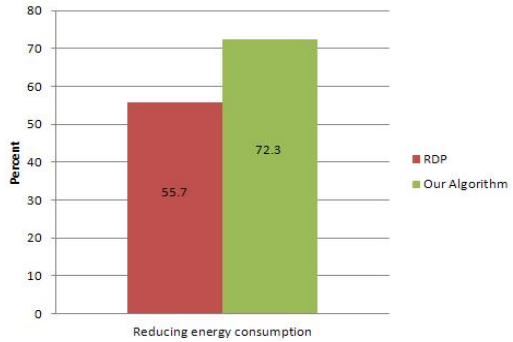

Fig. 23: Comparing RDP and the proposed algorithm in all the scenarios in terms of reducing energy consumption

We calculated the average of carelessness parameter in the implementations. As Fig. 24 shows, RDP algorithm responded to the queries with on average 11.3% carelessness. This level of carelessness in the previous works which used RDP algorithm remained the same.

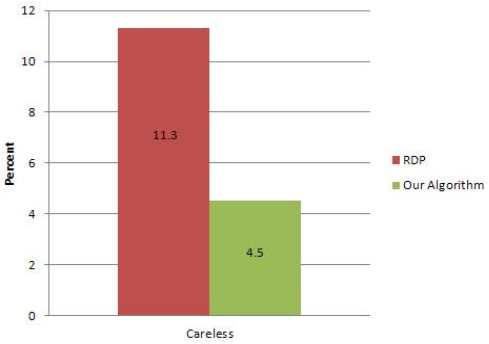

Fig. 24: comparing RDP and the proposed algorithm in the scenarios in terms of carelessness percentage.

However, our proposed algorithm could respond to queries with 4.5% carelessness. This lesser degree of carelessness was due to a more accurate simplification by our algorithm since fewer wrong areas were added and subtracted from the shape. This 4.5% degree of carelessness against 72.3% energy reduction can be ignored.

The most important achievement of this research is presenting an spatial query mechanism in sensor network that, when confronted with irregular areas, can have the best performance and, with the lowest degree of energy consumption, respond to queries. With respect to lesser energy consumption and maximised network lifetime, it can respond to more queries so that more human lives could be saved at times of crisis.

In future researches we can improve the quadrilateral merging phase because in this research we merged the quadrilaterals in columns and in horizontal rows. Since the number of quadrilaterals is high, there are numerous ways to merge them, while only the best one ought to be selected so that we can experience the highest reduction if the number of points. Using genetic algorithm is recommended. The next stage which has the potential to be improved is the act of determining whether the quadrilaterals are inside or outside the shape. If two angles of the quadrilateral are inside the shape, we consider it as inside, which is not very accurate though. If we can decide on the part of the quadrilateral which falls inside the shape, carelessness decreases.

References

[1] J. Löffler, J. Schon, V. Hernandez-Ernst, J. Pottebaum, and R. Koch, "Intelligent use of geospatial information for emergency operation management," in Proceedings of the fourth international conference on information systems for crisis management, ISCRAM, 2007.

[2] A. Soheili, V. Kalogeraki, and D. Gunopulos, "Spatial queries in sensor networks," in Proceedings of the 13th annual ACM international workshop on Geographic information systems, 2005, pp. 61-70.

[3] M. Careem, C. De Silva, R. De Silva, L. Raschid, and S. Weerawarana, "Demonstration of Sahana: free and open source disaster management," in Proceedings of the 8th annual international conference on Digital government research: bridging disciplines & domains, 2007, pp. 266-267.

[4] P. K. Chitumalla, D. Harris, B. Thuraisingham, and L. Khan, "Emergency response applications: dynamic plume modeling and real-time routing," IEEE Internet Computing, vol. 12, pp. 38-44, 2008.

[5] M. A. M. Vieira, C. N. Coelho, D. da Silva, and J. M. da Mata, "Survey on wireless sensor network devices," in Emerging Technologies and Factory Automation, 2003. Proceedings. ETFA'03. IEEE Conference, 2003, pp. 537-544.

[6] J. Yick, B. Mukherjee, and D. Ghosal, "Wireless sensor network survey," Computer Networks, vol. 52, pp. 2292-2330, 2008.

[7] J. Zheng and A. Jamalipour, Wireless sensor networks: a networking perspective: John Wiley & Sons, 2009.

[8] S. R. Madden, M. J. Franklin, J. M. Hellerstein, and W. Hong, "TinyDB: an acquisitional query processing system for sensor networks," ACM Transactions on database systems (TODS), vol. 30, pp. 122-173, 2005.

[9] Z. Can and M. Demirbas, "A survey on in-network querying and tracking services for wireless sensor networks," Ad Hoc Networks, vol. 11, pp. 596-610, 2013.

[10]J. Gehrke and S. Madden, "Query processing in sensor networks," IEEE Pervasive Computing, vol. 3, pp. 46-55, 2004.

[11]A. Coman, M. A. Nascimento, and J. Sander, "A framework for spatio-temporal query processing over wireless sensor networks," in Proceeedings of the 1st international workshop on Data management for sensor networks: in conjunction with VLDB 2004, 2004, pp. 104-110.

[12]Google map - a desktop web mapping service. Available: https://maps.google.com

[13]W. R. Tobler, "AN EXPERIMENT IN THE COMPUTER GENERALIZATION OF MAPS," DTIC Document1964.

[14]A. H. Robinson, J. Morrison, P. C. Muehrcke, A. Kimerling, and S. Guptill, "Elements of cartography, john wiley&sons," Inc., New York, USA, 1995.

[15]P. S. Heckbert and M. Garland, "Survey of polygonal surface simplification algorithms," DTIC Document1997.

[16]D. H. Douglas and T. K. Peucker, "Algorithms for the reduction of the number of points required to represent a digitized line or its caricature," Cartographica: The International Journal for Geographic Information and Geovisualization, vol. 10, pp. 112-122, 1973.

[17]U. Ramer, "An iterative procedure for the polygonal approximation of plane curves," Computer graphics and image processing, vol. 1, pp. 244-256, 1972.

[18]T. Gökgöz, A. Sen, A. Memduhoglu, and M. Hacar, "A New Algorithm for Cartographic Simplification of Streams and Lakes Using Deviation Angles and Error Bands," ISPRS International Journal of Geo-Information, vol. 4, pp. 2185-2204, 2015.

[19]P. Chandrasekara, T. Mahaulpatha, D. Thathsara, I. Koswatta, and N. Fernando, "Landmarks based route planning and linear path generation for mobile navigation applications," Spatial Information Research, pp. 1-11, 2016.

[20]M. Lucena, J. M. Fuertes, A. L. Martinez-Carrillo, A. Ruiz, and F. Carrascosa, "Efficient classification of Iberian ceramics using simplified curves," Journal of Cultural Heritage, vol. 19, pp. 538-543, 2016.

[21]A. Jelinek, L. Zalud, and T. Jilek, "Fast total least squares vectorization," Journal of Real-Time Image Processing, pp. 1-17, 2016.

[22]R. I. da Silva, D. F. Macedo, and J. M. S. Nogueira, "Duty cycle aware spatial query processing in wireless sensor networks," Computer Communications, vol. 36, pp. 149-161, 2013.

[23]W. Li, Y. Li, P. Yu, J. Gong, and S. Shen, "The Trace Model: A model for simulation of the tracing process during evacuations in complex route environments," Simulation Modelling Practice and Theory, vol. 60, pp. 108-121, 2016.

[24]R. I. da Silva, V. D. D. Almeida, A. M. Poersch, and J. M. S. Nogueira, "Spatial query processing in wireless sensor network for disaster management," in 2009 2nd IFIP Wireless Days (WD), 2009, pp. 1-5.

[25]N. Fernández-García, L. D.-M. Martínez, A. Carmona-Poyato, F. Madrid-Cuevas, and R. Medina-Carnicer, "A new thresholding approach for automatic generation of polygonal approximations," Journal of Visual Communication and Image Representation, vol. 35, pp. 155-168, 2016.

[26]R. I. Da Silva, D. F. Macedo, and J. M. S. Nogueira, "Spatial query processing in wireless sensor networks–A survey," Information Fusion, vol. 15, pp. 32-43, 2014.

[27]W.Cao, Y. Li, "DOTS: An online and near-optimal trajectory simplification algorithm",Systems and Software, Vol 126, Pages 34–44, 2017.

[28] V. Canellidis, J. Giannatsis, V. Dedoussis "Evolutionary Computing and Genetic Algorithms: Paradigm Applications in 3D Printing Process Optimization", Intelligent Computing Systems
Vol 627 , pp 271-298, 2016.

[29]"MATLAB - Simulink-Mathematical Software."

Mohammad Shakeri received the B.Sc. degree in Islamic Azad university of Neyshabur, Neyshabur, Iran, in 2011. He received the M.Sc. degree in software engineering from Khorasan Razavi,Neyshabur, Science and Research branch, Islamic Azad university, Neyshabur, Iran, in 2016. He is currently work in Department of Information Technology in blood transfusion organization of Khorasan Razavi . His area research interests include Computer Networks, Wireless Sensor Networks and Image Processing. His email address is: Alborz.corp@gmail.com

Sayyed Majid Mazinani was born in Mashhad, Iran on 28 january 1971. He received his Bachelor degree in Electronics from Ferdowsi University , Mashhad, Iran in 1994 and his Master degree in Remote Sensing and Image Processing from Tarbiat Modarres University, Tehran, Iran in 1997. He worked in IRIB from 1999 to 2004. He also received his phD in Wireless Sensor Networks from Ferdowsi University , Mashhad, Iran in 2009. He is currently assistant professor at the faculty of Engineering in Imam Reza International University, Mashhad, Iran. He was the head of Department of Electrical and Computer Engineering from 2009 to 2012. His research interests include Computer Networks, Wireless Sensor Networks and Smart Grids.

Node Classification in Social Network by Distributed Learning Automata

Ahmad Rahnamazadeh
Department of Electrical Engineering, Qazvin branch, Islamic Azad University, Qazvin, Iran
rahnamazade@gmail.com
Mohammad Reza Meybodi*
Department of Electrical Engineering, Amirkabir University, Tehran, Iran
mmeybodi@aut.ac.ir
Masoud Taheri Kadkhoda
Department of Electrical Engineering, Qazvin branch, Islamic Azad University, Qazvin, Iran
Taheri.masood@gmail.com

Received: 07/Sep/2016 Revised: 14/Nov/2016 Accepted: 05/Des/2016

Abstract

This paper presented a multiple Distributed Learning Automata (DLA) random walk model for node classification on a social network task. The purpose of this work is to improve the accuracy of node classification in social network by using of DLA. When dealing with large graphs, such as those that arise within the context of online social networks, a subset of nodes may be labeled. These labels can indicate demographic values, interest, beliefs or other characteristics of the nodes. A core problem is to use this information to extend the labeling so that all nodes are assigned a label.

Due to the high accuracy of local similarity measures, in the proposed algorithms, we will use them to build the transition matrix. As a standard in social network analysis, we also consider these networks as graphs in which the nodes are connected by edges and the transition matrix is used as weight value of edges. Now we partition this graph according to labeled nodes. Every sub-graph contains one labeled node along with the rest of unlabeled nodes. Then corresponding DLA on each partition. In each sub-graph we find the maximal spanning tree by using of DLA. Finally, we assign label by looking at rewards of learning automata. We have tested this algorithm on three real social network data sets. The result of Experiments show that the expected accuracy of a presented algorithm is achieved.

Keywords Social Network, Classification, Distributed Learning Automata, Node Labeling, Local Similarity Measure.

1. Introduction

The rise of online social networks in the past decade leads to generate more information to the people, ideas and their thoughts. Much of this information can be a model by labels that related with the people. These labels contain diverse information of nodes such as age, location, religion idea and etc.

Node classification in a social network in fact, assigns a label for unlabeled nodes from set of labels. There are many new applications for this kind of labeling, such as:

- Suggesting new connections or contacts to individuals, based on finding others of similar interests, demographics, or experiences.
- Recommendation system is to suggest objects (music, movies, and activities) based on the interests of other individuals with overlapping characteristics.
- Question answering systems which direct questions to those with the most relevant experience to a given question.
- Advertising systems is, which show advertisements to those individuals most likely to be interested and receptive to advertising on a particular topic.
- Sociological study is of communities, such as the extent to which communities form around particular interests or affiliations.
- Epidemiological study of how ideas and "memes" spread through communities over time.

Of course, these are just a few examples of the many different ways social network data is of interest to businesses, researchers, and operators of social networks. They have in common the aspect that knowing labels for individuals is a key element of each application.

So far, other methods are presented in two categories: iterative classification and random walk. The first category methods are based on iterative classification. Between researchers that have been done in this area, we can mention Neville and Jensen [1]. They originally used a Naive Bayesian classifier to derive labels in their instantiation of the ICA framework. An important special solution is the method of Macskassy and Provost[2], who used a simpler classification method based on taking a weighted average of the class probabilities in the neighborhood (effectively "voting" on the label to assign). Bhagat et al [3] proposed a method that considers the labeled nodes in the entire graph. This can be viewed as an instance of ICA using a nearest neighbor classifier to find a labeled node that is most similar to an unlabeled

* Corresponding Author

node being classified. Chakrabarti et al. in their method used features from neighboring documents to aid the classification, which can be viewed as an instance of ICA on a graph formed by documents [4].

The second category method is based on random walk. The node classification method of Zhu et al. [5] was proposed within the context of semi-supervised learning, where a symmetric weight matrix W is constructed using Eq. (1). More generally, we consider it to take as input graph $G(V,E,W)$, from which we derive the matrix $T = D^{-1}W$. Nodes $V_l$have initial labels $Y_l$from the label set Y.

$$w_{ij} = \exp(-\frac{\|v_i - v_j\|^2}{2\sigma^2}) \quad (1)$$

Jaakkola and Szummer [6] considered the variation where the labeled nodes are not forced to be absorbing states. A recently proposed method by Zhou et al. [7] considers partitioning a graph based on both structural and attribute similarity of nodes on the graph. A central example is the work by Kleinberg and Tardos that describes the problem of Metric Labeling [8]. A different approach studied by McSherry is to use spectral methods (study of eigenvalues and eigenvectors) to recover a labeling [9]. Goldberg et al. make the observation that nodes may link to each other, even if they do not have similar labels [10]. Leskovec et al. [11] study the problem of classifying edges as positive and negative through the lens of two theories from social science literature: Balance and Status. Goyal et al. [12] studied a problem of edge labeling with applications such as viral marketing, where it is useful to know the influence that a user has on his neighbors. XiaohuaXu et al. [13] proposed algorithm based on multiple ant colonies for node classification. HuanXu et al. [14] presented a model by name of a factor graph. This model created a hidden graph model from main transition graph. In this model type of relation between nodes depend on direct or undirected relation in a transition graph. In continue they classified node with a loopy back propagation algorithms.

2. Problem Definition

Social network is defined by a graph $G = (V,E,W,Y)$, where V is set of nodes, E is set of edges that shown a relation between nodes in social network, W is weight matrix then shown similarity between nodes (more similarity, more weight) and Y is set of label of nodes. This label can be age, sex and other profile information and or other singed such as favorites.

In the classification in social network problem, we are given a graph $G(V, E, W)$ with a subset of nodes $V_l \subset V$ labeled, where V is the set of n nodes on the graph (possibly augmented with other features), and $V_u = V - V_l$ is the set of unlabeled nodes. Here W is the weight matrix, and E is the set of edges. Let Y be the set of m possible labels, and $Y_l = \{y_1, y_2, \ldots, y_l\}$ be the initial labels on nodes in these V_l. The task is to infer label's Y on all nodes V of the graph.

Let $Y_l = \{y_1, y_2, \ldots, y_l\}$ be the initial labels from the label set Y, on nodes in the set V_l.

For clarity, we provide some illustrative example of how (social) network data may be captured by a variety of choices of graph models:

Example: As an example of a different kind os a network, consider the picture and video sharing website, Flickr. Let graph $G(V,E,W)$ represent the Flickr user network, where:

- **Nodes V**: A node $v_i \in V$ represents a user.
- **Edges E**: An edge $(i,j) \in E$ between two nodes v_i, v_j could be an explicit link denoting subscription or friend relation; alternately, it could be a derived link where v_i, v_j are connected if the corresponding users have been co-viewed more than a certain number of picture or videos.
- **Node Labels Y**: The set of labels at a node may include the user's demographics (age, location, gender, occupation), interests (hobbies, movies, books, pictures), a list of recommended videos extracted from the site, and so on.
- **Edge Weights W**: The weight of an edge could indicate the strength of the similarity, could be created from local similarity measure, denoting subscription or friend relation.

3. Learning Automata and Distributed Learning Automata

3.1 Learning Automata

A learning automaton is an adaptive decision-making unit that improves its performance by learning how to choose the optimal action from a finite set of allowed actions through repeated interactions with a random environment. The action is chosen at random based upon a probability distribution kept over the action-set and at each instant, the given action is served as the input to the random environment. The environment responds to the taken action in turn with a reinforcement signal. The action probability vector is updated based upon the reinforcement feedback from the environment. The objective of a learning automaton is to find the optimal action from the action-set so that the average penalty received from the environment is minimized [15]. The environment can be described by a triple $E \equiv \{\alpha, \beta, c\}$ where a $\alpha \equiv \{\alpha_1, \alpha_2, \ldots, \alpha_r\}$ represents the finite set of inputs (actions), $\beta \equiv \{\beta_1, \beta_2, \ldots, \beta_r\}$ denotes the set of values can be taken by the reinforcement signal, and $c \equiv \{c_1, c_2, \ldots, c_r\}$ denotes the set of the penalty probabilities is called penalty set. If the penalty probabilities are constant, the random environment is said to be a stationary random environment, and if they vary with time, the environment is called a non-stationary

environment. The environments depending upon the nature of the reinforcement signal b can be classified into P-model, Q-model and S-model. The environments in which the reinforcement signal can only take two binary values 0 and 1 are referred to as P-model environments. Another class of the environment allows a finite number of the values within the interval $[0, 1]$ can be taken by the reinforcement signal. Such an environment is referred to as Q-model environment. In S-model environments, the reinforcement signal lies in the interval $[a, b]$. The relationship between the learning automaton and its random environment has been shown in Fig. (1).

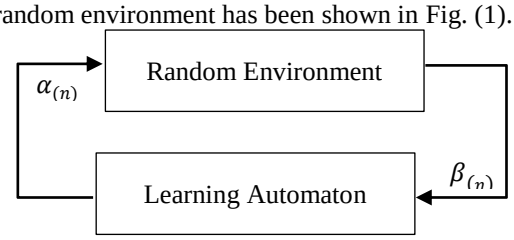

Fig. 1: The relationship between the learning automaton and its random environment

Learning automata can be classified into two main families: fixed structure learning automata and variable structure learning automata. Variable structure learning automata is represented by a quadruple $\mathrm{LA} \equiv \{\alpha, \beta, \mathrm{p}, \mathrm{T}\}\}$ where $\beta \equiv \{\beta_1, \beta_2, \dots, \beta_r\}$ is the set of inputs, $\alpha \equiv \{\alpha_1, \alpha_2, \dots, \alpha_r\}$ is the set of actions, $\mathrm{T} \equiv \mathrm{p(n+1)} = \mathrm{T}[\alpha(\mathrm{n}), \beta(\mathrm{n}), \mathrm{p(n)}]$ is learning algorithm, and $\mathrm{p} \equiv \{\mathrm{p}_1, \mathrm{p}_2, \dots, \mathrm{p}_r\}$ is the Action probability vector. The learning algorithm is a recurrence relation which is used to modify the action probability vector. Let $\alpha(\mathrm{k})$ and $\mathrm{p(k)}$ denote the action chosen at instant k and the action probability vector on which the chosen action is based, respectively. The recurrence equation shown by (2) and (3) is a linear learning algorithm by which the action probability vector p is updated. Let $\alpha_i(\mathrm{k})$ be the action chosen by the automaton at instant k. The action probabilities are updated as given in Eq. (2), when the chosen action is rewarded by the environment (i.e., $\beta(\mathrm{n}) = 0$). When the taken action is penalized by the environment, the action probabilities are updated as defined in Eq. (3) (i.e., $\beta(\mathrm{n}) = 1$).

$$p_i(n+1) = \begin{cases} p_i(n) + a.\left(1 - p_i(n)\right) & \alpha(n) = \alpha_i \\ p_j(n) - a.p_j(n) & \alpha(n) = \alpha_i \ \forall j \ j \neq i \end{cases} \quad (2)$$

$$p_i(n+1) = \begin{cases} (1-\mathrm{b}).p_i(n) & \alpha(n) = \alpha \\ \frac{b}{r-1} + (1-\mathrm{b}).p_j(n) & \alpha(n) = \alpha_i \ \forall j \ j \neq i \end{cases} \quad (3)$$

Where r the number of actions is can be chosen by the automaton; a and b denoted the reward and penalty parameters and determined the amount of increases and decreases of the action probabilities, respectively. If $a = b$, the recurrence Eq. (2) and Eq. (3) are called linear reward-penalty (L_{RP}) algorithm, if $a \gg b$ the given equations are called linear reward-e penalty ($L_{R\varepsilon P}$), and finally if $b = 0$ they are called linear reward-inaction (L_{RI}). In the latter case, the action probability vectors remain unchanged when the taken action is penalized by the environment.

3.2 Distributed Learning Automata

A distributed learning automata (DLA) is a network of the learning automata which collectively cooperated to solve a particular problem. Formally, a DLA can be defined by a graph $\mathrm{DLA} = (\mathrm{V}, \mathrm{E})$, T and A_0, where $\mathrm{V} = \{\mathrm{LA}_1, \mathrm{LA}_2, \dots, \mathrm{LA}_n\}$ is the set of learning automata, $\mathrm{E} \subset \mathrm{V} \times \mathrm{V}$ is the set of the edges in which edge e_{ij} corresponds to the action e_j of the automaton LA_i, T is the set of learning schemes with which the learning automata updated their action probability vectors, and A_1 is the root automaton of DLA from which the automation activation is started. An example of a DLA has been shown in Fig. (2). LA_j is activated when action j of LA_i is selected. The number of actions for LA_i equal with a number of outgoing edge from node LA_i.

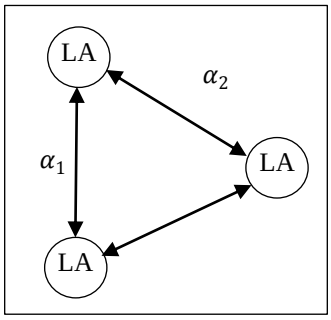

Fig. 2: Distributed learning automata

4. Distributed Learning Automates Random Walk

4.1 Similarity Matrix by Local Measure

Due to the good results of local similarity measures in various articles, in this paper we use, eight measures base on common friends or common relation to create a transition matrix. In continue we describe eight measures that used for this article and other articles.

Jaccard Coefficient: This coefficient one of the popular measures in a data recovery field [16, 17]. This coefficient defined as a ratio of a common friends in a union of a friend for two nodes. Equation of a coefficient shown in Eq. (4).

$$JC(x, y) = |\Gamma(x) \cap \Gamma(y)| / |\Gamma(x) \cup \Gamma(y)| \quad (4)$$

Where $\Gamma(\mathrm{x})$ is the number of a friend for node x.

Adamic/Adar Index: This measure is useful for find a relation between webpages, and is linked with a common features of two webpages [17, 18]. Equation of this index shown in Eq. (5).

$$AA(x,y) = \sum_{z \in \Gamma(x) \cap \Gamma(y)} \frac{1}{\log |\Gamma(z)|} \quad (5)$$

Where $\Gamma(z)$ is outgoing of a common friends between nodes x, y.

Hub promoted index: This measure is used for determine to overlap between two nodes [19]. This index defines as a ratio of a common friends to a minimum of friends between two nodes. Equation of this index shown in Eq. (6).

$$PI(x,y) = |\Gamma(x) \cap \Gamma(y)| / \min(|\Gamma(x)|, |\Gamma(y)|) \quad (6)$$

Hub depressed index: This measure is the same before at with difference that the denominator is the maximum of friends between two nodes [20]. Equation of this index shown in Eq. (7).

$$HDI(x,y) = |\Gamma(x) \cap \Gamma(y)| / \max(|\Gamma(x)|, |\Gamma(y)|) \quad (7)$$

Link weight: this measure containing two measures first sum of weight and second product of weight [20]. At the first for each node, edge weights were calculated separately according to Eq. (8). Then link weight calculated as summation or production of two node weight (Eq. (9) and Eq. (10)).

$$(x) = \frac{1}{\sqrt{1+\Gamma(x)}}, w(y) = \frac{1}{\sqrt{1+\Gamma(y)}} \quad (8)$$

$$SW(x,y) = w(x) + w(y) \quad (9)$$

$$PW(x,y) = w(x) \times w(y) \quad (10)$$

Salton index: This measure defines as a ratio number of common friend to geometric mean of each node friends [17]. Equation of this index shown in Eq. (11).

$$SI(x,y) = |\Gamma(x) \cap \Gamma(y)| / \sqrt{|\Gamma(x)|.|\Gamma(y)|} \quad (11)$$

Sorenson index: This measure define as ratio number of common friends to arithmetic mean of each node friends [17]. Equation of this index shown in Eq. (12).

$$SI(x,y) = |\Gamma(x) \cap \Gamma(y)| / \sqrt{|\Gamma(x)|.|\Gamma(y)|} \quad (12)$$

In this study, we use measures defined above for create the transition matrix.

4.2 General Description of Proposed Algorithm

In this proposed algorithm, at first we use graph partitioning: each sub-graph containing labeled node and set of an unlabeled nodes. Now for each sub-graph is a corresponding network of distributed learning automata. Set of action for each automata is equally to be out-degrees of a node. In addition for better convergence, we let automates use the transition matrix value as the initial probability vector. Our object is achieved to be maximal spanning tree in each sub-graph**.**

In each sub-graph labeled node as root and random select any action from action set. This choice of action has two consequences:

1: activated automata on another side selected action and put the activated automata in an active group.

2: inactive selected action on another automata for avoid cycle in a graph

This trend continues to get all the automaton in the active group. Finally if cost of a tree improved, considers its environment as favorable response and all automata in a tree rewarded. Otherwise, all automata is fined. We use linear reinforcement learning in proposed algorithm. When the chosen action is rewarded by the environment, the action probabilistic update as given in Eq. (1) and when the chosen action is penalized by the environment, the action probabilistic update as given in Eq. (2).

Because of being inactive some action of automata for avoid of a cycle in a sub-graph, before selected one action, probabilistic vector divided to a summation possibility of active actions. This subject is shown in Eq. (13).

$$p_i = prob[\alpha(n) = \alpha_i | V(n),\ \alpha_i \in v(n)] = \frac{p_i(n)}{K(n)} \quad (13)$$

Where $V(n)$ is set of active action's automata.

In the end of each iterative, we update the probabilistic action's vector because of activating, inactive action. This subject is shown in Eq. (14) and Eq. (15).

$$p_j(n+1) = p_j(n+1)K(n) \quad \text{for all j}, \alpha_j \in \text{V(n)} \quad (14)$$

$$p_j(n+1) = p_j(n) \quad \text{for all j}, \alpha_j \notin \text{V(n)} \quad (15)$$

The finishing condition of an algorithm achieved the product of weight selected tree edge to a threshold. In final unlabeled node given the label of winner automata (the most of acquired rewarded).

The general idea of our proposed algorithm is illustrated in Fig. (3), Fig. (4)

In the algorithm of Fig. (4) X_m is set of a labeled nodes and Y_m is set of labels. The target of algorithm is assigned labels to X_u from set of Y_m . P is a transition matrix calculated with LSM in section (4-1). For each sub-graph contains one labeled node as root and all other unlabeled nodes, finding MST by network of learning automata according to the algorithm Fig. (3).

Input: The node label l and a sub-graph G_l $=(V,E,Q^t_l)$, where V , Q^t_l is the probabilistic rule at generation t

Output: V_{new} and E_{new} , which describe a DLA; ΔR, wich is used for reward update

1. $V_{new} \leftarrow \{v_l\}$, where v_l is the labled node (root node) from V, $E_{new} \leftarrow \emptyset$.
2. **repeat**
3. Choose an edge (v_j,v_k) randomly by action probability vector of automata (value in Q^t_l probability) such that $v_j \in V_{new}$ and v_k is not. (LA on v_k is active)
4. Remove all edge connected to v_j (For avoid cycle in graph)
5. Add v_k to V_{new} and to E_{new}

Fig. 3: ALGORITHM: Finding Maximal Spanning Tree With DLA

Input: training set (X_m,Y_m), test set X_u
Output: Y_u

1. Initialize parameters;
2. Compute P according to Similarty Indexes
3. Construct sub-graph G
4. While termination conditions is not met Do
5. For each node v_l do
6. Crawled out recording path form root to unlabeled nodes (Algorithm Fig .(3))
7. Traverse this tree and update Reward $R(:,l)$ (if improved weight of tree)
8. Update P Accroding to Learning Algorithm
9. End for
10. End while
11. Assign labels to Y_u according to R

Fig. 4: ALGORITHM: Classifier of DLA Maximal Spanning Tree

To give a better explanation of the above algorithm, we show the detailed process based upon the example of Fig. (5).

V1 and V2 are a labeled nodes (White nodes) and V3, V4, V5 is an unlabeled nodes (Dark nodes). So we partition this graph to two sub-graph with root labeled node V1, V2 shown in Fig. (6), Fig. (7). Two DLA is assigned to sub-graphs DLAa, DLAb. Weight of each edge is calculated with Local Similarity Measure in section (4-1). Now in each sub-graph finding MST with labeled node as root vertex, by DLA and dividing reward and penalty to LA's in each DLA (Algorithm Fig. (3)). After initial generation of automata random walk, each unlabeled vertex will be attached by two kinds of rewards, and their intensities are given according to ΔR1: and ΔR2:. Fig. (7) Exactly illustrates the reward increments on the entire unlabeled graph after first generation. Both kinds of reward increment are computed according to their generated MSTs and the equation proposed. For example, in this sample in a vertex V3, kind of automata in DLAa is a dominant ($\Delta R_{13} > \Delta R_{23}$) then assign label V1 for V3 and likewise for the rest.

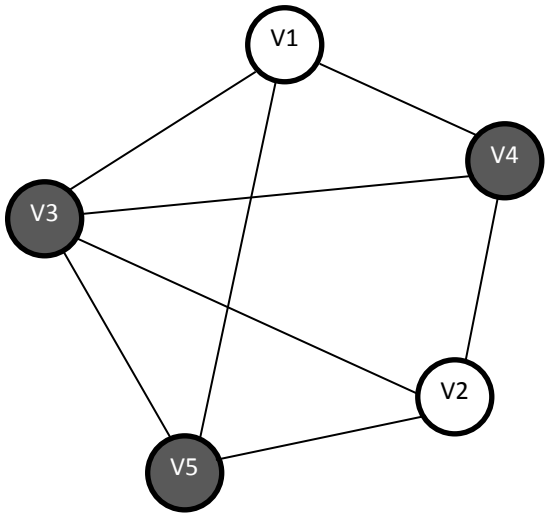

Fig. 5: A simple social network graph with 5 node and relation between

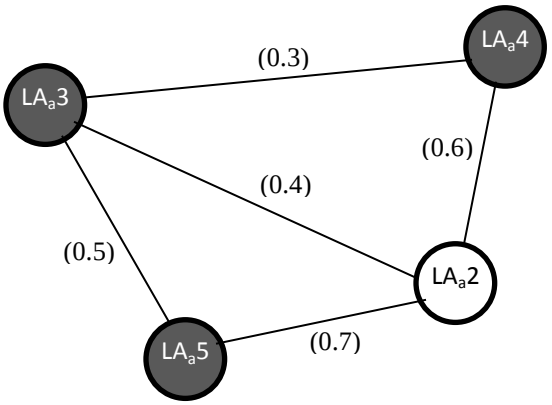

Fig. 6: Sub-graph with DLA_a and weight of relation by root V_2

4.3 Definition of Reward Matrix

In order to keep the rewards of belonging to each automaton, we use the matrix of rewards. Value of each column in our matrix is shown total rewards of each type learning automata. Value of each row in our matrix is shown total rewards of each labeled node for all types of learning automata. In another side equation in Eq. (16) shown reward of learning automate type l on unlabeled node I in tth iterative.

$$R_{il}^{t} = R^{t}(j,l) \quad (16)$$

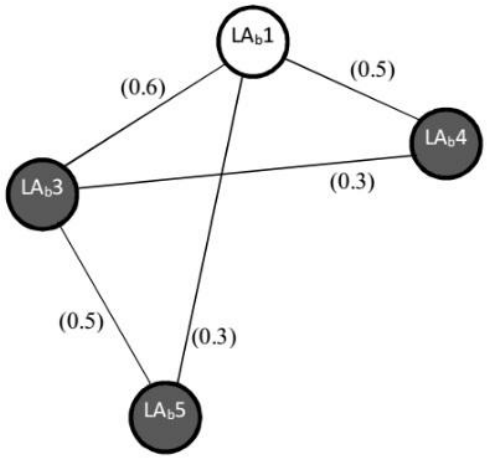

Fig. 7: Sub-graph with DLA_b and weight of relation by root V_1

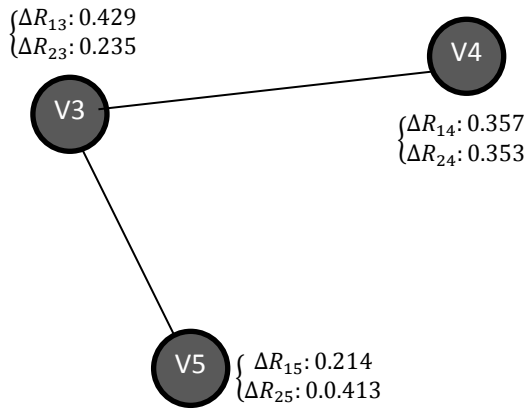

Fig. 8: Reward increment of each vertex after first generation of automata activation

4.4 Integrated Probabilistic Transition Rule

In the end of each iterative and activate every automata in per sub graph, if cost of a tree improved, considers its environment as favorable response and every automata in a tree rewarded. Otherwise, all automats is penalized. We use linear reinforcement a learning algorithm in proposed method.

5. Experiments

5.1 Test Datasets

The four data sets are obtained for experiment. First, data set publicly available from the SNAP data repository, Second and third data set getting from Network Economic group and related MySpace, Netlog social networks and fourth data set derived from Flickr social network by Elena Zheleva and Lise Getoor [21]. Detailed information is provided in Table (1).

Table 1: Used Dataset Detail

Dataset Name	*Number of Node*	*Number of Class*
Organization Network	46	7
Myspace	621	39
Netlog	1484	52
Flicker	14451	55

5.2 Test Results

We decided to node classification on four data set with various percentages of unlabeled node and local similarity measures. You can see the accuracy of probable label assigning in Table (2) to Table (5).

Table 2: Result of experiment by Organizational Network Dataset

		Percentage of initially known labels			
		50%	*67%*	*75%*	*80%*
Local similarity measure	Adamic/Adar	0.24	0.36	0.45	0.69
	Salton	0.27	0.47	0.45	0.67
	Sorenson	0.26	0.43	0.48	0.75
	Jaccard	0.34	0.42	0.55	0.79
	HPI	0.34	0.44	0.54	0.79
	HDI	0.31	0.40	0.56	0.76
	PW	0.37	0.40	0.52	0.85
	SW	0.39	0.47	0.58	0.92

Table 3: Result of experiment by Myspace Dataset

		Percentage of initially known labels			
		50%	*67%*	*75%*	*80%*
Local similarity measure	Adamic/Adar	0.25	0.35	0.44	0.73
	Salton	0.23	0.37	0.43	0.69
	Sorenson	0.28	0.40	0.45	0.73
	Jaccard	0.25	0.41	0.52	0.79
	HPI	0.31	0.42	0.58	0.81
	HDI	0.33	0.43	0.55	0.82
	PW	0.36	0.43	0.51	0.84
	SW	0.32	0.57	0.62	0.91

Table 4: Result of experiment by Netlog Dataset

		Percentage of initially known labels			
		50%	*67%*	*75%*	*80%*
Local similarity measure	Adamic/Adar	0.26	0.38	0.45	0.64
	Salton	0.24	0.40	0.41	0.62
	Sorenson	0.30	0.38	0.42	0.74
	Jaccard	0.29	0.39	0.44	0.73
	HPI	0.37	0.42	0.54	0.75
	HDI	0.26	0.43	0.49	0.78
	PW	0.33	0.43	0.64	0.88
	SW	0.32	0.56	0.64	0.9

Table 5: Result of experiment by Flickr Dataset

		Percentage of initially known labels			
		50%	67%	75%	80%
Local similarity measure	Adamic/Adar	0.25	0.36	0.40	0.61
	Salton	0.24	0.39	0.41	0.64
	Sorenson	0.31	0.38	0.44	0.74
	Jaccard	0.25	0.37	0.43	0.76
	HPI	0.28	0.41	0.58	0.76
	HDI	0.29	0.38	0.41	0.74
	PW	0.33	0.45	0.51	0.82
	SW	0.29	0.46	0.58	0.88

In another experiment on first dataset is attempted to modify a value of reward parameter and penalty parameter. A result of this experiment viewed in Fig. (3).

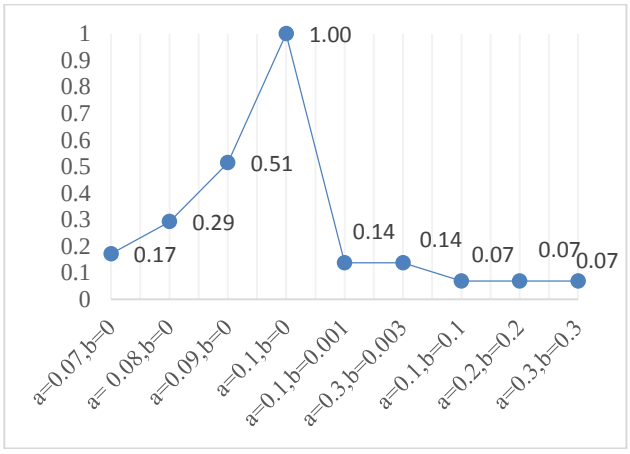

Fig. 9: Chart of change convergence rate with change reward and penalty parameter

Fig. (6) To Fig. (9) Show compare the accuracy of node classification between Multiple Ant Colony (MAC) [13], Factor Graph Model (FGM) [14] and our model with DLA on all datasets, with all local similarity measures. 80% of nodes are labeling in these experiments.

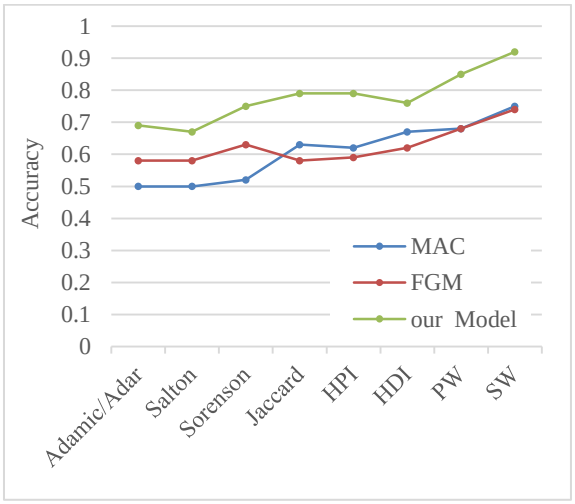

Fig. 10: Acuracy of node classification on Organizational Networks

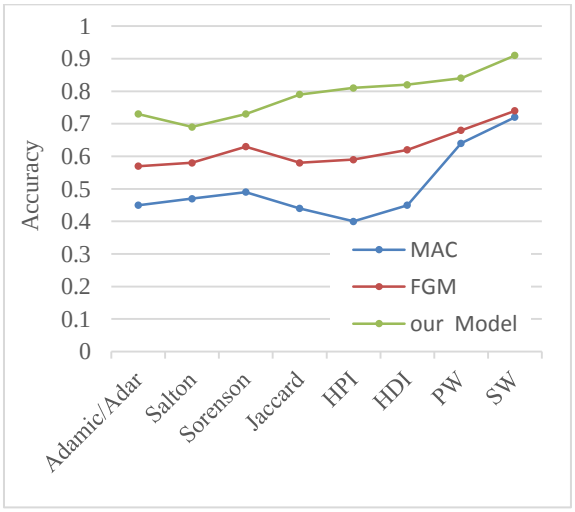

Fig. 11: Accuracy of node classification on Myspace

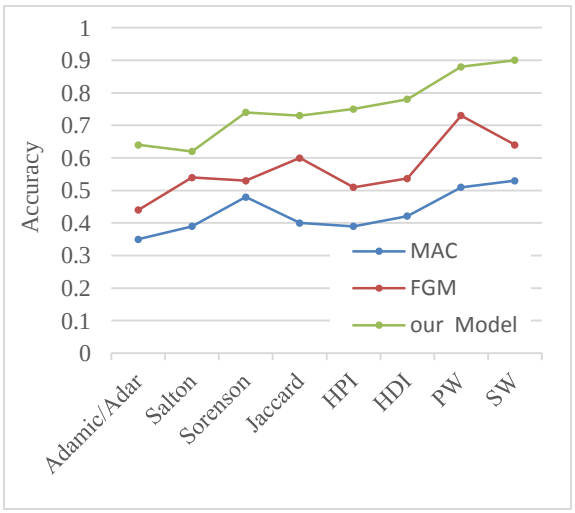

Fig. 12: Accuracy of node classification on Netlog

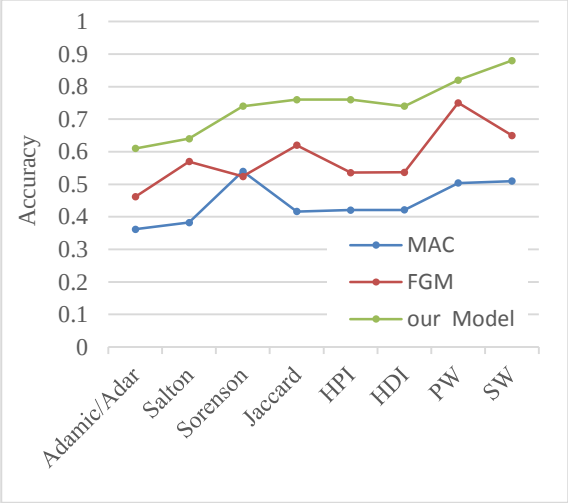

Fig. 13: Accuracy of node classification on Flickr

6. Conclusions

According to the result, the best of Local Similarity Measures is edge weight, and poor are Adamic/Adar. According to the Fig. (2) Convergence, rate is come down in L_{RP} and $L_{R\varepsilon P}$ .it shows that suboptimal behavior of learning automata in real environment preferred to optimal behavior. Also in L_{RI} the optimal value of a reward parameter is equal to 0.1. Convergence rate is come down with decrease or increase reward parameter. On an accuracy score, our model is more than better than others.

References

[1] J. Neville and D. Jensen, "Iterative classification in relational data," in Proc. AAAI-2000 Workshop on Learning Statistical Models from Relational Data, 2000, pp. 13-20.

[2] S. A. Macskassy and F. Provost, "A simple relational classifier," DTIC Document2003.

[3] S. Bhagat, I. Rozenbaum, and G. Cormode, "Applying link-based classification to label blogs," in Proceedings of the 9th WebKDD and 1st SNA-KDD 2007 workshop on Web mining and social network analysis, 2007, pp. 92-101.

[4] S. Chakrabarti, B. E. Dom, and P. Indyk, "Enhanced hypertext categorization using hyperlinks," ed: Google Patents, 2002.

[5] X. Zhu, Z. Ghahramani, and J. Lafferty, "Semi-supervised learning using gaussian fields and harmonic functions," in ICML, 2003, pp. 912-919.

[6] M. S. T. Jaakkola and M. Szummer, "Partially labeled classification with Markov random walks," Advances in neural information processing systems (NIPS), vol. 14, pp. 945-952, 2002.

[7] Y. Zhou, H. Cheng, and J. X. Yu, "Graph clustering based on structural/attribute similarities," Proceedings of the VLDB Endowment, vol. 2, pp. 718-729, 2009.

[8] J. Kleinberg and E. Tardos, "Approximation algorithms for classification problems with pairwise relationships: Metric labeling and Markov random fields," Journal of theACM (JACM), vol. 49, pp. 616-639, 2002.

[9] F. McSherry, "Spectral partitioning of random graphs," in Foundations of Computer Science, 2001. Proceedings. 42nd IEEE Symposium on, 2001, pp. 529-537.

[10] A.B.Goldberg, X. Zhu, and S. J. Wright, "Dissimilarity in graph-based semi-supervised classification," in International Conference on Artificial Intelligence and Statistics, 2007, pp. 155-162.

[11] J. Leskovec, D. Huttenlocher, and J. Kleinberg, "Predicting positive and negative links in online social networks," in Proceedings of the 19th international conference on World wide web, 2010, pp. 641-650.

[12] A. Goyal, F. Bonchi, and L. V. Lakshmanan, "Learning influence probabilities in social networks," in Proceedings of the third ACM international conference on Web search and data mining, 2010, pp. 241-250.

[13] X. Xu, L. Lu, P. He, Y. Ma, Q. Chen, and L. Chen, "Semi-supervised classification with multiple ants maximal spanning tree," in Web Intelligence (WI) and Intelligent Agent Technologies (IAT), 2013 IEEE/WIC/ACM International Joint Conferences on, 2013, pp. 315-320.

[14] H. Xu, Y. Yang, L. Wang, and W. Liu, "Node classification in social network via a factor graph model," in Pacific-Asia Conference on Knowledge Discovery and Data Mining, 2013, pp. 213-224.

[15] H. Beigy and M. R. Meybodi, "Utilizing distributed learning automata to solve stochastic shortest path problems," International Journal of Uncertainty, Fuzziness and Knowledge-Based Systems, vol. 14, pp. 591-615, 2006.

[16] M. Al Hasan and M. J. Zaki, "A survey of link prediction in social networks," in Social network data analytics, ed: Springer, 2011, pp. 243-275.

[17] C. A. Bliss, M. R. Frank, C. M. Danforth, and P. S. Dodds, "An evolutionary algorithm approach to link prediction in dynamic social networks," Journal of Computational Science, vol. 5, pp. 750-764, 2014.

[18] L. Adamic and E. Adar, "How to search a social network," Social networks, vol. 27, pp. 187-203, 2005.

[19] Y.-X. Zhu, L. Lü, Q.-M. Zhang, and T. Zhou, "Uncovering missing links with cold ends," Physica A: Statistical Mechanics and its Applications, vol. 391, pp. 5769-5778, 2012.

[20] W. Cukierski, B. Hamner, and B. Yang, "Graph-based features for supervised link prediction," in Neural Networks (IJCNN), The 2011 International Joint Conference on, 2011, pp. 1237-1244.
[21] E. Zheleva and L. Getoor, "To join or not to join: the illusion of privacy in social networks with mixed public and private user profiles," in Proceedings of the 18th international conference on World wide web, 2009, pp. 531-540.

Ahmad RahnamaZadeh received the M.Sc degree in Software Engineering from Faculty of Electrical and Computer Engineering in Qazvin Islamic Azad University. He already received his B.Sc. of Computer Engineering, Hardware Engineering, at Islamic Azad University of Qazvin, Iran. His research interests include Social Network Analysis, Machine Learning and Graph Theory

Mohammad Reza Meybodi received the B.Sc and M.Sc degrees in Economics from Shahid Beheshti University, Tehran, Iran, in 1973 and 1977, respectively. He also received the M.Sc and Ph.D. degrees from the Oklahoma University, USA, in 1980 and 1983, respectively, in Computer Science. Currently he is a Full Professor in Computer Engineering Department, Amirkabir University of Technology (Tehran Polytechnic), Tehran, Iran. Prior to current position, he worked from 1983 to 1985 as an Assistant Professor at the Western Michigan University, and from 1985 to 1991 as an Associate Professor at the Ohio University, USA. His research interests include channel management in cellular networks, learning systems, parallel algorithms, soft computing and software development.

Masoud Taheri Kadkhoda received the M.Sc degree in Artificial Intelligence from Faculty of Electrical and Computer Engineering in Qazvin Islamic Azad University and received his B.Sc. of Computer Engineering, Software Engineering, at Mazandaran University of Science and Technology, Iran.

Improving Accuracy, Area and Speed of Approximate Floating-Point Multiplication Using Carry Prediction

Marzie Fathi*
Faculty of Computer Engineering, Najafabad Branch, Islamic Azad University, Najafabad, Iran
fathi.marziye@gmail.com
Hooman Nikmehr
Department of Computer Architecture, University of Isfahan, Isfahan, Iran
nikmehr@eng.ui.ac.ir

Received: 27/Jul/2016 Revised: 31/Aug/2016 Accepted: 26/Sep/2016

Abstract

Arithmetic units are essential in digital circuit construction, and the enhancement of their operation would optimize the whole digital system. Among them, multipliers are the most important operational units and are used in a wide range of digital systems such as telecommunication signal processing, embedded systems, and mobile technology. The main drawback to a multiplication unit is its high computational load, which leads to considerable power consumption and an increased area of silicon. This also reduces the speed, which negatively affects the digital host functionality. Estimating arithmetic is a new branch of computer arithmetic implemented by discarding or manipulating a portion of arithmetic circuits and/or intermediate computations. Applying estimated arithmetic in arithmetic units would improve the speed, power consumption, and the implementation area by sacrificing a slight amount of result accuracy. This article develops and analyzes an estimated truncated floating-point multiplier for single precision operands that is capable of compensating for errors to a desired level by applying the least significant columns of the partial product matrix. These errors are caused by removing a number of carry digits in the partial product matrix which make a direct contribution to rounding the floating-point numbers. The evaluation results indicate that the proposed method improves speed, accuracy, and silicon area, in comparison with common truncated multiplication methods.

Keywords: estimated arithmetic; partial product matrix; rounding; truncated multiplier; error correction.

1. Introduction

Multipliers are one of the major arithmetic units commonly applied to digital systems like digital signal processing, telecommunication signal processing, embedded systems, and mobile systems. The major deficiency in these systems is their low speed, high power consumption, and high silicon-covered area, which cause a shortfall in digital system operation [1]. The Fast Fourier Transform (FFT) constitutes the basis of most telecommunication systems, like DVBT, UWB, WIMAX, WLAN, ADSL, and wireless telecommunication systems [2]. This function is implemented by multiplication and represents a complex function of products applied for converting the signal from frequency to time phase and vice versa.

$$x_k = \sum_{n=0}^{N-1} d_n . e^{\frac{j2\pi nk}{N}} \qquad k = 0, 1, 2, \cdots, N-1 \tag{1}$$

This function is applicable in telecommunication signal processing as well as image processing and digital signal processing. Optimized implementation of this block influences telecommunication systems with respect to speed and accuracy [3]-[4]. In addition to its multiplication or Multi-Accumulate (MAC) on some sources of Fused Multiply-Add (FMA), this function is a component other major arithmetical factors like Finite Impulse Response (FIR) [5], Discrete Cosine Transform (DCT) [5]-[6], and Multiple Input Multiple Output (MIMO) [7]. Consequently, any improvement in the multiplying algorithm would also contribute to both of these functions and to the telecommunication system in general.

In today's applications, where high-value calculation is of the essence, applying floating-point unit in FFT calculations and other telecommunication signal processing functions could be beneficial and efficient. In the recent past, the mentality and assumption was that floating-point has big area and high power; therefore, designs preferred to convert codes into fixed points or simulate floating-point functionality. This, of course, was a time-consuming and erroneous, with 30% of software design time attributed to it [8]. Nevertheless, this point is not always accurate , while applying optimized floating-point unit in telecommunication digital signal can even reduce energy consumption by 30% [9]-[10]. The focus of most research is now on approximated or estimated computations as a new approach in applications where the circuit would be able to generate inaccurate and faulty results. This approach is implemented by eliminating a portion of intermediate calculation. Although this function causes an increase in speed and a decrease in the silicon-covered area and power consumption, it slightly reduces arithmetic circuit accuracy [11]. Implementation of arithmetic units like multiplication have different methods. This counter, which replaces the common method and 3:2 counters, when using a 4:2 counter (four entry and two exit bits) in an 8×8 tree multiplier, is illustrated in Fig. 1. When all four bits are 1, an error

* Corresponding Author

occurs. In part (b) of Fig. 1, a reduction in multiplication, circuit capacity, and implementation time are observed [12].

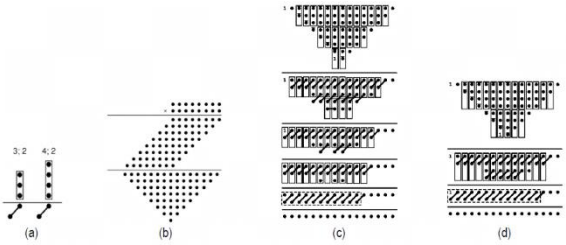

Figure.1. a) 4:2 and 3:2 counters, b) partial product generation in $(\mathbf{8}\times\mathbf{8})$-bit multiplier, c) the $(\mathbf{8}\times\mathbf{8})$ marked accurate multiplier using 3:2 counter, d) the$(\mathbf{8}\times\mathbf{8})$ estimated marked accurate multiplier using 4:2 counter[12]

The parallel truncated multiplier, developed in 1992 [13], was the first sample applied in estimated computing techniques and accepted in this field. In this method, eliminating the partial product LSP (Least Significant Part) matrix and keeping the MSP (Most Significant Part) section would lead to circuit area reduction. Of course, this phenomenon would generate error; so far, there exist no studies regarding removal of these errors [14]-[15].

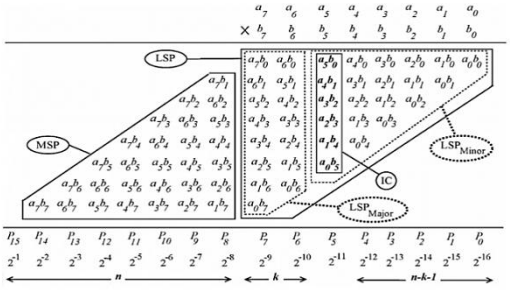

Figure. 2. The $(\mathbf{8}\times\mathbf{8})$ truncated multiplier and different elements of the partial product matrix for errror correction

Applying the LSP column of partial products to estimate the carry digit to MSP is another method that has been used in [16]-[17]. This method depends on multiplying the circuit entrance by a complicated estimating circuit but retaining accuracy. Here, we see implementation of a sequential estimated truncated floating-point digit at single precision, where the partial product of the matrix yield from the multiplication of mantissas of two digit floating-points are involved. By applying the four columns in LSP of the matrix and applying one small circuit for the carry digit estimation from the 5th column, the error is reduced in a significant manner and the outcome converges to the real value of multiplication.

In this article, the rounding of floating-point technique is introduced in Sec. 2, the combinational estimated multiplier is described in Sec. 3, the probability of maximum error is computed in Sec. 4, the proposed simulation method and its comparison with other states is addressed in Sec. 5, and the article is concluded in Sec. 6.

2. Rounding Floating –Point Numbers

Since 1990, floating-point numbers have been exhibited in accordance with IEEE 754-2008 standard. The two single and double precision widths are introduced for these numbers in this standard [1]. The partial product matrix generated from multiplying the mantissas by two floating-point digits at single precision is shown in Fig. 3. This product has 48 bits, but due to the standard limitations, only 24 MSP bits (23 bits of mantissas and one bit, the product of normalization) are held. To compensate for the error caused by eliminating the LSP bits, the rounding is performed by applying the three sticky (S), Gard (G) and Round (R) bits located in the LSP, calculated in accordance with Standard S from Eq. (2) [1].

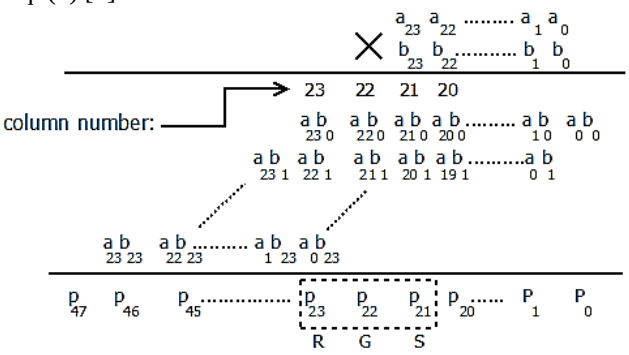

Figure. 3. Partial product matrix and the two mantissas floating-point digits at single precision

$$S = P_{21}\,\mathrm{OR}\,P_{20}\,\mathrm{OR}\ldots P_0 \tag{2}$$

3. Sequential Estimated Multiplier Capable of Error Compensation

3.1 Algorithm

Hardware implementation of this multiplier, including the 20 bits register A (for storing the 1st to 20th multiplicand), the 24 bits register B (for storing the multiplier), and 28 bits register P (for storing the product) with initial value of zero, is illustrated in Fig. 4. Since this multiplier is a sequential truncated to 28 bits and there is no need for the final response of the 20 LSP bits, the section of the circuit that computes these 20 LSP bits can be eliminated. To accomplish this, the 27 bits register, the Extended Register (Ex) with its initial value, is defined according to Eq. (3).

$$\begin{cases} Ex(3:0) = A(23:20) \\ A = A(19:0) \end{cases} \tag{3}$$

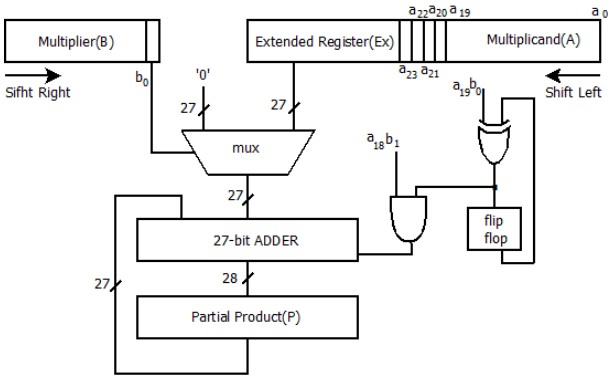

Figure. 4. Hardware implementation of multiplier, W4CE state

The operation of this multiplier is subject to the following steps:

1. In the first cycle, provided that the least significant bit of register *B* (b_0) is 1, the initial value of *EX* is added to *P* and the product is placed in *P*; otherwise, *P* holds its previous value.

$$P(i)=\begin{cases} P_{i-1}+Ex(i) & \text{if} \quad b_i=1 \\ P_{i-1} & \text{if} \quad b_i=0 \end{cases} \tag{4}$$

2. In every cycle *i*, first the *P* and *A* registers shift to the left by one bit and the exiting bit enters the *EX* register. Here, *B* shifts to the right by one bit.
3. In cycle *i*, step one is repeated 24 times until the last cycle yield is placed in *P*.

3.2 Error Compensating Circuit

As explained earlier, in the proposed multiplier, 20 columns have been eliminated from the LSP section of the partial product matrix, which in turn would lead to the elimination of the carry digit in this section, an error occurs. To compensate for this error, it should be estimated somehow; hence, what bits are involved in the creation of this carry digit should be known.

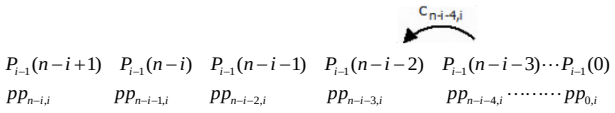

Figure. 5. Adding function in cycle i^{th} of partial product matrix

In this proposed method, this digit is estimated from the 19th column in cycle$i$ $(c_{n-i-4,i})$, three bits are required:

- The partial product created in the i^{th} cycle and at the $(n-i-4)^{th}$ space of $(pp_{n-i-4,i})$
- The intermediate total product in the $(i-1)^{th}$ cycle of $(P_{i-1}(n-i-3))$
- The carry generated in the i^{th} cycle and $(n-i-5)^{th}$ space of $(c_{n-i-5,i})$

These three elements are the entries of full adder; therefore, circuits must be designed that would receive these three entries and produce the $c_{n-i-4,i}$ and $P_{n-i-4,i}$ outputs. Since this proposed multiplier is of a sequential type and multiplication occurs in any part of the cycle, not all the above-mentioned entries are accessible. And among them, only $pp_{n-i-4,i}$ are accessible in every cycle and $c_{n-i-5,i}$ is the carry digit of the column adjacent, which in turn requires these three similar elements for its production and makes the circuit issue more complicated; for that reason, it is not considered. To compute $P_{i-1}(n-i-3)$, it can be said that this value in approximation is equal to the total of intermediate multiplication products in previous cycles, where the computation of function $c_{n-i-5,i}$ is not considered. Hence, to make a distinction between this estimated value and $P_{i-1}(n-i-3)$, it is presented as an accumulated value ($AV_{n-i-3,i-1}$) with a name change; that is, the total partial product must be protected in any cycle to allow access to $AV_{n-i-3,i-1}$. Here, a flip-flop with an initial value of 0 can be applied, the value of which in the i^{th} cycle would equal FF_i.

$$AV_{n-i-3,i-1}=FF_i=\begin{cases} 0 & \text{if} \quad i=0 \\ FF_{i-1}+pp_{n-i-3,i-1} & \text{if} \quad 0<i\le 20 \end{cases} \tag{5}$$

Equation 5 describes the total of two bits, for implementation of which a half adder could be applied. According to the descriptions above and the half-adder equation, the $c_{n-i-4,i}$ value can be obtained from Eq. (6-7).

$$AV_{n-i-3,i-3}=FF_i=FF_{i-1}\ \text{XOR}\ pp_{n-i-3,i-3} \tag{6}$$

$$c_{n-i-4,i}=AV_{n-i-3,i-1}\ \text{AND}\ pp_{n-i-4,i} \tag{7}$$

The implementation of this circuit is illustrated in Fig. 6, where ECV is the carry digit that is added to the 20th column in every cycle.

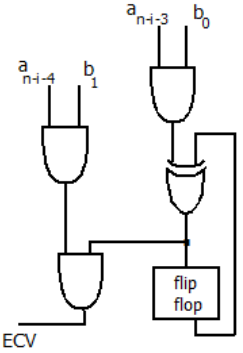

Figure. 6. Error compensation circuit

4. Computing Probability of Maximum Error

Maximum error occurs when the *R*, *G*, *S* bits and other effective bits are not available or, if available, their values are not appropriate for computing *S*; thus, no rounding takes place.

The bits *R* and *G*, in fact, represent the bits P_{23} and P_{22} respectively, (refer to Fig. 3), and $S=P_{21}\,\text{OR}\,P_{20}\,\text{OR}$

P_{19}. To compute the maximum error probability, it is necessary to calculate the probability of each one of P_{19} to P_{23} bits being 1 (here P_{19} is computed in both the truncated and estimated states).

To accomplish this task, the probabilities of the elements from partial product matrix involved in computing these bits being 1 must be computed. For example, the probability of P_{23} or *R* being 1 depends on the probability of every element being 1 in the 23rd column (Fig. 3) in every cycle, and each of these intermediate elements depends on another element; that is, every intermediate product like $P_i(n-i+1)$ in cycle *i* depends on $pp_{n-i+1,i}$ (intermediate product in cycle *i*), $P_{i-1}(n-i+2)$ (intermediate product in $(i-1)^{th}$ cycle), and $c_{n-i,i}$ (carry bit from adjacent column in cycle *i*).

If the probability of $P_i(n-i+1)$ being 1 is defined as $P_1(P_i(n-i+1))$. According to Table 1, its being 1 is achieved in different states.

Table 1. Possible states in computing $\boldsymbol{P_i(n-i+1)}$

$P_{i-1}(n-i+2)$	$pp_{n-i+1,i}$	$c_{n-i,i}$	$P_i(n-i+1)$	$c_{n-i+1,i}$
0	0	0	0	0
0	0	1	1	0
0	1	0	1	0
0	1	1	0	1
1	0	0	1	0
1	0	1	0	1
1	1	0	0	1
1	1	1	1	1

Consequently, the following equation is obtained:

$$\begin{aligned}P_1(P_i(n-i+1)) &= [\{P_1(P_{i-1}(n-i+2)) \times P_1(pp_{n-i+1,i})\} \\ &+ \{P_0(P_{i-1}(n-i+2) \times P_0(pp_{n-i+1,i})\}] \\ &\times P_1(c_{n-i,i}) \\ &+ [\{P_1(P_{i-1}(n-i+2)) \times P_0(pp_{n-i+1,i})\} \\ &+ \{P_0(P_{i-1}(n-i+2)) \times P_1(pp_{n-i+1,i})\}] \\ &\times P_0(c_{n-i,i})\end{aligned} \quad (8)$$

$P_1(pp_{n-i+1,i})$, $P_1(P_{i-1}(n-i+2))$, and $P_1(c_{n-i,i})$ are the probability of the intermediate product being 1 at i^{th} cycle, their being 1 at $(i-1)^{th}$ cycle, and their being 1 for carry digit bits from the adjacent column and i^{th} cycle, respectively (probability of being 0 is defined in the same order).

To compute the probability of $pp_{n-i+1,i}$ being 1, represented by $P_1(pp)$, it can be assumed that every intermediate bit is a random variable; thus:

$$P_1(pp) = \frac{1}{2} \times \frac{1}{2} = \frac{1}{4} \quad (9)$$

$$P_0(pp) = 1 - \frac{1}{4} = \frac{3}{4} \quad (10)$$

Likewise, it can be said that the probability $P_{i-1}(n-i+2)$ is in fact the probability $P_i(n-i+1)$, in the $(i-1)^{th}$ cycle; therefore, it depends on the same parameters but at i^{th} cycle, in a sense that it has a recessive state, the end condition of which is computation of $P_1(P_1(n-1))$ (an addition that occurs in the first cycle). This value in the first cycle is subject to values $pp_{n-1,1}$, $pp_{n-1,2}$ and $c_{n-3,2}$. By applying a table similar to Table 1, this can be presented as:

$$\begin{aligned}P_1(P_1(n-1)) &= [\{P_1(pp_{n-2,2}) \times P_1(pp_{n-1,1})\} \\ &+ \{P_0(pp_{n-2,2}) \times P_0(pp_{n-1,1})\}] \\ &\times P_1(c_{n-3,2}) \\ &+ [\{P_1(pp_{n-2,2}) \times P_0(pp_{n-1,1})\} \\ &+ \{P_0(pp_{n-2,2}) \times P_1(pp_{n-1,1})\}] \\ &\times P_0(c_{n-3,2}) \\ &= [\{\frac{1}{4} \times \frac{1}{4}\} + \{\frac{3}{4} \times \frac{3}{4}\} \times P_1(c_{n-3,2})] \\ &+ [\{\frac{1}{4} \times \frac{3}{4}\} + \{\frac{3}{4} \times \frac{1}{4}\}] \times P_0(c_{n-3,2}) \\ &= \frac{10}{16} \times P_1(c_{n-3,2}) + \frac{10}{16} \times P_0(c_{n-3,2})\end{aligned} \quad (11)$$

All values in Eq. (11) are random variables, the probability of which is computable through Eq. (9-10). To compute $P_1(c_{n-i,i})$ in Eq. (8), Eq. (12) must be applied, which is obtained from Table 1.

$$\begin{aligned}P_1(c_{n-i,i}) &= [P_1(P_{i-1}(n-i+1)) \times P_1(pp_{n-i,i})] \\ &+ [\{P_1(P_{i-1}(n-i+1) \times P_0(pp_{n-i,i})\} \\ &+ \{P_0(P_{i-1}(n-i+1) \times P_1(pp_{n-i,i}) \\ &\times P_1(c_{n-i-1,i})]\end{aligned} \quad (12)$$

Eq. (12) is a returnable one, the ending condition of it is determining the second cycle carry digit ($c_{n-2,2}$).

According to Fig. 7, computing $c_{n-2,2}$ is subject to two a_{n-2} and b_{n-2} values (intermediate product) and its value is1 when the volume of either a_{n-2} or b_{n-2} is 0 and the other is 1 and the carry digit of the adjacent column (c_{n-3}) is 1. This equation is a returnable one as well. Eventually, the need to compute the probability of c_1 would rise, which would be subject to the probability of a_0 and b_0 being 1; hence:

$$P_1(c_1) = P_1(a_0) \times P_1(b_0) = \frac{1}{4} \times \frac{1}{4} = \frac{1}{16} \quad (13)$$

Consequently, the probability of c_{n-2} being 1 can be computed through Eq. (14).

$$P_1(c_{n-2}) = (\frac{1}{4}\times\frac{1}{4}) + \frac{3}{8}(\frac{1}{4}\times\frac{1}{4}) + \ldots \frac{3}{8}(\frac{1}{4}\times\frac{1}{4}) = \frac{1}{16}\sum_{k=0}^{n-2}\left(\frac{3}{8}\right)^k \quad (14)$$

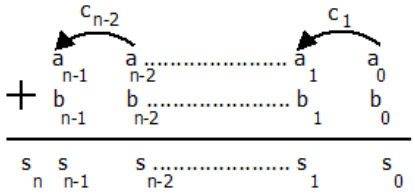

Figure. 7. Adding function of the two-bit digits

The $P_1(c_{n-3,2})$ and $P_0(c_{n-3,2})$ in Eq. (11) are computed with respect to the above-mentioned description. In the same sequence, all parameters in Eq. (8) can be computed.

4.1 Maximum Error Probability for No Error Compensation State

To determine the effectiveness of this proposed method of compensating for errors caused by truncation in a partial product matrix, different state of truncation is of concern.

In the first state, the product contains only 24 bits and no extra bit is held for rounding (WO3C). In the second state, in addition to the 24 bits, bits P_{23}, P_{22} and P_{21} are considered as *R*, *G*, and *S* bits held (W2CE). In the next state, bits P_{23}, P_{22}, and P_{21} are considered as *R*, *G*, and *S*, and P_{20} is considered as a bit following *S* (W3CE). In the last state, bits P_{23}, P_{22} and P_{21} are considered as bits *R*, *G*, and *S*, and bits P_{20}, P_{19} are considered as the two bits following *S*, which are held (W4CE). The maximum error and rounding are defined based on occurrences of different states of bits *R*, *G*, and S, Table 2.

Table 2. Rounding states occurrence

R	*G*	*S*	Rounding
0	0	0	0
0	0	1	0
0	1	0	0
0	1	1	0
1	0	0	0
1	0	1	1
1	1	0	1
1	1	1	1

Now, if the probabilities of *R*, *G*, and *S* bits being 1 equal $P_1(R)$, $P_1(G)$, and $P_1(S)$ respectively, and the probability of maximum error is $P_{\max}(e)$, Eq. (15) yields:

$$P_{\max}(e) = [P_1(R)\times P_0(G)\times P_1(S)] + [P_1(R)\times P_1(G)\times P_0(S)] + [P_1(R)\times P_1(G)\times P_1(S)] \quad (15)$$

In fact, Eq. (15) is the maximum error occurrence probability at WO3C state in Table 2. At W2CE, the maximum error occurs when *R*=1, *G*=0, *S*=0, and P_{20} = 1; but since this bit is not available, the rounding would be calculated wrongly. In W3CE, maximum error occurs when *R*=1, *G*=0, *S*=0, P_{20} = 0, and P_{19} =1. A similar result is obtained for W4CE state when *R*=1, *G*=0, *S*=0, P_{20} = 0, P_{19} = 0, and P_{18} = 1. The results obtained by these computations will be explained later. In all cases, the probability of every bit being 1 or 0 is calculated according to the method described in Sec. 4.

4.2 Maximum Error Probability for Error Compensation States

Computing probability at this state is related to a time when the error compensation circuit is applied for carry propagation estimation. Applying this circuit predicts the carry propagation wrongly in both states, Table 1, Therefore, by knowing the existence of error in computing carry propagation, and its appearance in the product, with reference to Eq. (16) the following is yielded:

$$AV_{n-i+1,i} = \begin{cases} AV_{n-i+2,i-1} \oplus pp_{n-i+1,i} & \text{if} \quad 2 < i \le 24 \\ AV_{n,i-1} & \text{if} \quad i = 2 \end{cases} \quad (16)$$

According to the definition of exclusive OR function function, this product would be equal 1, only if the number of bits that equal 1 is an odd number. Hence, $P_1(AV_i)$, the probability function of exclusive OR function can be represented as

$$P_1(AV_i) = \sum_{k=1}^{\left\lceil \frac{i}{2} \right\rceil} \binom{i}{2k-1} \left(\frac{1}{4}\right)^{2k-1} \left(\frac{3}{4}\right)^{i-(2k-1)} \quad (17)$$

The results obtained by replacing the digits in all the above-mentioned equations in both cases of error state, with and without compensation, are presented in Table 3. As observed these results are very close to one another, indicating the error compensation circuit accuracy.

Table 3. Digit values of muximum error probability

Proposed method	Maximum error probability for no compensation state	maximum error probability for error compensation state
WO3C	0.4977495060	—
W2CE	0.06249765004	0.062621245550
W3CE	0.0314991165	0.03143649401
W4CE	0.01581255649	0.01587555472

5. Simulation

This simulation is made through *MATLAB* software and the implementation area and delay are assessed through *Synopsys Design Compiler* with *TSMC18* typical library.

To determine the error compensation circuit effect, in addition to simulation of this proposed multiplier for

complete multiplication, the following steps are applied: elimination of LSP section (WO3C), LSP three columns (W3CO), two columns and carry propagation estimation from the third column (W2CE), three columns and carry propagation estimation from the fourth column LSP (W3CE).

5.1 Accuracy Assessment

Here, the absolute and relative error, a product of two random digit multiplications at 24 cycle, is calculated and its diagram is drawn (Fig. 8 and Fig. 9). The cycles presented are 1, 4, 8, 12, 16, 20, and 24 only.

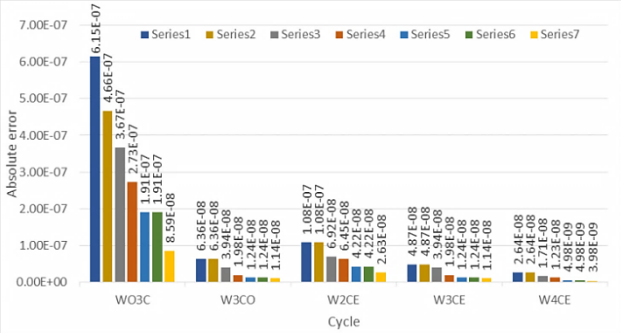

Figure. 8. Selected absolute error diagram in seven cycles

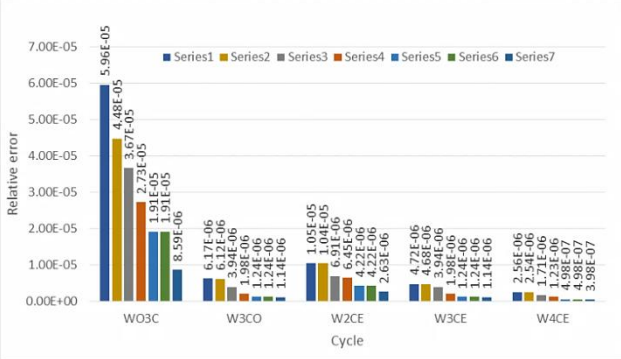

Figure. 9. Selected relative error diagram in seven cycles

The proposed design was simulated for 5,000 random digits as well, and the absolute and relative errors in the seven cycles defined were calculated and plotted (Fig. 10 and Fig. 11). The results indicate a reduction in error and the positive effect of the error compensation circuit.

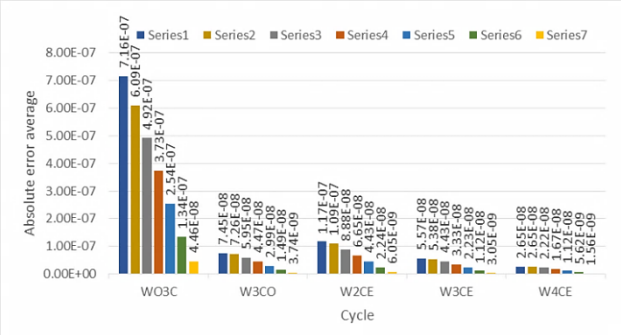

Figure. 10. Absolute error average of 5,000 random digits in seven cycles

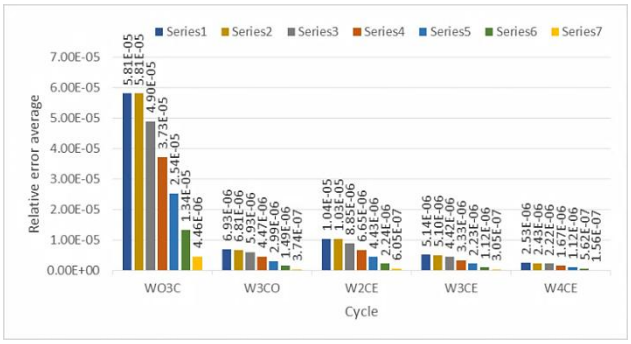

Figure. 11. Relative error average of 5,000 random digits in seven cycles

To determine error convergence, the fitting curve of the absolute and relative error average of 5,000 random digits for all states is drawn in Fig. 12. This curve indicates the error converges towards 0.

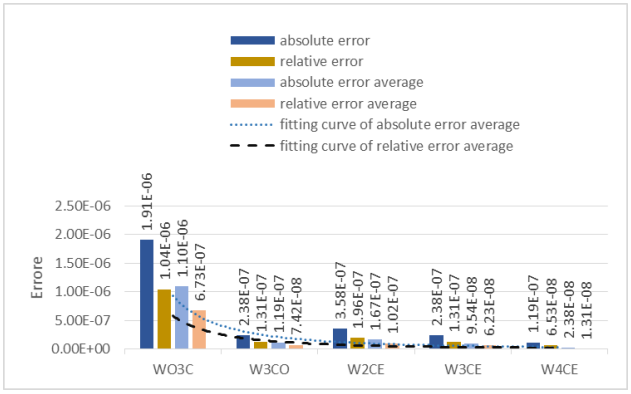

Figure. 12. The error coverges towards zero diagram

5.2 Area and Delay Assessment

In area assessment, the results of this proposed multiplier and truncated conditions are presented in the two combinational and non-combinational (TCA), and combinational and non-combinational area of circuits and intermediate connections (TA) are reported (Table 4). Comparison of different states, specifically, W2CE and W3CE, indicates the effective contribution of the estimating circuit.

Table 4. Truncated multipliers area report

	WO3C	W3CO	W2CE	W3CE	W4CE
TCA (um^2)	18431.894617	27219.185976	26255.382937	27071.902759	28077.475626
TA (um^2)	314113.38741	428701.223207	425790.735110	437927.316211	437626.215616

The timing report of all truncated multiplier states and this proposed multiplier are presented in Table 5. Comparison of different states, W2CE and W3CO in specific, indicates the effective contribution of the error compensation circuit. There exists a direct relation

between an increase in LSP column for error compensation and circuit delay.

Table 5. Truncated multipliers timing report

Truncated multipliers	WO3C	W3CO	W2CE	W3CE	W4CE
Delay (ns)	473.33	521.33	473.33	593.33	593.33

In Table 6, previous works has been summarized. Comparisons have been done for two parameters area and delay, and for both integer and floating-point numbers. In all of the papers presented, only two parameters area or delay have been discussed and have not been reported simultaneously.

As are observed, the proposed multiplier is in the proper position, exception in case [22] where this paper has not obtained any report about accuracy and area. Likewise, only there is one reported area that relates to a 16-bits integer multiplier.

Table 6. Comparison of proposed multiplier and previous work where fp represents floating-point numbers

Mult. method	Size (bits)	Area (um^2)	Delay (ns)
[18]	16 int	1.22×10^5	Not reported
[19]	8 int	Not reported	940.8
[20]	32 fp	Not reported	3055.2
[21]	16 int	Not reported	836.32
[22]	32 fp	Not reported	163.68
[23]	32 fp	Not reported	2099.424
[23]	32 fp	Not reported	2264.136
Proposed	32 fp	4.38×10^5	593.33

To determine the contribution of the LSP column number in error compensation, the diagram of relative error average and delay is presented in Fig. 13, where an increase in LSP column number for the purpose of compensation results in an increase in delay. This is why no attempt is made to increase the column number.

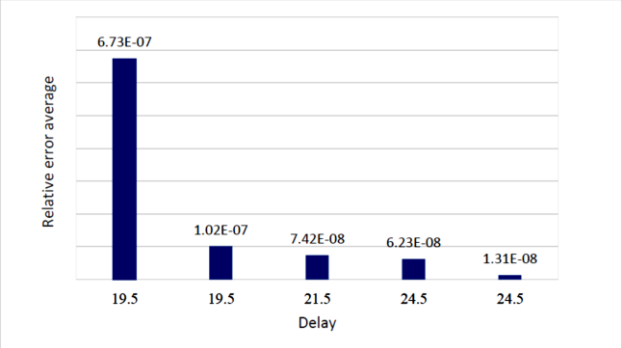

Figure. 13. Relative error average and delay diagram

6. Conclusion

The algorithm for and implementation of a sequential truncated multiplier for floating-point digits at single-precision that is capable of error compensation are proposed. This method is implemented by applying four MSPS from a semi-LSP matrix of a partial product and estimated carry from the fifth column using a small circuit. Results indicate that the error compensation circuit can significantly reduce the error caused by lake of carry digits from the eliminated columns. Among all simulation states, W4CE is the best candidate with respect to finding a trade-off between speed, accuracy, and area, and it can be used in digital signal processing, telecommunication signal processing, embedded systems, mobile systems that require a small area, and low power consumption.

References

] B. Parhami, Computer Arithmetic, New York: Oxford University Press, 2000.

[2] X. Guan, Y. Fei and H. Lin, "Hierarchical design of an application-specific instruction set processor for high-throughput and scalable FFT processing." IEEE Transactions on Very Large Scale Integration (VLSI) Systems, vol. 20, no.3, (2012), pp. 551-563.

[3] A. V. Oppenheim, R. W. Schafer and J. R. Buck, Discrete-Time Signal Processing, USA: Prentice-Hall, 1998.

[4] J. R. Choi, H. G. Kim, S. S. Han and S. C. Hwang, "Variable 2K/4K/8K-point FFT/IFFT with compact memory for OFDM-based DVB-T system," International Conference on Systems and Informatics (ICSAI), May 2012, pp. 977-980.

[5] H. M. Hassan, K. Mohammad and A. F. Shalash, "Implementation of a reconfigurable ASIP for high throughput low power DFT/DCT/FIR engine," EURASIP Journal on Embedded Systems, No.1, 2012, pp. 1-18.

[6] J. Sohn and E. E. Swartzlander Jr, "Improved architectures for a fused floating-point add-subtract unit," Circuits and Systems I: Regular Papers, IEEE Transactions on, vol. 59, no. 10, 2012, pp. 2285-2291.

[7] X. Chen, A. Minwegen, Y. Hassan, D. Kammler, S. Li, T. Kempf and G. Ascheid, "Efficient multi-mode MIMO detection using reconfigurable ASIP," 20th Annual International Symposium on Field-Programmable Custom Computing Machines (FCCM), April 2012, pp. 69-76.

[8] D. Menard, D. Chillet, F. Charot and O. Sentieys, "Automatic floating-point to fixed-point conversion for DSP code generation," ACM. In Proceedings of the 2002 international conference on Compilers, architecture, and synthesis for embedded systems, October 2002, pp. 270-276.

[9] S. Z. Gilani, N. S. Kim and M. Schulte, "Virtual floating-point units for low-power embedded processors," 23rd International Conference on Application-Specific Systems, Architectures and Processors (ASAP), July 2012, pp. 61-68.

[10] S. Z. Gilani, N. S. Kim and M. Schulte, “Energy-efficient floating-point arithmetic for software-defined radio architectures,” 2011 IEEE International Conference on Application-Specific Systems, Architectures and Processors (ASAP), September 2011, pp. 122-129.
[11] P. Korkmaz, B. E. Akgul and K. V. Palem, “Energy, performance, and probability tradeoffs for energy-efficient probabilistic CMOS circuits,” Circuits and Systems I: Regular Papers, IEEE Transactions on, vol. 55, no. 8, 2008, pp. 2249-2262.
[12] D. Kelly, B. Phillips and S. Al-Sarawi, “Approximate signed binary integer multipliers for arithmetic data value speculation,” In Conference on Design & Architectures for Signal and Image Processing, 2009.
[13] Y. C. Lim, “Single-precision multiplier with reduced circuit complexity for signal processing applications,” Computers, IEEE Transactions on, vol. 41, no. 10, 1992, pp. 1333-1336.
[14] N. Petra, D. D. Caro, V. Garofalo, E. Napoli and A. G. Strollo, “Truncated binary multipliers with variable correction and minimum mean square error,” Circuits and Systems I: Regular Papers, IEEE Transactions on, vol. 57, no. 6, 2010, pp. 1312-1325.
[15] V. Garofalo, N. Petra and E. Napoli, “Analytical calculation of the maximum error for a family of truncated multipliers providing minimum mean square error,” Computers, IEEE Transactions on, vol. 60, no. 9, 2011, pp. 1366-1371.
[16] E. J. King and E. E. Swartzlander, “Data-dependent truncation scheme for parallel multipliers,” Conference Record of the Thirty-First Asilomar Conference on Signals, Systems & Computers, vol. 2, November 1997, pp. 1178-1182.
[17] E. E. Swartzlander, “Truncated multiplication with approximate rounding,” Conference Record of the Thirty-Third Asilomar Conference on Signals, Systems, and Computers, vol. 2, October 1999, pp. 1480-1483.
[18] F. Farshchi, M. Abrishami, and S.M. Fakhraie, "New approximate multiplier for low power digital signal processing." The 17th CSI International Symposium on Computer Architecture & Digital Systems, October 2013, pp. 25-30.
[19] Z. Vasicek and L. Sekanina, "Evolutionary design of approximate multipliers under different error metrics." Design and Diagnostics of Electronic Circuits & Systems, 17th International Symposium on. 2014 Apr 23, pp.135-140.
[20] C. M. Guardia and E. Boemo, "FPGA implementation of a binary32 floating point cube root." Programmable Logic (SPL), Nov 2014, pp. 1-6.
[21] A. Sunny, B. K. Mathew and P. B. Dhanusha, "Area Efficient High Speed Approximate Multiplier with Carry Predictor." Procedia Technology 24, 2016, pp. 1170-1177.
[22] S. Sivanantham, "Design of low power floating point multiplier with reduced switching activity in deep submicron technology." International Journal of Applied Engineering Research, vol. 8, no. 7, 2013, pp. 851-59.
[23] P. Koneru, T. Sreenivasu and A. P. Ramesh, "Asynchronous Single Precision Floating Point Multiplier using Verilog HDL." IJ of Advanced Research in Electronics and Communication Engineering, 2013 Nov.

Marziye Fathi received her B.SC degree in Computer Hardware Engineering and M.SC degree in Computer Architecture Engineering both from Islamic Azad University of Najafabad (IAUN), Najafabad, Iran, in 2010 and 2015, respectively. Her area research interests include digital arithmetic, VLSI and image processing.

Hooman Nikmehr received his BSc in Electronic Engineering and MSc in Computer Architecture Engineering both from University of Tehran, Tehran, Iran, in 1992 and 1997, respectively, and PhD degree in Computer Engineering from the University of Adelaide, Adelaide, Australia, in 2005. He is an Assistant Professor with the Department of Computer Architecture, University of Isfahan, Isfahan, Iran. His current research interests include VLSI, digital arithmetic, computer architecture, reconfigurable hardware design and low-power design.

Improved Generic Object Retrieval In Large Scale Databases By SURF Descriptor

Hasan Farsi*
Department of Electrical and Computer Engineering, Birjand University, Birjand, Iran
hfarsi@birjand.ac.ir
Reza Nasiripour
Department of Electrical, Faculty of Engineering, Birjand University, Birjand, Iran
reza.nasiripour@birjand.ac.ir
Sajjad Mohammadzadeh
Department of Electrical, Faculty of Engineering, Birjand University, Birjand, Iran
s.mohamadzadeh@birjand.ac.ir

Received: 26/Nov/2016 Revised: 21/Jun/2017 Accepted: 08/Jul/2017

Abstract

Normally, the-state-of-the-art methods in field of object retrieval for large databases are achieved by training process. We propose a novel large-scale generic object retrieval which only uses a single query image and training-free. Current object retrieval methods require a part of image database for training to construct the classifier. This training can be supervised or unsupervised and semi-supervised. In the proposed method, the query image can be a typical real image of the object. The object is constructed based on Speeded Up Robust Features (SURF) points acquired from the image. Information of relative positions, scale and orientation between SURF points are calculated and constructed into the object model. Dynamic programming is used to try all possible combinations of SURF points for query and datasets images. The ability to match partial affine transformed object images comes from the robustness of SURF points and the flexibility of the model. Occlusion is handled by specifying the probability of a missing SURF point in the model. Experimental results show that this matching technique is robust under partial occlusion and rotation. The properties and performance of the proposed method are demonstrated on the large databases. The average of retrieval rate by the proposed method applied on Oxford landmarks and Corel dataset are 69.68% and 65.79%, respectively. Also, the average of ANMRR measure by the proposed method applied on Oxford landmarks is 0.223 and this criterion for Corel dataset is 0.269. The obtained results illustrate that the proposed method improves the efficiency, speeds up recovery and reduces the storage space.

Keywords: Object retrieval; Speeded Up Robust Features (SURF); Large-scale; Supervised; Training-Free.

1. Introduction

Recently, the problem of specific object retrieval from an image database is a very challenging area that many researchers look for the best solution. In the other words, by selection of a particular object in a given query image, an object retrieval system should return a set of representative images that contain object. Object detection plays important roles in computer vision which includes image retrieval, intelligent transportation systems and surveillance. Object detection has used in recent researches on object tracking, object recognition, and other object-based approaches.

Object retrieval is faced many challenges:

1. Illumination condition/position: Illumination changes that occur during a day can be added a shadow to object interesting. Also, climate condition causes changes in illumination condition.
2. Geometric distortions: change in the position of object is called as geometric distortion. When two objects in images are matching, object is geometric distortion, to reduce rate of recognition.
3. Rotation: an object retrieval system must have ability adapt when position of object is rotation.
4. Scale: this challenge occurs when the size of object in an image is changed.
5. Occlusion: when object in an image is not completely visible that is called occlusion.

Object retrieval is mainly divided into two parts: category retrieval and detection. The aim of object category retrieval is to classify a given object into several predefined categories whereas the aim of object detection is to separate desired objects from the background in a target image.

Generally, the object detection seeks any object of a particular class in a test image to answer the question "how many objects are in the image, and where do they are located.

The detection area is divided to two parts, appearance-based and contour-based approaches [1-5]. In contour-based approaches, learning algorithms are more common to use. In the other words, these methods first extract some features such as color, texture, and illumination change. Then they use learning methods [6-8].

In appearance-based approaches, first, 'interest points' are selected at distinctive locations in the image, such as corner, blobs, and T-junctions. An interest point detector has most valuable property that is its repeatability,

* Corresponding Author

whether it reliably finds the same interest points under different viewing conditions. Then, the neighbors of every interest point are represented by a path descriptor. This descriptor has to be distinctive, and also robust against noise, detection errors, geometric, and photometric deformations [9-10].

Category of retrieval is caused limitation within computer vision. To achieve this purpose, Agarwal et al. and Barnard et al. have proposed the methods that use learning algorithm [11]. In other words, this method used many number of training data. Then, training process is done by the classifier known. Finally, the test image is added to classifier to matching process with training images.

In the recent years, machine vision methods extract features of image and object to achieve the purpose of object recognition. There are some approaches that use low-level features. For example, volumetric descriptor [14], surface distribution [15], geometry [16-17] have used to extract the feature for object retrieval. While these methods act efficiently well under an engineered environment where object pose and illumination are strictly controlled, it is no longer feasible under slight positions or illumination variations because of the limited computation power and nearly infinite possible combinations of pose and lighting.

To overcome this problem, it is proposed to use high-level feature based methods instead of searching all possible model positions through the image. High-level feature based methods extract object features which are mostly invariant among different positions, orientations and lightings. Scale Invariant Feature Transform (SIFT) [-18] is an efficient algorithm that is widely used in object recognition, image stitching, stereo vision and various computer vision researches.

One of the popular methods to detect objects by using a single query image without training is keypoint-based matching. Most methods use many keypoints which are relatively stable in the image and calculate the local invariant descriptors of the patches around the keypoints, such as SIFT and shape context [19]. Therefore, the object matching is translated into a set of local descriptors on the keyoints. Some approaches use densely computed descriptors [20]. The reported method in [21] used local regression kernels the descriptor with a matrix generalization of the cosine similarity measure as the comparison method.

There are other methods which are based on re-ranking. In [22], the authors have proposed a query expansion (QE) which causes improvements of retrieval performance. In [23], a discriminative query expansion (DQE) which uses matching learning method has been proposed. In [24], the authors proposed the method based on vector similarity.

In this paper, we propose a new method which uses only one query image to detect the object, without training, as shown in Figure 1. The proposed method can be decomposed into two parts: first, learning the probabilistic model for a specific object, and second, matching the model in a test image. The model is constructed with SURF points that are acquired from the image. Information of relative positions, scale and orientation between SURF points are calculated and constructed into a probabilistic model of the object. Then, dynamic programming is used to find the best combination among all SURF points. In the matching step, dynamic programming is also used to find the best model among all SURF points. Since a SURF point in the model can be lost during matching in the test image, this situation is handled by defining a missing probability for a SURF point. When a SURF point is lost, a virtual SURF point with the best match in the model is inserted; this is necessary to calculate the probability of the relation among SURF points in the model.

We evaluate the proposed model on two datasets. First dataset is the building dataset that comprise 5K images of Oxford landmarks where “landmarks” means a particular part of the building. We use a set of images comprising 11 different landmarks. The images for each landmark are retrieved from [12]. In addition, we use the Corel dataset to evaluate the proposed system [13]. This dataset includes 1000 different images. The images are divided into 11 classes, including early humans, elephants, flowers, buses, horses, etc. that we used to three classes, including planes, buses and dinosaurs. Some examples of the images from these dataset are shown in figure 2

Fig. 1 Object detection using only one query.

Fig. 2 Example images from dataset. (a) 25 randomly sampled images from Oxford dataset, (b) 25 randomly sampled images from Corel dataset.

This paper is organized as follows: In Section 2, the proposed object retrieval system is introduced. The

proposed system can be divided into two parts, first part is object retrieval and second part is object detection. In section 3, experimental results have been explained. Finally, the conclusion is drawn in Section 4.

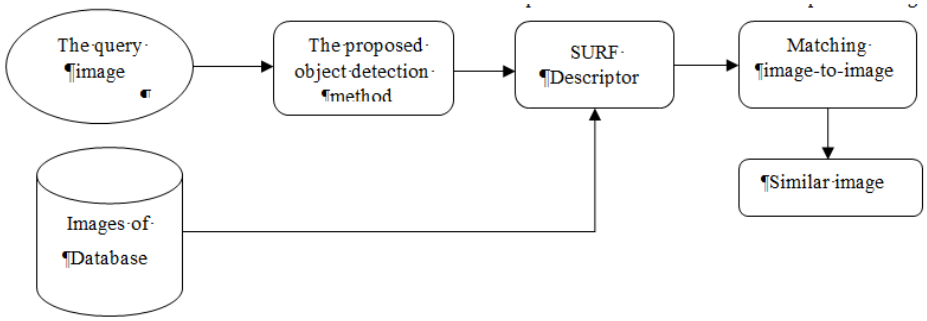

Fig. 3 Block diagram of the proposed Object Retrieval method.

2. Proposed Object Retrieval Method

The proposed method detects the objects with a single query image. The key problem is to represent the target class from the query image, which could be a typical real image. The detection process is very similar to "template matching". The query image is used as a standard "template", with the test images matched to this "template" to find the objects.

A block diagram of the proposed object retrieval method is illustrated inFigure3. The proposed method acts in different procedure using only one query image to detect the object without training. We extract features from query image and dataset images. This is achieved by SURF descriptor which is detailed in subsection 2.1. Since target image requires object detection, the proposed object detection for extraction of the target object is detailed in subsection 2.2. In subsection 2.3, the details of object matching using the proposed object retrieval method have been described.

2.1 SURF Algorithm

This section reviews the SURF algorithm which was proposed by Bay H, Tuytelaars, Gool L.V. in 2006. This algorithm is similar to SIFT algorithm. However, it is faster than SIFT in terms of calculation speed. In this section, SIFT descriptor is firstly described and then difference between SURF and SIFT descriptors is demonstrated. Both descriptors are applied in four steps:

2.1.1. Scale-space extreme detection
2.1.2. Key point localization
2.1.3. Orientation assignment
2.1.4. Key point descriptor

2-1-1- Scale-Space extreme detection

In SIFT, in order to detect the extreme or in other words position of interest point, image in a space called 'scale-space' is defined. The Interest points are stable features under different directions and scales. Scale space is performed by filtering image with sequence of Gaussian filter. Scale space of image is constructed as pyramid form. As observed in Figure 4, the scale space is composed of several octaves such that each octave is composed of five levels. In the first octave, the first level of image filtering is performed using Gaussian function with σ=0.5. Subsequently four levels are derived by convolution of image with Gaussian kernel $\sqrt{2}\sigma$, 2σ, $2\sqrt{2}\sigma$ and 4σ, respectively. In order to obtain the first level of the new octave, sub-sampling operation is performed by sampling the original image with 2:1 rate. The new levels in new octaves are constructed by using the same Gaussian kernels. The same process is performed for the construction of new octaves. The difference of levels in current scale is used to approximate the difference of Gaussian filters (DOG) or Laplace - Gaussian (LOG). Finally, the interest points are selected by local extreme points in the DOG scale space.

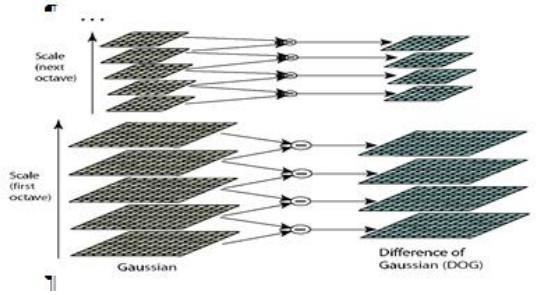

Fig. 4 Scheme of SIFT algorithm for extreme detection.

But in SURF descriptor uses a hessian matrix to find interest points. The determinant of a hessian matrix is an expression of the local change around the area. Given a point, $X = (x, y)$, in an image, I, the hessian matrix,H (x, σ), in Xat scale, σ, is defined as:

$$H(x,\sigma) = \begin{bmatrix} L_{xx}(x,\sigma) & L_{xy}(x,\sigma) \\ L_{xy}(x,\sigma) & l_{yy}(x,\sigma) \end{bmatrix} \quad (1)$$

Where $L_{xx}(x,\sigma)$, $L_{xy}(x,\sigma)$ and $L_{yy}(x,\sigma)$ denote the convolution of the second order Gaussian derivative $\frac{\partial^2 g(\sigma)}{\partial x^2}$, $\frac{\partial^2 g(\sigma)}{\partial xy}$, $\frac{\partial^2 g(\sigma)}{\partial y^2}$ with the image at point $X = (x, y)$, respectively. $g(\sigma)$ is given by:

$$g(\sigma) = \frac{1}{2\pi\sigma^2} e^{\frac{-(x^2+y^2)}{2\sigma^2}} \quad (2)$$

The convolution is very time-consuming. Hence, it is approximated and speeded-up by using integral images and approximated kernels-box filters. The integral image, I(X), at a location, X=(x,y), represents sum of all pixels in the input image, I, within a rectangular region formed between the origin and the position of X.

$$I(X) = \sum_{i=0}^{i\le x}\sum_{j=0}^{j\le y} I(x,y) \quad (3)$$

Using the box filters, the hessian determinant can be approximated by (4):

$$\det(H_{appx}) = D_{xx}D_{yy} - \left(wD_{xy}\right)^2 \quad (4)$$

D_{xx}, D_{xy} and D_{yy} denote the convolution of the box filters with the image at point,$X = (x, y)$, respectively.

Scale spaces are usually achieved by image pyramids. The image pyramids in SURF are constructed by changing the size of box filters rather than reducing the size of image. Initial scale layer is output of 9×9 filtering, and the corresponding scale, $\sigma = 1.2$. The following layers are obtained by filtering the image with gradually bigger masks, such as:9×9, 15×15 , 21×21, 27×27.

2.1.2. Key point localization

Both SURF and SIFT descriptors proceed at the way to locate the key points. In order to find the key points, each pixel is compared with 26 pixels. If the pixel value is lower or higher than all 26 pixels, this point is considered as a key point. Otherwise, this point is removed and the algorithm is applied on next pixel (or point). The computational complexity of the algorithm is low because most points in first stage of the algorithm are removed. Then the key points are interpolated in scale space image.

2-1-3- Orientation assignment

In SIFT method, in order to assign the orientation; a window is constructed around of each key point. Orientation histogram is constructed by using gradient directions of the points within the window. Each orientation histogram for each key point contains 36 parts which covers 360 degree of directions. In this histogram, the orientation having highest value is considered as the dominant orientation.

In SURF method, rotation invariance is achieved by detecting the dominant orientation of each feature point. The dominant orientation is estimated by calculating sum of the horizontal and vertical Haar wavelet responses within a sliding orientation window with angle of $\frac{\pi}{3}$. The two summed responses constitute a vector, and the longest vector lends its orientation to the feature point. The size of the Haar filter kernel is scaled to $4s \times 4s$where s is the scale of the feature point. The responses are weighted by a Gaussian function centred at the feature point.

Finally, these description vectors are normalized to unit vectors to provide robustness against contrast.

2.2 The proposed Object Detection Method

A block diagram of the proposed object detection method is illustrated in Figure 5. In this section, the gradients in different directions and scale have been calculated, and comparative operator is defined the inspired Retina eye model, and it is called Gabor functions. The simple method is proposed to combine multi-directional and multi-scale edge presentation. Eye map the input image to the various features that start in the retina. We have used a kind of Gabor filter by changing these parameters of filter. Therefore, many different scales of the edge of the image are extracted [25]. We have selected Gabor filter because frequency and orientation representations of Gabor filters are similar to those of the human visual system, and they have been found to be particularly appropriate for texture representation and discrimination.

Equations (5) models human visual system by a Gabor function which includes direction, scale, frequency and spatial model of the desired shape [26].

$$R(x-x_c, y-y_c)_{\lambda,\sigma,\theta,\varphi,\gamma} = R_0 \exp\left(-\frac{u^2 +,\gamma^2 v^2}{2\sigma^2}\right)\cos\left(2\pi\frac{u}{\lambda} + \varphi\right)$$

$$u(x-x_c, y-y_c, \theta) = (x - x\_c)cos\theta - (y - y\_c)sin\theta$$

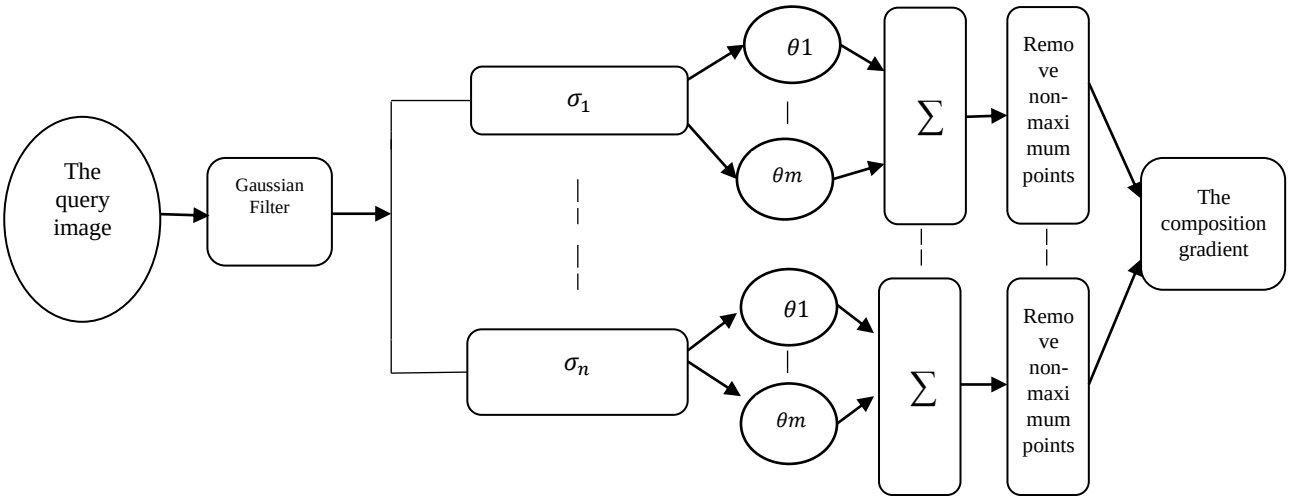

Fig. 5 Block diagram of the proposed object detection method.

$$v(x - x_c, y - y_c, \theta) = (x - x_c)sin\theta + (y - y_c)cos\theta \quad (5)$$

In this equation, x_c and y_c are the rotation center of the filter to the preferred angle, θ, that are placed relative to the origin. σ is standard deviation, λ length wave, and φ filter phase difference. Equation (6) has obtained by using query image and Equation (5):

$$t(x_c, y_c, \theta) = \iint I(x,y)\, R(x - x_c, y - y_c) d_x d_y \cong \sum_{m=1}^{M}\sum_{n=1}^{N} I(m\Delta x, n\Delta y) R(m\Delta x - x_c, n\Delta y - y_c)\, \Delta x \Delta y \quad (6)$$

In this section we have used from the following approximations: $\lambda = 2\pi\sigma^2, \emptyset = \frac{\pi}{2}$

First, we have used the Gaussian filter with fit σ to reduce noise input image. Second, for each scale, Gabor filter is convoluted with the original image in different scales (n) and different directions (m), -90 to +90 degrees. Therefore, the M × N gradient function are obtained from the original image. Then, the sum of weighted responses of Gabor filter is used to estimate the total gradient vector. In any scale, local gradient function with maximum values achieved by applying the remove the non-peak local maximum algorithm. So, in any scale, an approximate map has been achieved. Figure6 shows an illustration of target object (shape) extraction enhancement with the proposed object detection method.

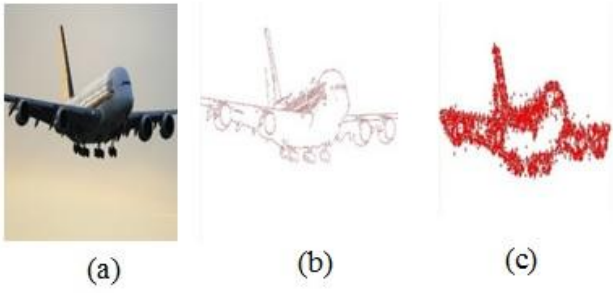

Fig. 6. Target object detection by the proposed Object Detection method and SURF descriptor. a) Original image, b) Detection method and c) extract SURF descriptor from object.

2.3 Object Matching

Figure7 shows object matching between two images for instance, where right image is query image and left image is matched image. We first acquire all the SURF points in the target image. In other words, each image is represented as isolated SURF points.

A model is defined by a set of N_m nodes. The set of nodes $M = m_a$is indexed by $\alpha = 1,2, \dots, N_m$ and each m_a will correspond to a SURF point in the image. Each node has attributes of $(z_\alpha, s_\alpha, \theta_a, A_\alpha)$ where z_α denotes the spatial location, s_α indicates the feature size, θ_a denotes the orientation, and $A_\alpha$represents the appearance. There is also a binary value variable,u_α, that specifies whether a node in the model could be found in the image.

There are $N_m - 2$ triplet-cliques C in a model; each triplet-clique is also labeled by α and is a set of 3 nodes $C_\alpha = \{m_\alpha, m_{\alpha+1}, m_{\alpha+2}\}$.

We define the model parameters as $\omega = (\omega^A, \omega^S)$, where $\omega^A = \{\omega_\alpha^A\}$ are the appearance parameters and $\omega^S = \{\omega_\alpha^S\}$ are the shape parameters. The model parameters, ω , can be decomposed into N_m nodes $m_1, \dots, m_{N_M}$ and $N_M - 2$ cliques $C_1, \dots, C_{N_{M-2}}$; each node represents an appearance vector u_a^A , $\alpha = 1, \dots, m$; each clique represents a shape vector u_a^S. To match the model to the image, first we match the SURF points in the target image to the first clique in the model. To reduce the enormous possible combinations of any 3 SURF points in the image, for each SURF point, we first find the nearest neighbour of its appearance vector among the appearance vectors of the first 3 nodes (m_1, m_2, m_3). We restrict them to only match to the closest one. We then store each 3 SURF points that matches (m_1, m_2, m_3)in the model as the chain,H_k, and its chain probabilities given the model parameters as P_h^k. $P_h^k$is defined as the clique probability P^c times the observed probability P^0.

For the first iteration every SURF point in image I_1 are added to one of the available cliques that would give the highest product of maximum P_i^c among images $I_2 \dots I_{NI}$. The P_i^cin Image I_i is calculated by assuming the model parameter u^A and u^S is equal to the appearance vector and shape vector of the corresponding SURF points in C_{1j}^a; and the model parameter $\sum A$ and $\sum S$ is set to the identity matrix. The maximum clique probability in I_i is the maximum among all combinations of Surf points in I_i.

Adding a new node to the clique would create a new clique which is composed of one new node and two previous nodes. In further iterations, new SURF points in I_1 will be added it this set of new clique instead of the previous ones; each SURF points would be added to the clique that would give the highest product of maximum clique probabilities among images$I_2 \dots I_{NI}$ times the chain probabilityP_{kt}^h.

The iteration is stopped when none of the chain probability is higher than a threshold.

In addition to 3 SURF points stored as the chain, we also store a case in which 1 SURF point is lost. We generate a virtual SURF point which has the appearance vector and the location giving the maximum$\mathrm{P^c}$, and store 2 actual SURF points and 1 virtual SURF point into a chain $\mathrm{H_k}$ with chain probability $\mathrm{P_h^k = P^c P^0}$. The only restriction is that one node in a clique could be a virtual SURF point. For each iteration, we match one of the SURF points in the image to one of the chains from the last iteration which corresponds to the maximum$\mathrm{P_h^k}$. The

iteration ends when all nodes in the model are matched. The chain H_k containing the highest P_h^k is the most possible location of the object in the image.

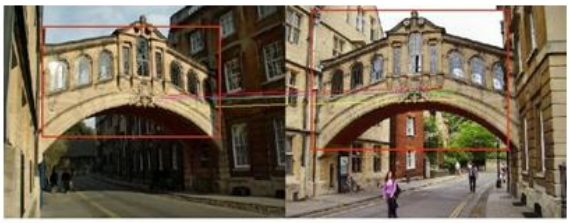

Fig. 7 Example of object matching.

3. Experimental Results

3.1 Evaluation Measures

There are many measures for evaluation of retrieval methods. In this paper, we use three measures ANMRR, precision and recall. Precision and recall are used for evaluation of most object retrieval methods.

The Average Normalized Modified Retrieval Rank (ANMRR) is an objective measure which summarizes the performance of system into a scalar value. It is defined from MPEG-7 research group [27].

First, we denote NG(q), K(q), R(k) as follows:

NG(q) : The number of the ground truth images for a query image, q.

K(q) =min[4. |NG) q)|,2. max{|NG(q)|, ∀q}]

R(k)= rank of an image, k, in retrieval results.

Rank(k) is obtained by:

ank(k) (7)

$$\begin{cases} R(k) & \text{if } R(k) \le K(q) \\ 1.25K & \text{otherwise} \end{cases}$$

Using Equation 9, Average Rank, AVR(q), for query q, is given by:

VR(q) = <Rank(k)>. (8)

However, for ground truth sets with different sizes, the AVR(q) value depends on NG(q). To minimize the influence of variations in NG(q), Modified Retrieval Rank, MRR(q), is obtained by:

[RR(q) = AVR(q)-0.5[1+|NG(q)|] (9)

The upper bound of MRR(q) depends on NG(q). To normalize this value, Normalized Modified Retrieval Rank, NMRR(q), is obtained by:

MRR(q) = $\frac{AVR(q)-0.5[1+|NG(q)|]}{1.25K(q)-0.5[1+|NG(q)|]}$ (10)

This measure is zero for perfect performance and approaches to one as performance worsens. The ANMRR of the dataset is finally given by averaging the NMRR(q) over all the q's

NMRR = <NMRR(q)>. (11)

Precision is the fraction of returned images that are relevant to the query image. Recall is the total number of relevant images with respect to the total number of relevant images in the dataset according to a priori knowledge. If we denote T as the set of returned images and R as the set of all images relevant to the query image, then the precision and recall criteria are given by Equations (12) and (13), respectively [28]

$$Precision = \frac{|T \cap R|}{|T|} \quad (12)$$

$$Recall = \frac{|T \cap R|}{|R|} \quad (13)$$

The number of relevant images is computed and the precision and recall in reach of retrieved images for all query images are obtained. We next consider the average of these precisions and recalls for each number of retrieved images as the precision and recall of each method for each number of retrieved images.

We use various methods to evaluate the proposed system. Montagna and Finlayson [29] proposed a method using the combination of precision and recall criteria as the performance measures for object retrieval method. According to Montagna and Finlayson [29], the following measures have been adopted:

P (0.5), precision at 50% recall (i.e. precision after retrieving 1/2 of the relevant documents).

P (1), precision at 100% recall (i.e. precision after retrieving all of the relevant documents, P(1) is the percent of crossover point of precision and recall). We use these values because precision and recall are considered in relation to each other and they are not meaningful if taken separately. To evaluate performance we use Mean Average Precision (MAP) for the landmark.

3.2 Indexing Results

In this section, we evaluate the performance of the proposed object retrieval on the building dataset of Oxford landmarks and Corel datasets. We use a set of images in Oxford dataset that comprising 11 different landmarks. The images for each landmark are retrieved from [12]. Also, Corel dataset include 1000 different images. These images are divided into 11 classes, including early humans, elephants, flowers, buses, horses, etc. that we use them into three classes, including planes, buses and dinosaurs.

3.2.1. The Corel Dataset

We evaluate the proposed method with color layout descriptor [30], dominant color descriptor [31], Patch based HOG-LBP [36] and Scalable color descriptor [30] in Corel dataset. We apply the proposed method to retrieve relative images, therefore we use query image. The P(0.5), P(1) and ANMRR of the proposed method, color layout descriptor, dominant color descriptor and Scalable color descriptor on Corel dataset are represented in Figure 8.

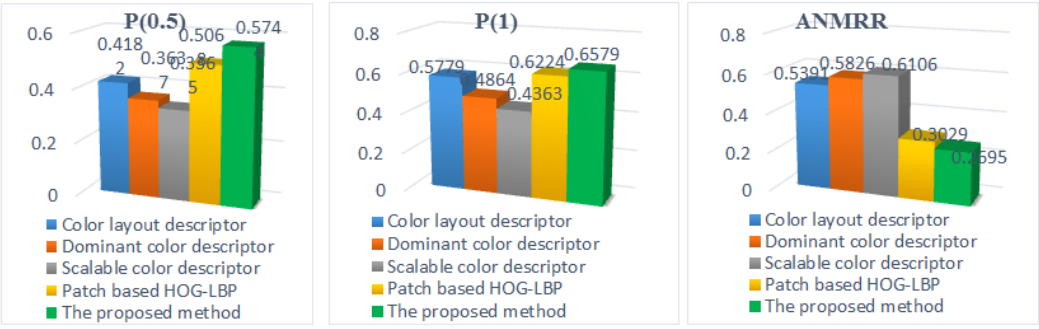

Fig. 8 P(0.5), P(1) and ANMRR for different landmarks on Corel dataset.

3.2.2. The Oxford Landmarks Datasets

In order to demonstrate the effectiveness of the proposed method, we apply the proposed method on Oxford landmarks datasets. We compare the proposed method with cosine model [32], general (content-unaware) language modeling approach (LM) [33] and two variants of the matting-based COR model [34]. The performance of the proposed method, Cosine, CORm, CORa and LM methods of the 11 landmarks on the Oxford 5K dataset is shown in Figure9. As observed, the performance of the proposed method in "All Souls"is better than other methods. After the proposed method, CORm, CORa, Cosine and LM have better performance, respectively. As observed, in each landmarks, the performance of the proposed method is better than other methods except in "Balliol" and "Keble" landmarks.

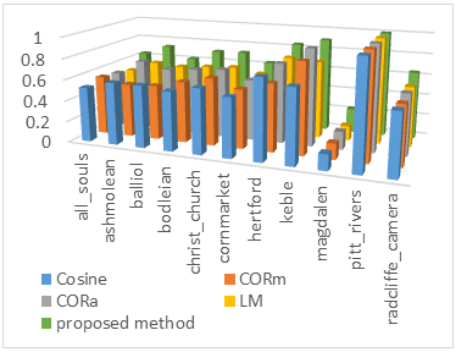

Fig. 9 P(1) for different landmarks on Oxford dataset.

We compare the proposed method with Ng et al [37], SPoC [38], R-MAC [39], CroW [40] and uCroW [40]. The MAP performance of the proposed method, Ng et al, SPoC, R-MAC, CroW and uCroW methods of the Oxford dataset is shown in Figure 10. Table 1 summarizes the test results on the Oxford 5K dataset. The P(0.5), P(1), ANMRR and average of these parameters of the proposed method, CORm, CORa and LM methods are represented in this table. Once again, in Table 2 the best score for each metric is in bold face.

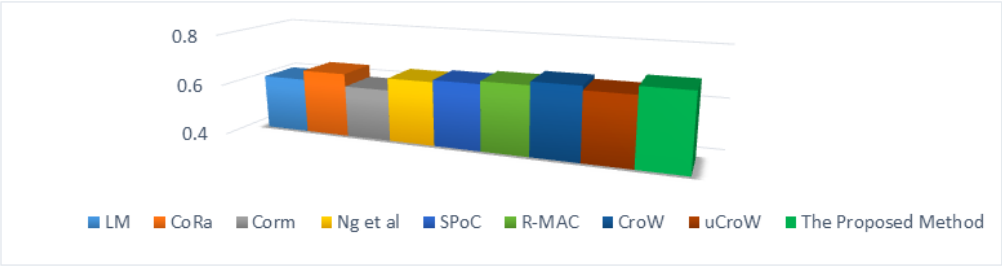

Fig. 10 MAP for different approaches on Oxford dataset.

Figure 11 shows the object matching of the proposed method on 11 landmarks of Oxford dataset. In this figure, each sub-figure has two images where right image is query image and left image is matched image. We present matched points by using color lines. These points are obtained by using SURF descriptor explained in section 3. According to these figures, the proposed matching method is robust under illumination, rotation, scaling and partial occlusion.

4. Conclusions

We proposed a new method for object retrieval object using a single query image without training or free-training. We used SURF algorithm for object matching. The detection process is very similar to "template matching". The query image is used as a standard "template", with the test images matched to this "template" to find the objects. The obtained results

Table 1. P(1), P(0.5) and ANMRR of different method in Oxford 5K dataset.

Method	Datasets												
		All Souls	Ashmolean	Balliol	Bodleian	Christ Church	Cornmarket	Hertford	Keble	Magdalen	Pitt rivers	Radcliffe Camera	Average
Cosine	P(0.5)%	61.72	59.09	71.21	66.34	62.87	59.71	82.21	70.01	17.13	50	68.89	60.83
	P(1)%	53.21	62.17	61.18	57.09	62.50	57.21	78.24	71.15	13.76	100	59.31	61.43
	ANMRR	0.321	0.182	0.361	0.241	0.290	0.354	0.072	0.061	0.721	0	0.352	0.269
CORm	P(0.5)%	65.70	51.08	63.12	68.34	65.37	58.90	70.02	86.32	15.13	50	66.79	60.07
	P(1)%	56.09	49.47	53.33	58.12	64.01	57.05	65.29	85.81	8.76	100	64.10	60.19
	ANMRR	0.289	0.191	0.426	0.236	0.275	0.349	0.090	0.056	0.721	0	0.371	0.273
CORa	P(0.5)%	63.74	68.02	**73.25**	74.34	67.32	61.71	82.00	**92.00**	17.21	50	68.91	64.41
	P(1)%	55.11	67.47	**63.31**	65.18	67.14	58.14	78.07	**91.11**	11.71	100	59.09	65.12
	ANMRR	0.311	0.156	**0.335**	0.185	0.262	0.338	0.065	**0.034**	0.710	0	0.351	0.250
LM	P(0.5)%	60.68	61.10	70.00	71.30	63.87	62.02	82.17	74.22	14.45	50	67.65	61.59
	P(1)%	53.17	59.47	59.24	61.20	64.41	59.78	77.90	73.39	8.61	100	59.02	61.47
	ANMRR	0.329	0.168	0.361	0.205	0.289	0.332	0.081	0.074	0.741	0	0.364	0.268
The proposed method	P(0.5)%	**73.10**	**74.28**	72.09	**81.41**	**73.37**	**65.72**	**88.17**	91.11	**24.45**	50	**73.91**	**69.78**
	P(1)%	**64.17**	**73.02**	61.72	**71.30**	**72.05**	**63.21**	**84.05**	90.06	**22.81**	100	**64.11**	**69.68**
	ANMRR	**0.261**	**0.137**	0.352	**0.106**	**0.231**	**0.298**	**0.059**	0.039	**0.670**	0	**0.305**	**0.223**

showed that using the proposed system object retrieval could improve the performance in the two datasets; Oxford landmarks and Corel datasets. In addition, the proposed method results in improving efficiency, speeds up recovery and reduces the required space for storage. The experimental results also show that the proposed matching technique is robust under partial occlusion, rotation and scaling. This method is very useful for generic or immediate object detection tasks, because of using single query image.

Fig. 11 Example of object matching on the Oxford landmarks database. Right image is query image and left image is image matched.

References

[1] P. Kontschieder, H. Riemenschneider, M. Donser, H. Bischof, "Discriminative learning of contour fragments for object detection", In Proc. Brit. Mach. Vis. Conference. pp. 1-12, 2011.#

[2] X. Meng, Z. Wang, L. Wu, "Building global image feature for scene recognition", Pattern Recognition. pp. 373-380, 2012.#

[3] B. Leibe, K. Schindler, N. Cornelis, L. Van Gool, "Coupled object detection and tracking from static cameras and moving vehicles", IEEE Transaction. Pattern. Anal Mach Intelligence, pp. 1683-1698, 2008.#

[4] H. Riemenschneider, M. Donoser, H. Bischof, "Using partial edge contour matches for efficient object category localization", in Proc. Europa Conference Computer, pp. 29-42, 2010.#

[5] X. Yang, H. Liu, Latecki, "Contour-based object detection as dominant set computation", Pattern Recognition, pp. 1927-1936, 2012.#

[6] V. Ferrari, T. Tuytelaars, and L. Van Gool, "Object detection by contour segment networks", In (ECCV), 2006.#

[7] V. Ferrari, F. Jurie, and C. Schmid, "Accurate object detections with deformable shape models learnt from images", In (CVPR), 2007.#

[8] V. Ferrari, L. Fevrier, F. Jurie, and C. Schmid, "Groups of adjacent contour segments for object detection", (PAMI), 2008.#

[9] X. Meng, Z.Wang, and L.Wu, "Building global image features for scene recognition", Pattern Recognition, Vol.45, No.1, pp. 373–380, 2012.#

[10] B. Leibe, K. Schindler, N. Cornelis, and L. Van Gool, "Coupled object detection and tracking from static cameras and moving vehicles", IEEE Trans. Pattern Anal. Mach. Intell, Vol.30, No.10, pp. 1683–169, 2008.#

[11] S. Agarwal, A. Awan, and D. Roth, "Learning to detect objects in images via a sparse, part-based representation", IEEE PAMI, 2004.#

[12] Pages. Available: http://www.flickr.com.#

[13] Pages. Available http://wang.ist.psu.edu/docs/related.#

[14] J. Tangelder, R. Veltkamp, "Polyhedral model retrieval using weighted point sets", Int. J. Image Graph, 2003.#

[15] R. Osada, T. Funkhouser, B. Chazelle, D. Dobkin, "Shape distributions", ACM Transaction, 2002.#

[16] A.Makadia, K.Daniilidis, "Spherical correlation of visual representations for 3D model retrieval", Int.J.Computer, Vol.89, No.2, 2010.#

[17] L. Zhu, Y. Chen, A. Yuille, "Unsupervised learning of a probabilistic grammar-Markov models for object categories", Pattern Analysis and Machine Intelligence, IEEE Transactions, pp. 114-128, 2009.#

[18] D. G. Lowe, "Object recognition from local scale-invariant feature", In Proceedings of the International Conference on Computer Vision, pp. 1150-, 1999.#

[19] S. Malik, J. Puzicha, "Shape matching and object recognition using shape context", IEEE Transaction. pp. 509-522, 2002.#

[20] E. Shechtman, M. Irani, "Matching local self-similarities across images and videos", IEEE Conference on Computer Vision and Pattern Recognition, 2007.#

[21] H. Seo, P. Milanfar, "Training-free, generic object detection using locally adaptive regression kernels", IEEE Transaction, pp. 1688-1704, 2010.#

[22] O. Chum, J. Philbin, J. Sivic, M. Isard, A.A. Zisserman, "Total recall: automatic query expansion with a generative feature model for object retrieval", IEEE 11th International Conference, 2007.#

[23] R.Arandjelović, A.Zisserman, "Three things everyone should know to improve object retrieval", IEEE Conference on Computer Vision and Pattern Recognition (CVPR), 2012.#

[24] D.Qin, S.Gammeter, L.Bossard, T.Quack, L.V.Gool, "accurate object retrieval with k-reciprocal nearest neighbors", IEEE Conference on Computer Vision and Pattern Recognition (CVPR), 2011.#

[25] S. E. Grigoresco, N. Petkov, P. Kruizinga, "Comparision of texture features based on Gabor filters", IEEE Transaction, pp. 1160-1167, 2002.#

[26] C. Grigorescu, N. Petcov, M. A. Westenberg, "Contour detection based on nonclassical receptive field inhibition", IEEE Transaction, pp. 729-739, 2003.#

[27] Chun, Kim, Jang, "Content-based image retrieval using multi-resolution color and texture features", IEEE Transaction, pp. 1073-1084, 2008.#

[28] Veganzones M. A, Grana, M, "A spectral/spatial CBIR system for hyper spectral images", IEEE J. Sel. Top. Earth Obs. Remote Sens, pp. 488-500, 2012.#

[29] Montagna R, Finlayson, G.G, "Padua point interpolation and L^P-norm minimization in color-based image indexing and retrieval", IET Image Process. pp. 139-147, 2012.#

[30] R. Troncy, B. Huet, S. Schenk, "Multimedia semantics, desktop edition (XML): metadata, analysis and interaction", John Wiley & Sons Inc., New York, (1st edition), pp. 36-54, 2011.#

[31] A. Ibrahim, A. Zou'bi, R. Sahawneh, M. Makhadmeh, "Fixed representative colors feature extraction algorithm for moving picture experts group-7 dominant color descriptor", Journal of Computer Science, pp. 773-777, 2009.#

[32] J. Philibin, O. Chum, M. Isard, J. Sivic, A. Zisserman, "Object retrieval with large vocabularies and fast spatial matching", Computer Vision and Pattern Recognition (CVPR), pp. 1-8, 2007.#

[33] B. Geng, L. Yang, C. Xu, "A study of language model for image retrieval", IEEE Int. Conf. Data Mining Workshops, IEEE Computer Society, pp. 158-163, 2009.#

[34] Linjun Yang, Bo Geng, Yang Cai, Alan Hanjalic, Xian-Sheng Hua, "Object retrieval using visual query context", IEEE Transactions on multimedia, 2011.#

[35] B. Herbert, E. Andreas, T. Tinne, V.G. Luc, "Speeded-up robust features (SURF)", Computer vision and image understanding (CVIU), pp. 346-359, 2008.#

[36] J. YU, Z. C, T. W AND X. ZHANG, "Feature integration analysis of bag-of-features model for image retrieval", Nero computing, [On-line], 2013.#

[37] J. Ng, F. Yang, and L. Davis. "Exploiting local features from deep networks for image retrieval", In Computer Vision and Pattern Recognition Workshops (CVPRW), 2015.#

[38] A. Babenko and V. Lempitsky, "Aggregating local deep features for image retrieval", In International Conference on Computer Vision (ICCV), 2015.#

[39] G. Tolias, R. Sicre, and H. J_egou, "Particular object retrieval with integral max-pooling of CNN activations", arXiv preprint arXiv:1511.05879, 2015.#

[40] Y. Kalantidis, C. Mellina, and S. Osindero, "Cross-dimensional weighting for aggregated deep convolutional features", arXiv:1512.04065, 2015.#

Hasan Farsi received the B.Sc. and M.Sc. degrees from Sharif University of Technology, Tehran, Iran, in 1992 and 1995, respectively. Since 2000, he started his Ph.D in the Centre of Communications Systems Research (CCSR), University of Surrey, Guildford, UK, and received the Ph.D degree in 2004. He is interested in speech, image and video processing on wireless communications. Now, he works as professor in communication engineering in department of Electrical and Computer Eng., University of Birjand, Birjand, IRAN.

Reza Nasiripour was born in Mashad in 1990. He received the B.Sc. and M.Sc. degrees in electrical communication engineering from University of Birjand, Birjand, Iran in 2012 and 2014, respectively. He is currently Ph.D. student in Department of Electrical and Computer Engineering, University of Birjand, Birjand, Iran. His research interests include Image and Video Processing, Pattern Recognition and Machine Learning

Sajjad Mohammadzadeh received the B.Sc. degree in communication engineering from Sistan & Baloochestan, University of Zahedan, Iran, in 2010. He received the M.Sc. and Ph.D. degree in communication engineering from South of Khorasan, University of Birjand, Birjand, Iran, in 2012 and 2016, respectively. Now, he works as assistant professor in Faculty of Technical and Engineering of Ferdows, University of Birjand, Birjand, Iran. His area research interests include Image and Video Processing, Retrieval, Pattern recognition, Digital Signal Processing, Sparse Representation, and Deep Learning.

A Novel Resource Allocation Algorithm for Heterogeneous Cooperative Cognitive Radio Networks

Mahdi Ghamari Adian*
Department of Electrical Engineering , University of zanjan, Zanjan, Iran
ghamari@znu.ac.ir

Received: 22/Sep/2016 Revised: 02/Jul/2017 Accepted: 11/Jul/2017

Abstract

In cognitive radio networks (CRN), resources available for use are usually very limited. This is generally because of the tight constraints by which the CRN operate. Of all the constraints, the most critical one is the level of permissible interference to the primary users (PUs). Attempts to mitigate the limiting effects of this constraint, thus achieving higher productivity is a current research focus and in this work, cooperative diversity is investigated as a promising solution for this problem. Cooperative diversity has the capability to achieve diversity gain for wireless networks. Therefore, the possibility of and mechanism for achieving greater utility for the CRN are studied when cooperative diversity is incorporated. To accomplish this, a resource allocation (RA) model is developed and analyzed for the heterogeneous, cooperative CRN. In the model, during cooperation, a best relay is selected to assist the secondary users (SUs) that have poor channel conditions. Overall, the cooperation makes it feasible for virtually all the SUs to improve their transmission rates while still causing minimal harm to the PUs. The results show a marked improvement in the RA performance of the CRN when cooperation is employed in contrast to when the CRN operates only by direct communication.

Keywords: Cognitive Radio Networks; Cooperative Diversity; Heterogeneous Networks; Resource Allocation.

1. Introduction

The measurements in various locations on the usage of the allotted spectrum spaces by the networks have shown a rather high level of inefficiency in spectrum usage [1, 2]. An outstanding attempt to resolve the issue are cognitive radio networks (CRN) [3]. Generally, with the CRN, unlicensed cognitive or secondary users (SUs) are made to access and utilize the same spectrum space that has been preallocated to primary users (PUs) of the spectrum, provided certain preconditions. In order to achieve an optimal productivity level for the resource allocation of the CRN, it is best to allocate low data rates to subchannels where the interference gains to PUs are quite high. This is understandable; as allocating high data rates to such subchannels would imply high transmit power by the SUs and high interference to the PUs because of the high interference gain. This smart move by the allocating algorithms of the SUs increases the throughput of the CRN. However, the achieved throughput is still very limited. In this work, as a result of recruiting cooperative diversity, a significant increase in reliability and capability of the system is realized.

2. Related Work

The concept of RA in CRN is no longer entirely new. Several research projects have been undertaken in this regard, and a review of relevant ones is performed in this section. Resource allocation in CRN actually deals with devising and describing mechanisms for assigning resources (frequency spectrum, transmit power, bandwidth, time slot, modulation scheme, etc) fairly and optimally to all users so that the highest possible productivity level is achieved.

A number of RA problems for underlay CRN have been identified, and attempts at solving them (both optimally and sub-optimally) have been investigated. In [4] Using game theory approach, the strong duality in convex optimization and the primal decomposition method, a low complexity semi-distributed algorithm was proposed for spectrum sharing and power allocation for MIMO-MB-CRNs. Other similar works that have developed RA models for underlay CRN can be found in [5-13]. References [14-15] have all developed models that describe possible cooperation between SUs in a CRN to help achieve a higher utility level. In [14], relays using decode-and-forward protocol are made to assist the SUs of the CRN. A similar model is developed in [15], where a decode-and-forward cooperative relay network is used to assist the SUs, thereby improving throughput.

As a means of addressing some of the limitations of the underlay and overlay arrangements, recent attempts at introducing user cooperation into RA in CRN have been made. A number of studies [14]–[17] have all developed models that describe possible cooperation between SUs in a CRN to help achieve a higher utility level. In two studies [14] relays using decode-and-forward protocol are made to assist the SUs of the CRN. For the optimization problem that has been developed to be solvable, the subchannels are first assigned to the SUs on the basis of their channel gains and possible interference to PUs. Thereafter, power is allocated to each subchannel.

* Corresponding Author

A similar model is developed in [10] where a decode-and-forward cooperative relay network is used to assist the SUs, thereby improving throughput. The nonconvex optimization problem that was developed is solved by first dualizing, then decomposing into relay assignment and power allocation. A primary decomposition method is also used in the work of Du et al, [16] after the power allocation problem in the developed model has been formulated. The sum rate of both PUs and SUs is jointly maximized in [17] while the SUs cooperate to transmit their signals. To achieve a result close to optimal, subchannels are first allocated to the SUs; thereafter, power is assigned to each SU and PU iteratively.

While the above reviewed works have incorporated some kind of cooperation, this work differs from them all in that the cooperative diversity approach developed in this work is targeted directly at addressing the problem of PU interference. Thus, the interference problem is first taken care of by the cooperation model even before the RA to SUs is performed. More specifically, in this work, through SU cooperation, the impact of the interference to PUs is mitigated, thus achieving greater throughput for the heterogeneous CRN. The heterogeneity in the CRN has been approached from 2 perspectives. Firstly, the channels are assumed to be heterogeneous, meaning that the available channels for the CRN do not all have the same characteristics. To capture the differing effects of channel heterogeneity, the network has been developed using an orthogonal frequency division multiple access (OFDMA) platform. With the OFDMA, the system can dynamically and optimally use different portions of the spectrum for different users at the same time. Secondly, the SUs in the network are heterogeneous. Users in each category are then serviced on the basis of their priority and/or their varying demands. During cooperation, the selection scheme used is the single-best-relay selection scheme used alongside the store-and-forward cooperative diversity technique. With this scheme, a best relay among the SUs is selected as the cooperator, which, during cooperation receives data from the source user and transmits to the destination. Overall, the heterogeneous cooperative CRN model, as developed and studied, reveals that much greater productivity is achievable by the CRN when its users cooperate. The contributions of this work are as follows:

- Investigating the use of cooperative diversity as a means of mitigating the limiting effects of interference to PUs in the RA problem of the CRN.
- Developing and analyzing methods for obtaining solutions to the RA problem in heterogeneous, cooperative CRN.

Section 3 describes the system model, Section 4 deals with the problem formulation and optimal solutions, Section 5 presents the heuristic developed to reduce the computational complexity, Section 6 presents the results and finally, Section 7 concludes the paper.

3. System Model

The CRN model consists of K heterogeneous SUs and L PUs, all within the coverage range of the secondary user base station (SUBS). N OFDMA subchannels are available for the SUs. The K heterogeneous SUs have different demands and priorities. These SUs are thus categorized as K_1 : SUs with minimum rate guarantee, and $(K-K_1)$: SUs with best effort service. All subchannels are in slow fading. Fig. 1. shows the network when cooperation is employed. The SU that needs cooperation, as it intends to communicate with a destination terminal (D), is referred to as the source secondary user (SSU). This SSU has a potentially high interference channel gain to the PU on the direct link and would therefore either not have been allocated subchannels at all or would have been given only a few subchannels to transmit at low data rates if direct communication alone had been considered. To help mitigate this limitation, the SSU selects a cooperating secondary user (CSU) with good channel quality and poor interference channel gain to the PU. The combined channel condition of the SSU and the CSU is obtained as follows:

Denote $H_{k,n}^{s}$ as the channel gain between the SSU and the *k*-th SU, employed as the CSU, at the *n*-th subchannel and $H_{k,n}^{r}$ as the channel gain between the CSU and the destination terminal D over the *n*-th subchannel. The SSU transmits signals to the *k*-th relay on the *n*-th subchannel with power $P_{k,n}^{s}$ in the first slot, while the *k*-th relay (CSU) transmits signals to D on the *n*-th subchannel with power $P_{k,n}^{r}$ in the second slot.

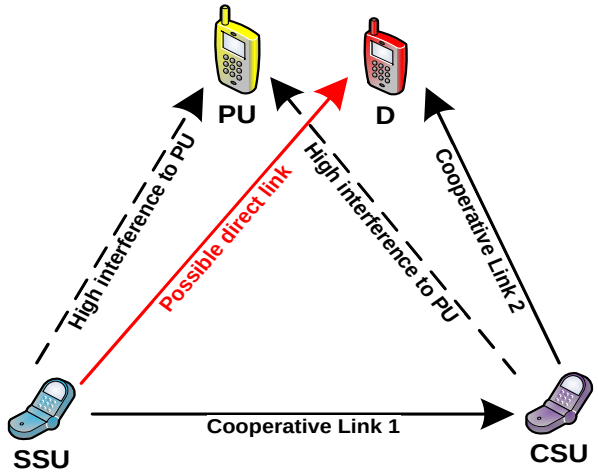

Fig. 1 System Model

Thus, the data rate of each slot is given as:

$$c_{k,n}^{s}=\log\left(1+\frac{P_{k,n}^{s}\left|H_{k,n}^{s}\right|^{2}}{\sigma_r^{2}+\sum_{l=1}^{L}J_{k,n}^{l}}\right),c_{k,n}^{r}=\log\left(1+\frac{P_{k,n}^{r}\left|H_{k,n}^{r}\right|^{2}}{\sigma^{2}+\sum_{l=1}^{L}J_{n}^{l}}\right)$$

where σ_r^2 and σ^2 are the noise powers at the *k*-th relay (CSU) and D respectively and the interference to the *k*-th relay and that to D on the *n*-th subchannel by the *l*-th PU's signal are denoted by $J_{k,n}^l$ and J_n^l.

The cooperative data rate is limited by the minimum of the two hops:

$$c_{k,n,C} = \min\left(c_{k,n}^s, c_{k,n}^r\right) \tag{2}$$

$c_{k,n,D}$ denotes the data rate over direct path from the SU to D. This data rate c for each subchannel is dependent on the modulation scheme. In this work, four modulation schemes, which are binary phase shift keying (BPSK), 4-quadrature amplitude modulation (QAM), 16-QAM and 64-QAM, are considered. The modulation schemes transmit $c = 1, 2, 4$ and 6 bits per OFDMA symbol respectively. For a given BER ρ, the minimum power for BPSK modulation is given as $P(c,\rho) = N_\phi\left[c \times erfc^{-1}(2\rho)\right]^2$ (where $c = 1$), while for the M-ary QAM, the minimum power is given as $P(c,\rho) = \frac{2\left(2^c - 1\right)N_\phi}{3}\left[erfc^{-1}\left(\frac{c\rho\sqrt{2^c}}{2\left(\sqrt{2^c}-1\right)}\right)\right]^2$ where N_ϕ is the single-sided noise power spectral density. The minimum power $P_{k,n}\left(c_{k,n},\rho\right)$ required at the *k*-th SU over the nth subchannel to transmit $c_{k,n}$ bits is obtained by dividing the power of that user *k* on the *n*-th subchannel by the channel gain between the SUBS and the user *k* over that subchannel n. This is thus given as:

$$P_{k,n}\left(c_{k,n},\rho\right) = \frac{P\left(c_{k,n},\rho\right)}{H_{k,n}^c} \tag{3}$$

4. Problem Formulation

Let the minimum data rate assigned to user *k* in category one be R_k and the normalized proportional fairness factor for each SU in category two be γ_k with data rate R_i indicating the rate for the element *i*. The total power on the *n*-th subchannel is represented as $\Phi_n = \sum_{k=1}^{K} P_{k,n}$ with $P_{k,n}$ being the transmit power of user *k* over the nth subchannel. Also let the interference power gain matrix between the SUBS and the available PU be represented as $\mathbf{H}^p \in \square^{L\times N}$. The vector $\mathbf{H}_{l,n}^p$ therefore denotes the subchannel interference power gain between the SUBS and PU *l* over subchannel *n*. The maximum permissible level of interference to the *l*-th PU from all the transmitting SUs is represented as ε_l while $P_{\max}$ denotes the maximum transmit power at the SUBS. Also let $X_{k,n,D}$ be a binary variable employed to limit each subchannel to direct or cooperative communication. The resource allocation problem for the heterogeneous cooperative CRN is formulated as:

$$z = \max \sum_{n=1}^{N}\left(\sum_{k=1}^{K_1}\left[X_{k,n,D}c_{k,n,D} + \left(1 - X_{k,n,D}\right)c_{k,n,C}\right] + \sum_{k=K_1+1}^{K}\left[X_{k,n,D}c_{k,n,D} + \left(1 - X_{k,n,D}\right)c_{k,n,C}\right]\right) \tag{4}$$

subject to

$$\sum_{n=1}^{N}\left(c_{k,n,D} + c_{k,n,C}\right) \geq R_k; k = 1, 2, \ldots, K_1 \tag{5}$$

$$\frac{R_k}{\sum_{i=K_1+1}^{K} R_i} = \gamma_k; k = K_1 + 1, K_1 + 2, \ldots, K \tag{6}$$

$$\sum_{n=1}^{N}\left(\sum_{k=1}^{K}\left[X_{k,n,D}P_{k,n,D} + \left(1 - X_{k,n,D}\right)P_{k,n,C}\right]\right) \leq P_{\max} \tag{7}$$

$$\sum_{n=1}^{N}\Phi_n \mathbf{H}_{l,n,D}^p \leq \varepsilon_l; l = 1, 2, \ldots, L \tag{8}$$

$$\sum_{n=1}^{N}\Phi_n \mathbf{H}_{l,n,C}^p \leq \varepsilon_l; l = 1, 2, \ldots, L \tag{9}$$

$$\begin{cases} c_{k,n,D} = 0 & \text{if } c_{k',n,D} \neq 0, \\ c_{k,n,C} = 0 & \text{if } c_{k',n,C} \neq 0, \end{cases}, \forall k' \neq k; k = 1, 2, \ldots, K \tag{10}$$

$$X_{k,n,D} \in \{0,1\}, X_{k,n,D} = \begin{cases} 1 & \text{if } c_{k,n,D} \neq 0 \\ 0 & \text{otherwise} \end{cases} \tag{11}$$

The equation in constraint (6) can be equally expressed as:

$$R_k = \gamma_k \times \sum_{i=K_1+1}^{K} R_i$$

Representing $\gamma_k \times \sum_{i=K_1+1}^{K} R_i$ by $\tilde{\gamma}_k$, Equation (6) becomes:

$$R_{K_1+1} : R_{K_1+2} : \ldots : R_K = \tilde{\gamma}_{K_1+1} : \tilde{\gamma}_{K_1+1} : \ldots : \tilde{\gamma}_K \tag{12}$$

The above formulation of the RA problem is not a linear programming problem. However, the problem can be reformulated as an integer linear programming (ILP) problem. The reformulated problem can easily be solved by using any of the classical optimization techniques. The branch-and-bound (BnB) approach is used in this work. The reformulation is achieved as described below:

Define $\mathbf{x}_I$ as the bit allocation vector for all subchannels assigned to all users in category one and also define $\mathbf{x}_{II}$ as the bit allocation vector for all subchannels assigned to all users in category two. $\mathbf{x}_I$ and $\mathbf{x}_{II}$ are given as:

$$\mathbf{x}_I = \left[\left(\mathbf{x}_{I,N}^1\right)^T \quad \left(\mathbf{x}_{I,N}^2\right)^T \quad \ldots \quad \left(\mathbf{x}_{I,N}^N\right)^T\right]^T \in \{0,1\}^{NK_1C\times 1} \tag{13}$$

$$\mathbf{x}_{II} = \left[\left(\mathbf{x}_{II,N}^1\right)^T \quad \left(\mathbf{x}_{II,N}^2\right)^T \quad \ldots \quad \left(\mathbf{x}_{II,N}^N\right)^T\right]^T \in \{0,1\}^{N(K-K_1)C\times 1} \tag{14}$$

where $\mathbf{x}_{I,N}^n = \left[x_{I,1,n}^T \quad x_{I,2,n}^T \quad \ldots \quad x_{I,K,n}^T\right]^T \in \{0,1\}^{KC\times 1}$ indicates that subchannel *n* has been assigned to a category one SU with

$\mathbf{x}_{I,k,n} = \left[x_{k,n,1} \quad x_{k,n,2} \quad \dots \quad x_{k,n,M} \right]^T \in \{0,1\}^{C\times 1}$; $n = 1,\dots,N$; $k = 1,\dots,K$; M indicates the overall number of modulation schemes being employed (for this work, $M = 4$). The implication is that $\mathbf{x}_{I,k,n} = \left[x_{k,n,1} \quad x_{k,n,2} \quad x_{k,n,3} \quad x_{k,n,4} \right]^T$. Similar explanations apply to $\mathbf{x}_{II}$. The combined bit allocation vector $\mathbf{x} = \mathbf{x}_I + \mathbf{x}_{II}$. Because of the mutually exclusive constraint, $\mathbf{x}_{I,N}^n$ and $\mathbf{x}_{II,N}^n$ can be any of the vectors $\left\{ [0 \ 0 \ \dots \ 0]^T, [1 \ 0 \ \dots \ 0]^T, [0 \ 1 \ \dots \ 0]^T, \dots, [0 \ 0 \ \dots \ 1]^T \right\}$

Hence, only one component in $\mathbf{x}_{I,N}^n$ is 1, while the other components are all 0s. If $x_{k,n,c}$ is 1, it means that subchannel *n* has been assigned to user *k* to transmit *c* bits per symbol. If $\mathbf{x}_{I,N}^n$ has all its components as 0s, subchannel *n* is not being assigned to any user. For the two user categories, define the modulation order vectors $\mathbf{b}_I$ and $\mathbf{b}_{II}$ as:

$$\mathbf{b}_I = \left[\left(b_{I,N}^1 \right)^T \quad \left(b_{I,N}^2 \right)^T \quad \dots \quad \left(b_{I,N}^N \right)^T \right]^T \in \mathbb{Z}^{NK_1C\times 1} \quad (15)$$

$$\mathbf{b}_{II} = \left[\left(b_{II,N}^1 \right)^T \quad \left(b_{II,N}^2 \right)^T \quad \dots \quad \left(b_{II,N}^N \right)^T \right]^T \in \mathbb{Z}^{N(K-K_1)C\times 1} \quad (16)$$

where $\mathbf{b}_{I,N}^n = \left[b_{I,1,n}^T \quad b_{I,2,n}^T \quad \dots \quad b_{I,K,n}^T \right]^T$, $\mathbf{b}_{I,k,n}^n = \left[b_{k,n,1}^T \quad b_{k,n,2}^T \quad \dots \quad b_{k,n,C}^T \right]^T$. Similar explanations also apply to $\mathbf{b}_{II}$. Having considered only four modulation schemes, $\mathbf{b}_{1,k,n} = [1 \ 2 \ 3 \ 4]^T$ (the same applies to $\mathbf{b}_{II,N}^n$). For the two categories of SUs, data rate matrices $\mathbf{B}_i \in \mathbb{Z}^{K_1\times NK_1C}$ and $\mathbf{B}_j \in \mathbb{Z}^{(K-K_1)\times N(K-K_1)C}$ are defined respectively as:

$$\mathbf{B}_i = \begin{bmatrix} b_1 & b_1 & \dots & b_1 \\ b_2 & b_2 & \dots & b_2 \\ \vdots & \vdots & \ddots & \vdots \\ b_{K_1} & b_{K_1} & \dots & b_{K_1} \end{bmatrix}, \left\{ \begin{array}{l} b_1 = \left[b^T \quad 0_C^T \quad \dots \quad 0_C^T \right] \in \mathbb{Z}^{1\times K_1C} \\ b_2 = \left[0_C^T \quad b^T \quad \dots \quad 0_C^T \right] \in \mathbb{Z}^{1\times K_1C} \\ \qquad\qquad \vdots \ \vdots \ \ddots \ \vdots \\ b_{K_1} = \left[0_C^T \quad 0_C^T \quad \dots \quad b^T \right] \in \mathbb{Z}^{1\times K_1C} \end{array} \right\} \quad (17)$$

$$\mathbf{B}_j = \begin{bmatrix} b_{K_1+1} & b_{K_1+1} & \dots & b_{K_1+1} \\ b_{K_1+2} & b_{K_1+1} & \dots & b_{K_1+1} \\ \vdots & \vdots & \ddots & \vdots \\ b_K & b_K & \dots & b_K \end{bmatrix}, \left\{ \begin{array}{l} b_{K_1+1} = \left[b^T \quad 0_C^T \quad \dots \quad 0_C^T \right] \in \mathbb{Z}^{1\times (K-K_1)C} \\ b_{K_1+2} = \left[0_C^T \quad b^T \quad \dots \quad 0_C^T \right] \in \mathbb{Z}^{1\times (K-K_1)C} \\ \qquad\qquad \vdots \ \vdots \ \ddots \ \vdots \\ b_K = \left[0_C^T \quad 0_C^T \quad \dots \quad b^T \right] \in \mathbb{Z}^{1\times (K-K_1)C} \end{array} \right\} \quad (18)$$

Define $\mathbf{R}_k \in \left[R_1 \quad R_2 \quad \dots \quad R_{K_1} \right]^T$ and $\tilde{\gamma}_k \in \left[\tilde{\gamma}_{K_1+1} \quad \tilde{\gamma}_{K_1+2} \quad \dots \quad \tilde{\gamma}_K \right]^T$, the constraint of Equation (5) can be written as $\mathbf{B}_i \mathbf{x}_I \geq \mathbf{R}_k$, while the data rate constraint for category two SU can be written as $\mathbf{B}_j \mathbf{x}_{II} = \tilde{\gamma}_k$. A power transmission vector $\mathbf{p}$ is defined as:

$$\mathbf{p} = \left[\left(\mathbf{p}_N^1 \right)^T \quad \left(\mathbf{p}_N^2 \right)^T \quad \dots \quad \left(\mathbf{p}_N^N \right)^T \right]^T \in \mathbb{Z}^{NKC\times 1} \quad (19)$$

where $\mathbf{p}_N^n = \left[\mathbf{p}_{1,n}^T \quad \mathbf{p}_{2,n}^T \quad \dots \quad \mathbf{p}_{K,n}^T \right]^T$, $\mathbf{p}_{k,n} = \left[p_{k,n,1} \quad p_{k,n,2} \quad \dots \quad p_{k,n,C} \right]^T$; $p_{k,n,c}$ is the power required to transmit *c* bits over subchannel *n* for user *k*. Equation (7) can be written as $\mathbf{p}^T \mathbf{x} \leq P_{\max}$. The transmit power is the sum of the powers used for both direct and cooperation transmission, $\mathbf{p} = \mathbf{p}_D + \mathbf{p}_C$, where $\mathbf{p}_D$ and $\mathbf{p}_C$ are the transmit power vectors during direct and cooperation transmission respectively. The power constraint therefore becomes $\left(\mathbf{p}_D + \mathbf{p}_C \right)^T \mathbf{x} \leq P_{\max}$. To write Equation (8), the interference power constraint in terms of the bit allocation vector $\mathbf{x}$, define a matrix $\mathbf{A} \in \{0,1\}^{N\times NKC}$ as:

$$\mathbf{A} = \begin{bmatrix} 1_{KC}^T & 0_{KC}^T & \dots & 0_{KC}^T \\ 0_{KC}^T & 1_{KC}^T & \dots & 0_{KC}^T \\ \vdots & \vdots & \ddots & \vdots \\ 0_{KC}^T & 0_{KC}^T & \dots & 1_{KC}^T \end{bmatrix}, 1_{KC} = \begin{bmatrix} 1 \\ 1 \\ \vdots \\ 1 \end{bmatrix} \in \{1\}^{KC\times 1}, 0_{KC} = \begin{bmatrix} 0 \\ 0 \\ \vdots \\ 0 \end{bmatrix} \in \{0\}^{KC\times 1} \quad (20)$$

Let $\mathbf{p} \otimes \mathbf{x}$ be the Schur-Hadamard (or entry-wise) product of $\mathbf{p}$ and $\mathbf{x}$. By defining $\varepsilon_l \in \left[\varepsilon_1 \quad \varepsilon_2 \quad \dots \quad \varepsilon_L \right]^T \in \mathbb{Z}^{L\times 1}$, Equation (8) can then be written as:

$$\left[\mathbf{H}_{l.n,D}^p \left(\mathbf{A} \left(\mathbf{P}_D \otimes \mathbf{x} \right) \right) \right] \leq \varepsilon_l \quad (21)$$

Likewise, the constraint in Equation (9) can be written as:

$$\left[\mathbf{H}_{l.n,C}^p \left(\mathbf{A} \left(\mathbf{P}_C \otimes \mathbf{x} \right) \right) \right] \leq \varepsilon_l \quad (22)$$

Thus, the resource allocation problem for the modeled heterogeneous cognitive CRN described in Equations (4) - (11) can be described in the ILP form as:

$$z^* = \max_{\mathbf{x}} \left[\left(\mathbf{b}_I \right)^T \mathbf{x}_I + \left(\mathbf{b}_{II} \right)^T \mathbf{x}_{II} \right] \quad (23)$$

subject to $\mathbf{B}_i \mathbf{x}_I \geq \mathbf{R}_k ; k = 1,2,\dots,K_1$ (24)

$$\mathbf{B}_j \mathbf{x}_{II} = \tilde{\gamma}_k ; k = K_1 + 1, K_1 + 2, \dots, K \quad (25)$$

$$\left(\mathbf{p}_D + \mathbf{p}_C \right)^T \mathbf{x} \leq P_{\max} \quad (26)$$

$$\left[\mathbf{H}_{l.n,D}^p \left(\mathbf{A} \left(\mathbf{P}_D \otimes \mathbf{x} \right) \right) \right] \leq \varepsilon_l \quad (27)$$

$$\left[\mathbf{H}_{l.n,C}^p \left(\mathbf{A} \left(\mathbf{P}_C \otimes \mathbf{x} \right) \right) \right] \leq \varepsilon_l \quad (28)$$

$$\mathbf{0}_N \leq \mathbf{A}\mathbf{x} \leq \mathbf{1}_N \quad (29)$$

$$\mathbf{x}_I, \mathbf{x}_{II}, \mathbf{x} \in \{0,1\} \quad (30)$$

The formulation above is an ILP problem in which, in this work, the BnB approach has been employed to obtain solutions. BnB optimization is a very useful and well-developed technique for solving such problems.

5. Iterative based Heuristic

In this section, a fast, iterative-based heuristic is developed to solve the ILP problem. The algorithm involves two steps:

- subchannel allocation

- iterative bit and power allocation.

Subchannel Allocation

In carrying out the subchannel allocation for the different categories of SUs, the constraint $\mathbf{x} \in [0,1]$ is integer-relaxed such that the constraint becomes:

$$0 \le \mathbf{x} \le 1 \tag{31}$$

By solving this integer-relaxed formulation at the first iteration, the values of $\mathbf{x}$ are obtained. The data rate for the *k*-th SU at the *n*-th subchannel becomes $\left(\mathbf{b}_{k,n}^T \mathbf{x}_{k,n}\right)$. The subchannel *n* is only allocated to user k after ascertaining that $\left(\mathbf{b}_{k,n}^T \mathbf{x}_{k,n}\right) \ge \left(\mathbf{b}_{m,n}^T \mathbf{x}_{m,n}\right) \quad \forall m \ne k$. Clearly then, each subchannel is allocated to the SU that has the highest achievable data rate over that subchannel. It is important to realize too that once the suchannels have been allocated to the different SUs using the above criterion at the first iteration, the dimension of $\mathbf{x}$ reduces from its initial value of $\mathbf{x} \in [0,1]^{KNC \times 1}$ to the smaller value of $\mathbf{x} \in [0,1]^{NC \times 1}$.

5.1 Binary SAR Architecture

Once the subchannels have been assigned to the SUs, it remains to determine how many bits and what power can be associated with each subchannel. This is performed in an iterative manner. The optimization process occurs in a number of iterations, say *y*. In general, the following optimization problem has to be solved at the *y*-th iteration step:

$$\max_{\mathbf{x}^y} \left[\left(\mathbf{b}_I^y\right)^T \mathbf{x}_I^y + \left(\mathbf{b}_{II}^y\right)^T \mathbf{x}_{II}^y \right] \tag{32}$$

$$\text{subject to} \quad \mathbf{B}_i \mathbf{x}_I^y \ge \left[\mathbf{R}_k - \mathbf{f}^{(y-1)} \right]^+, k = 1,2,\ldots,K_1 \tag{33}$$

$$\mathbf{B}_j \mathbf{x}_{II}^y = \left[\tilde{\gamma}_k - \mathbf{g}^{(y-1)} \right]^+, k = K_1+1, K_1+2, \ldots, K \tag{34}$$

$$\left(\mathbf{p}^{(y-1)}\right)^T \mathbf{x}^y \le P_{\max} - \left\| \mathbf{u}^{(y-1)} \right\|_1 \tag{35}$$

$$\mathbf{H}^p \left[\mathbf{A}\left(\mathbf{p}^{(y-1)} \square \mathbf{x}^y\right) \right] \le \varepsilon_l - \mathbf{H}^p \mathbf{u}^{(y-1)} \tag{36}$$

$$\mathbf{0}_N \le \mathbf{A}\mathbf{x}^y \le \mathbf{1}_N \tag{37}$$

$$\mathbf{0}_{KNC} \le \mathbf{x}^y \le \mathbf{1}_{KNC} \tag{38}$$

where $\mathbf{f}^{(y-1)}$ and $\mathbf{g}^{(y-1)}$ are the allocated bits for category one and category two users at the *y*-th iteration respectively, and $\mathbf{u}^{(y-1)}$ is the allocated power at the *y*-th iteration. Here, a detailed explanation on the iteration process is given. Recall that the bit allocation to the *n*-th subchannel assigned to a category one SU, $\mathbf{b}_{I,n} = \left[b_{I,n}^T \quad \ldots \quad b_{K_1,n}^T \right]^T$ is a vector of size $K_1 C \times 1$ with possible entries 1, 2, 4 and 6. Assume that during the subchannel allocation carried out in the last subsection, the first subchannel has been allocated to the second user, which happens to be a category one SU. Then, $\mathbf{b}_{I,1} = [0 \;\; 0 \;\; 0 \;\; 0, 1 \;\; 2 \;\; 4 \;\; 6, 0 \;\; 0 \;\; 0 \;\; 0, 0 \;\; 0 \;\; 0 \;\; 0]$ for users in category one (assuming there are four users). If it had been the third subchannel that was allocated to the first user, which happens to be a category two SU, then $\mathbf{b}_{II,3} = [1 \;\; 2 \;\; 4 \;\; 6, 0 \;\; 0 \;\; 0 \;\; 0, 0 \;\; 0 \;\; 0 \;\; 0, 0 \;\; 0 \;\; 0 \;\; 0]$ (assuming there are also four users in this category) and so on. Once this has been done and certain elements of $\mathbf{b}_I$ and $\mathbf{b}_{II}$ are zeros according to the subchannel allocation, the vectors $\mathbf{b}_I$ and $\mathbf{b}_{II}$ are renamed $\mathbf{b}_I^1$ and $\mathbf{b}_{II}^1$ respectively. Consequently, at the first iteration (i.e. when $y = 1$), the following optimization problem is solved:

$$\max_{\mathbf{x}^1} \left[\left(\mathbf{b}_I^1\right)^T \mathbf{x}_I^1 + \left(\mathbf{b}_{II}^1\right)^T \mathbf{x}_{II}^1 \right] \tag{39}$$

$$\text{subject to} \quad \mathbf{B}_i \mathbf{x}_I^1 \ge \mathbf{R}_k, k = 1,2,\ldots,K_1 \tag{40}$$

$$\mathbf{B}_j \mathbf{x}_{II}^1 = \tilde{\gamma}_k, k = K_1+1, K_1+2, \ldots, K \tag{41}$$

$$\mathbf{p}^T \mathbf{x}^1 \le P_{\max} \tag{42}$$

$$\mathbf{H}_{l,n,D}^p \left[\mathbf{A}\left(\mathbf{p}_D \square \mathbf{x}^1\right) \right] \le \varepsilon_l \tag{43}$$

$$\mathbf{H}_{l,n,C}^p \left[\mathbf{A}\left(\mathbf{p}_C \square \mathbf{x}^1\right) \right] \le \varepsilon_l \tag{44}$$

$$\mathbf{0}_N \le \mathbf{A}\mathbf{x}^1 \le \mathbf{1}_N \tag{45}$$

$$\mathbf{0}_{KNC,1} \le \mathbf{x}^1 \le \mathbf{1}_{KNC,1} \tag{46}$$

The rates $\mathbf{B}_i \mathbf{x}_I^1$ and $\mathbf{B}_i \mathbf{x}_{II}^1$ and power $\mathbf{p}^T \mathbf{x}^1$ obtained at the first iteration are passed on as $\mathbf{f}^1, \mathbf{g}^1$ and $\mathbf{u}^{(1)}$ respectively for the second iteration. Vector $\mathbf{x}^1$ is used along with the power vector $\mathbf{p}$ to determine the initial modulation scheme for each SU at various subchannels. The total power allocated to the first subchannel can then be calculated as $\left(p_{k,n}^T x_{k,n}^1\right)$. To generalize, if the *n*-th subchannel is allocated to the *k*-th SU, the total power allocated to it is calculated as $\left(p_{k,n}^T x_{k,n}^1\right)$. The modulation scheme q (with bits c_q) that can be employed without exceeding the power $\left(p_{k,n}^T x_{k,n}^1\right)$ can be obtained as:

$$q = \arg\max_q \left\{ q \in [0,1,2,3,4] : p_{k,n,q} \le p_{k,n}^T x_{k,n}^1 \right\} \tag{47}$$

The interference leakage to PU will still be less than ε. As a result, it is most likely that there will be some residual power available for use. Hence $y = 2$ becomes feasible. Since the first subchannel has been allocated to the second user, which happens to be in category one, to transmit 2 bits, then, $\mathbf{b}_{I,2,1}$ can be modified as $\mathbf{b}_{I,2,1} = [0 \;\; 0 \;\; 2 \;\; 4]^T$. To have allocated 2 bits to this subchannel, the power $\mathbf{p}_{2,1,2}$ must have been used. With the realization of excess power available for use, the allocation might then be upgraded to, say, a 16-QAM (to transmit 2 more bits) or 64-QAM. For this to take place would require additional power of $\left(p_{2,1,3} - p_{2,1,2}\right)$ (for 16-QAM) or $\left(p_{2,1,4} - p_{2,1,2}\right)$ (for 64-QAM) respectively.

Hence, the new power vector at the second iteration $\mathbf{p}_{2,1}^1 = \left[p_{2,1,1} \quad p_{2,1,2} \quad \left(p_{2,1,3} - p_{2,1,2}\right) \quad \left(p_{2,1,4} - p_{2,1,2}\right) \right]^T$. If u_n^1 denotes the power that was allocated to the *n*-th subchannel in the first iteration, then $\mathbf{u}^1 = \left[u_1^1 \quad \dots \quad u_N^1 \right]^T$ It therefore implies that $P_{\max} - \sum_{n=1}^{N} u_n^1$ is the residual power available for the second iteration step. This total power is given as $\upsilon_n^2 = u_n^1 + \left(\mathbf{p}_{k,n}^1\right)^T \mathbf{x}_{k,n}^2$. This new power is used to decide about the modulation scheme q of the *n*-th subchannel should be upgraded to:

$$q = \arg\max_q \left\{ q \in [0,1,2,3,4] : p_{k,n,q} \le \upsilon_{k,n}^2 \right\} \quad (48)$$

Similarly, the interference to PUs as a result of the power allocated in the first iteration step is given as $\mathbf{H}^p \mathbf{u}^1$. The remaining interference permissible must be less than $\left(\varepsilon_l - \mathbf{H}^p \mathbf{u}^1\right)$ for the second iteration. Since, at this second iteration, f_k^1 already becomes the data rate allocated to the *k*-th SU in category one during the first iteration and g_k^1 becomes the data rate already allocated to the *k*-th SU in category two during the first iteration, $\mathbf{f}^1$ and $\mathbf{g}^1$ are defined as $\mathbf{f}^1 = \left[f_1^1 \quad \dots \quad f_1^k \right]^T$ and $\mathbf{g}^1 = \left[g_1^1 \quad \dots \quad g_1^k \right]^T$ respectively. Hence, the data rate requirement at the second iteration for category one users would be $\left(\mathbf{R}_k - \mathbf{f}^1\right)$, while the available data rate for category two users at the second iteration would be $\left(\tilde{\gamma}_k - \mathbf{g}^1\right)$. The constraints on data rate then become $\mathbf{B}_i \mathbf{x}_I^2 \ge \left[\mathbf{R}_k - \mathbf{f}^1\right]^+$ for category one users and $\mathbf{B}_j \mathbf{x}_{II}^2 = \left[\tilde{\gamma}_k - \mathbf{g}^1\right]^+$ for category two users. This whole iteration process is repeated continuously and only stopped when no further improvement can be achieved on the total achievable data rate for each user. The stopping criterion is thus given as:

$$\left[\left(\mathbf{b}_I^y\right)^T \mathbf{x}_I^y + \left(\mathbf{b}_{II}^y\right)^T \mathbf{x}_{II}^y \right] - \left[\left(\mathbf{b}_I^{y-1}\right)^T \mathbf{x}_I^{y-1} + \left(\mathbf{b}_{II}^{y-1}\right)^T \mathbf{x}_{II}^{y-1} \right] = \varsigma \quad (49)$$

where ς is a predetermined (very small) value. After the *y*-th iteration, the vectors $\mathbf{f}^{(y+1)}$ and $\mathbf{g}^{(y+1)}$ will contain the allocated bits for each subchannel assigned to category one and category two users respectively. The pseudo-code given in Table 1 summarizes both the subchannel allocation and the iterative bit and power allocation.

6. Simulation Results

In this section, the performance of the proposed algorithms is evaluated using appropriate simulations. A static system level simulation is done as a single cell, which contains 8 SUs, 4 PUs, with category one SUs $K_1 = 2$, category two SUs $\left(K - K_1\right) = 2$ and SUs as possible cooperators from which the best relay (CSU) is selected = 4. The minimum data rate requirement for category one SUs is 64 bits/user. The area covers 2 km × 2 km and the SUs are uniformly distributed in the area. It is assumed here that 64 subchannels are available for secondary usage, meanwhile used by the PUs. The elements of the channel matrices follow a Rayleigh distribution and are independent of each other. The path-loss exponent is 4, and the standard deviation of shadowing is 6 dB. The noise power is $\sigma^2 = 10^{-12}$ W/Hz.

Table 1. Pseudo-code for the proposed iterative-based heuristic

• Pseudo-code for the subchannel allocation
• solve for x using Equations (23) - (29) and (31) • set subchannel index $n = 0$ • $n \leftarrow n + 1$ • if $\mathbf{b}_{k,n}^T \mathbf{x}_{k,n} \ge \mathbf{b}_{m,n}^T \mathbf{x}_{m,n}$, $\forall m \ne k$ • n -th subchannel is allocated to user *k* • end if • until $n < N + 1$
• Pseudo-code for the bit and power allocation
• set $n = 0, y = 0, \mathbf{u}^{(0)} = \mathbf{0}_N, \mathbf{p}^{(0)} = \mathbf{p}$ • $y \leftarrow y + 1$ • set $\mathbf{f}^y = \mathbf{0}_K, \mathbf{g}^y = \mathbf{0}_K, \upsilon^y = \mathbf{0}_N$ • solve the problem (32) - (38) • repeat • $n < N + 1$ • $\upsilon_n^y = u_n^{y-1} + \left(\mathbf{p}_{k,n}^{y-1}\right)^T \mathbf{x}_{k,n}^y$ • if $q = \arg\max_q \left\{ q \in [0,1,2,3,4] : p_{k,n,q} \le \upsilon_n^y \right\}$ then • use modulation scheme *q* on *n*-th subchannel • set $u_{k,n}^y = p_{k,n,l}; f_k^y = f_k^y + c_q; g_k^y = g_k^y + c_q$ • set $p_{k,n,m}^y = p_{k,n,m} - p_{k,n,l}, \forall m > l$ • set $b_{k,n,m}^{y+1} = b_{k,n,l} - c_q, \forall m > l$ • set $b_{k,n,m}^{y+1} = 0, \forall m \le l$ • end if • until $n < N + 1$ • until no further improvement on total data rate (Equation (49)) • the vectors $\mathbf{f}^{y+1}$ and $\mathbf{g}^{y+1}$ contain the bits allocated for each subchannel in category one and two respectively • the vector $\mathbf{u}^{y+1}$ contains the power allocated for each subchannel

Figure 2 shows the interference channel gain patterns for the various PUs. At high interference gain, the subchannels are allocated low data rates to reduce the adverse effect of high power and/or interference gain on the PUs and vice versa. The combined interference to the PUs on subchannels 2, 3, 9, 57, 63, and 64 is lower than the combined interference on the other subchannels. On subchannels 14 to 27 and 39 to 52, the combined interference to PUs is quite high, and the subchannels have been allocated low data rates to transmit. This is the fundamental principle by which the bit allocation is performed to obtain optimal results on the overall throughput of the network.

Figure 3 gives the average data rate (bits per OFDMA symbol) for each category of SUs against the maximum interference power to the PUs for both direct communication and cooperative communication, where the SUBS maximum transmit power is at 20 dBm. From the results obtained, it is obvious that for the developed RA problem to have feasible solutions, the minimum rate constraint of the high priority category 1 users has to be met at all times. Importantly, the result shows that a marked improvement in performance of the network is achieved during cooperation, compared to when direct communication alone is used. The reason for this is the improved interference gain to PUs that the cooperative network achieves, which means that the subchannels can transmit at a higher rate than they would ordinarily have been allocated by direct communication. It is also worth noting that in Figure 3, the average data rate during cooperation eventually converges to nearly that of direct communication. This shows that as the permissible interference level to PUs increases, the need for and/or effect of cooperation diminishes. It would be better to transmit directly if the PUs are robust to the SUs' interference than to transmit using cooperation, as cooperation generally requires much more signaling overhead than direct communication.

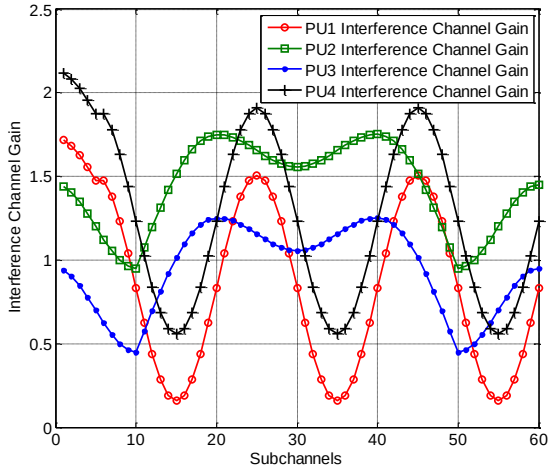

Fig. 2 Interference gain of PUs

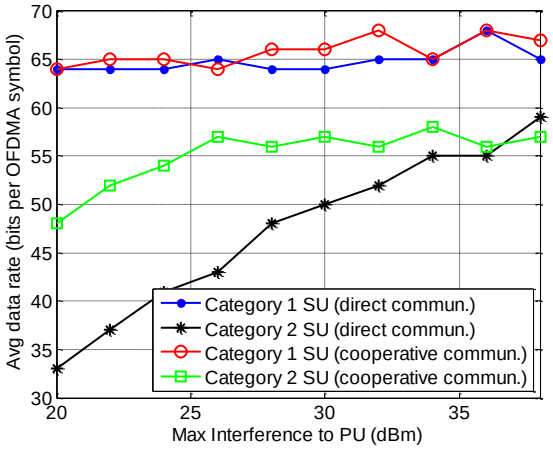

Fig. 3 Average data rate different categories of SUs

Figure 4 describes the average data rate performance for increasing SUBS power. The 2 categories of SUs are covered, and both direct and cooperative communications are considered. In Fig. 4, a maximum interference power to PUs of 25 dBm is used. At all times, the minimum rate guarantee of the category 1 SUs must be met for the problem to have feasible solutions. Again, as the SUBS power is increased, the average data rate improves, particularly for category 2 SUs. After a while though, no further improvement can be observed, irrespective of whether or not the SUBS power is increased. The reason for this is that the other constraints also come into play, thus making it impossible for the data rate to keep increasing indefinitely with increasing SUBS power. It is significant to note the improvement that cooperative communication achieves over direct communication. This improvement can be seen when the interference limit is at 25 dBm. These results clearly show that the network would rather transmit using direct communication when the SUBS power is limited so as to maximize the power use and reduce signalling overhead. At higher power, however, cooperative communication is preferred, as the overall capacity is remarkably better.

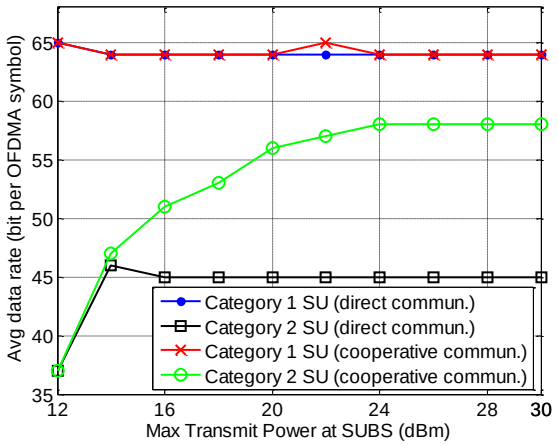

Fig. 4 Average data rate different categories of SUs

7. Conclusions

In CRN, RA models that can yield outstanding productivity even with very stringent constraints are critical. This work develops such a model whereby, in a heterogeneous CRN environment, cooperative diversity is used in mitigating the limiting effects of the interference to the PUs of the network. To make the model feasible and close to practical, only one single best relay is selected from the available ones as the cooperating relay. Also, cooperation is only used by users that have subchannels with a high interference gain to the PU. The problem that has been developed is first solved by a careful reformulation of the non-deterministic polynomial-time-hard problem into an ILP problem, and optimal solutions are obtained using the BnB method for solving ILP problems. To reduce computational complexity, an iterative-based heuristic is developed to solve the problem in a much reduced time frame. The results presented compare the average data rates and total data rates for the different categories of SUs when direct and cooperative communications are used. The optimality and computational complexity of the developed heuristic are compared with those obtained using ILP as well. The improvement in the performance of the network when cooperation is used is quite remarkable, as the results have shown.

References

[1] F. C. Commission, "Report of spectrum efficiency working group," 2002, spectrum policy task force, Washington, DC, USA.

[2] Cognitive radio technologies proceeding," 2003, rep. ET Docket, no. 03-108.

[3] L. E. Doyle, Essentials of Cognitive Radio, The Cambridge Wireless Essentials Series, New York, USA: Cambridge University Press, 2009.

[4] M. G. Adian, H. Aghaeinia and Y. Norouzi, "Spectrum Sharing and Power Allocation in MIMO Multi-Band Underlay Cognitive Radio Networks," IET Communications, vol. 7, no. 11, pp. 1140-1150, 2013.

[5] M. G. Adian and H. Aghaeinia, "Low Complexity Resource Allocation in MIMO-OFDM based Cooperative Cognitive Radio Networks," Trans. Emerging Telecommun. Tech., vol. 27, no. 1, pp. 92-100, 2016.

[6] M. G. Adian and H. Aghaeinia, "Resource Allocation in MIMO-OFDM Based Cooperative Cognitive Radio Networks: Optimal and Sub-Optimal Low Complexity Approaches," Int'l. J. Commun. Sys., doi: 10.1002/dac.2804, 2014.

[7] M. G. Adian and H. Aghaeinia, "Optimal Resource Allocation in MIMO-OFDM Based Cooperative Cognitive Radio Networks," IEEE Trans. Commun., vol. 62, no. 7, pp. 2224-2235, 2014.

[8] M. G. Adian and H. Aghaeinia, "Spectrum Sharing and Power Allocation in Multiple-In Multiple-Out Cognitive Radio Networks via Pricing," IET Commun., vol. 6, no. 16, pp. 2621-2629, 2012.

[9] M. G. Adian and H. Aghaeinia, "Optimal Resource Allocation in Heterogeneous MIMO Cognitive Radio Networks," Wireless Pers. Commun., vol. 76, no. 1, pp. 23-39, 2014.

[10] M. G. Adian and H. Aghaeinia, "Optimal Resource Allocation for Opportunistic Spectrum Access in MIMO-OFDM based Cooperative Cognitive Radio Networks," IET Sig. Process., vol. 7, no. 7, pp. 549-557, 2013.

[11] M. G. Adian, "A Coalitional and Two-Level Game Based Approach for Spectrum Leasing in MIMO Cooperative Cognitive Radio Networks," Wireless Personal Commun., DOI: 10.1007/s11277-017-4198-z, May 2017.

[12] M. G. Adian and H. Aghaeinia, "An Auction Based Approach for Resource Allocation in Multi-Cell MIMO-OFDM Based Cognitive Radio Networks," Wireless Pers. Commun., vol. 80, pp. 261–276, 2015.

[13] M. G. Adian, H. Aghaeinia, "An auction-based approach for spectrum leasing in cooperative cognitive radio networks: When to lease and how much to be leased," Wireless Networks, vol. 20, no. 3, pp. 411-422, 2014.

[14] S.Wang, M. Ge, and C.Wang, "Efficient resource allocation for cognitive radio networks with cooperative relays," IEEE J. Sel. Areas in Commun., vol. 31, no. 11, pp. 2432-2441, 2013.

[15] M. G. Adian and H. Aghaeinia, "Optimal resource allocation for opportunistic spectrum access in MIMO-OFDM based cooperative cognitive radio networks," IET Sig. Process., vol. 7, no. 7, pp. 549-557, 2013.

[16] S. Du, F. Huang, S. Wang, "Power allocation for orthogonal frequency division multiplexing-based cognitive radio networks with cooperative relays," IET Commun., vol. 8, no. 6, pp. 921-929, 2014.

[17] M. Pischella, D. Le Ruyet, "Cooperative allocation for underlay cognitive radio systems," Signal Processing Advances in Wireless Communications (SPAWC), 2013 IEEE 14th Workshop on, Darmstadt, Germany; June 2013, pp. 165-169.

[18] Y. Rahulamathavan, S. Lambotharan, C. Toker, A. Gershman, "Suboptimal recursive optimisation framework for adaptive resource allocation in spectrum-sharing networks," IET Signal Proc., vol. 6, no. 1, pp. 27-33, 2012.

Mahdi Ghamari Adian received his B.Sc. degree from Amirkabir University of Technology (Tehran Polytechnic) Tehran, Iran in 2004, his M.Sc. degree from Sharif University of Technology, Tehran, Iran in 2006 and his Ph.D. degree from Amirkabir University of Technology (Tehran Polytechnic) Tehran, Iran in 2014, both in Electrical Engineering (Communication Systems). He is currently an assistant professor in the Electrical Engineering department in University of Zanjan, Zanjan, Iran. His current research focus is in the areas of cognitive radio networks, cooperative communications and the applications of game theory and benefits of incorporating the MIMO systems in the cooperative cognitive radio networks.